INVESTIGATION OF STRENGTH OF A HYBRID ADHESIVE ANCHOR SYSTEM USED IN PRECAST CONCRETE WELDED REPAIR APPLICATIONS SUBJECTED TO TENSILE AND ECCENTRIC SHEAR LOADING

A DISSERTATION IN
Engineering
and
Mathematics

Presented to the Faculty of the University
of Missouri-Kansas City in partial fulfillment of
the requirements for the degree

DOCTOR OF PHILOSOPHY

by
MICHAEL GLENN EILERS

B.S., University of Missouri-Rolla, 2002
M.S., University of Missouri-Kansas City, 2006

Kansas City, Missouri
2012

INVESTIGATION OF STRENGTH OF A HYBRID ADHESIVE ANCHOR SYSTEM USED IN PRECAST CONCRETE WELDED REPAIR APPLICATIONS SUBJECTED TO TENSILE AND ECCENTRIC SHEAR LOADING

Michael Glenn Eilers, Candidate for the Doctor of Philosophy Degree

University of Missouri-Kansas City, 2012

ABSTRACT

A common precast industry repair for missing or misplaced connection plates is the use of an adhesive anchor system to fasten repair plates to precast members. Typically, the repair plate will experience elevated temperatures during the welding of the loose erection plate to the repair plate. Limited testing and theoretical data are currently available to provide design guidelines on how the elevated temperatures induced by welding affect the behavior and capacity of the adhesive anchoring systems. This dissertation outlines bond tests, eccentric shear tests, and a temperature investigation performed using a hybrid adhesive system in precast concrete repair applications. In addition, limited bond strength testing data using a high strength two-part epoxy adhesive is also included. The overall aim of this work is to provide test data and guidance to the industry and design professionals when designing adhesive anchoring systems for repair applications exposed to welding.

APPROVAL PAGE

The faculty listed below, appointed by the Dean of the School of Graduate Studies, have examined a dissertation titled "Investigation of Strength of a Hybrid Adhesive Anchor System used in Precast Concrete Welded Repair Applications Subjected to Tensile and Eccentric Shear Loading," presented by Michael Glenn Eilers, candidate for the Doctor of Philosophy degree, and certify that in their opinion it is worthy of acceptance.

Supervisory Committee

Ganesh Thiagarajan, Ph.D., P.E., Committee Chair
Department of Civil and Mechanical Engineering

Kevin Truman, Ph.D.
Department of Civil and Mechanical Engineering

Khosrow Sohraby, Ph.D., P.E.
Department of Computer Science and Electrical Engineering

Noah Rhee, Ph.D.
Department of Mathematics and Statistics

John Kevern, Ph.D., P.E.
Department of Civil and Mechanical Engineering

TABLE OF CONTENTS

LIST OF ILLUSTRATIONS

LIST OF TABLES

ACKNOWLEDGEMENTS

Without the following people and their contributions, this research project would not have been completed: Christian Fogstad, Christopher Gamache, Andrew Shouse, and Todd Chandler with Hilti North America provided technical and testing support, adhesives, anchors, and installation materials; Coreslab Structures (KANSAS), Inc. and Coreslab Structures (MISSOURI), Inc. provided plant access, materials, and technical support; Ada Alexander and David Kidd, both undergraduate research assistants provided help in specimen set-up, installation, and testing; Erich Martz and Scott Ford, both colleagues, provided help with technical assistance and testing. Words cannot express the gratitude for your support and patience on this research project.

Thank you, Dr. Ganesh Thiagarajan, and members of my committee. Your experience, knowledge, and patience provided throughout this project were invaluable in making this research project a valuable resource to the design community.

Lastly, and most importantly, thank you to my wife, Heather. Her support, love, and encouragement have been unconditional since the start of my graduate school endeavors. Without her, my graduate studies and this research would be nonexistent.

CHAPTER 1

INTRODUCTION

1.1 Introduction

The precast concrete industry typically uses embed plate connections consisting of flat bar stock of plate material with headed stud anchors (HSA), deformed bar anchors (DBA), weldable rebar, or a combination of these materials as shown in Figure 1 (a), (b), and (c), respectively. These embed plates used in connections are designed to match or exceed design loads transferred by pure tension, pure shear, eccentric shear, or combinations thereof. Some situations in practice, embed plates are located improperly or left out of precast members as illustrated by Figure 2. Such errors and omissions are typically remedied using an adhesive anchoring system to attach an external steel plate to the precast concrete element. The adhesive anchoring system's steel elements replace the HSA, DBA, and/or weldable rebar materials that were originally integrated into the embed plate.

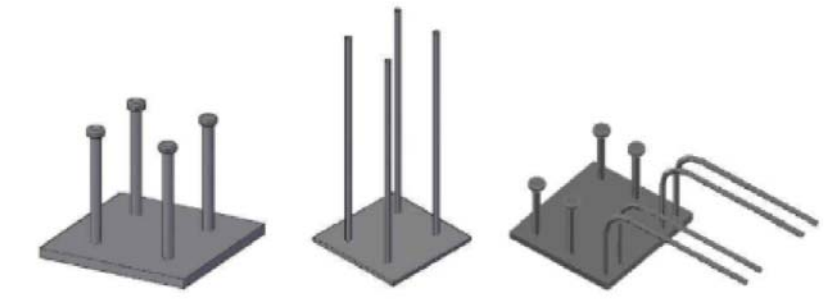

Figure 1: Common Embed Types Used in the Precast Industry

Figure 2: Improperly Located Embed Connection Plates

Due to their versatility, adhesive anchor systems have come to play an increasingly important role in the precast concrete industry. Their primary use is correcting fabrication errors and repair conditions in the field. More recently, the use of adhesive anchor systems has been seen in new construction. The flexibility and versatility they allow for in planning and job site coordination. Some of the advantages of using adhesive anchors instead of mechanical anchors in precast concrete repair applications include: less susceptibility to bond loss due to hole sizes and geometry, decreased spacing and edge distance reduction factors in design parameters, better suited for vibration loading conditions, and the possibility of variable and deeper embedment depths. The decreased spacing and edge distance reduction factors are especially beneficial as most precast connections are located at the edge of a member where it is intended to attach one element to another. Longer steel anchor elements used with adhesive anchoring systems allows for deeper embedment depths than mechanical anchors, which helps reduce concrete failure modes from being a controlling factor in the design of the fastening. Recent

advancements in adhesives have provided fast-cure adhesives, which allow a repair to be made and loaded within minutes.

It is common in the precast industry to cast embed plates in different product types. Such embed plates are part of the overall structural system that transfer gravity and lateral loads, as well as provide stability to the overall system, during both erection and in-service periods of the structure's existence. Typical embed plates cast into a precast member require welding of additional steel materials for load transfer. The simple span construction and frequent corner type connections required in precast systems generally result in eccentric shear loading conditions as seen in Figure 3.

Figure 3: Common Precast Connections Subjected to Eccentric Shear

Typical industry repair for embed plates that are missing or improperly located is the use of a post-installed adhesive anchor system that attaches a steel repair plate to the precast concrete member as seen in Figure 4. The adhesive anchoring system transfers the repair plate loading to the precast concrete member in a similar manner to how a cast-in embed would if it were present or in the correct location. Most of the time, it is not permissible to pre-weld bearing assemblies or other connecting elements prior to the

anchor installation due to the need for anchor adjustment to miss prestressing and mild steel reinforcement and still attain required bearing elevations and adjacent plates.

Figure 4: Common Precast Welded Repair using an Adhesive Anchor System

The use of adhesive anchoring systems subjected to large amounts of welding such as moment connections and corbel assemblies as shown per Figure 5, is controversial among design professionals. Some professionals argue the heat generated from the repair connection weld is higher than the degradation temperature of the adhesive, thereby causing a permanent reduction in the adhesive bond capacity. On the other hand, others reason that the repair embed plate and concrete act as a heat sink. The heat transfer to the anchor adhesive combined with the minimal duration at elevated temperatures does not adversely affect the adhesive bond capacity.

Figure 5: Post-Installed Corbel Assembly using an Adhesive Anchor System

Ultimately, the decision to weld, or not to weld in conjunction with embed plate repairs using adhesive anchor systems are left to the judgment of the design professional. This judgment is difficult to make if the actual behavior and maximum temperature gradients are not known or correctly understood. Industry standards briefly address the use of adhesive anchors and most often reference the adhesive system manufacturer's specification and product guidelines. Adhesive manufacturer's do address strength reductions of published loads for in-service base material temperatures up to about 160° F (71° C) to 180°F (82° C), but provide very limited guidance regarding design capacities when temperatures induced by welding are unknown along the steel anchor elements.

The scientific purpose of this research project is to study and characterize the strength of a common precast repair plate or augmentation using a hybrid adhesive anchoring system subjected to considerable welding and subsequent tensile and eccentric

shear loading. The hybrid adhesive anchoring system specifically used for this research is Hilti HIT-HY 150 MAX and HAS threaded anchor elements.

This specific aim of this research is to examine whether embed repair plates fastened to precast concrete elements using a hybrid adhesive anchoring system with threaded steel anchor elements subjected to tension and eccentric shear loading after welding is performed on or near the steel anchor elements will provide adequate structural strength when compared to reference tests and design capacities. Current research has not specifically verified the behavior of adhesive anchor systems subjected to eccentric shear and tension in combination with large amounts of welding.

A preliminary prediction of capacities is presented, and specific experiments are proposed to research the specific aim. A comprehensive experimental testing program would lead to a greater degree of confidence in designing and using similar types of repairs by the design professionals, specifically ensuring that adequate structural strength in the adhesive anchor system is attained.

1.2 Literature Survey

In 1970, American Concrete Institute (ACI) established ACI Committee 355, *Anchorage to Concrete* (American Concrete Institute). The purpose of ACI Committee 355 was, and still is, to develop design provisions for anchoring to concrete. In 2002, ACI Committee 355 successfully incorporated the first detailed strength design provisions into Appendix D, *Anchoring to Concrete*, of ACI 318-02 (ACI Committee 318 2002), *Building Code Requirements for Structural Concrete* (Wollmershauser 2003). Appendix D in the ACI 318-02 (ACI Committee 318 2002), 318-05 (ACI Committee 318 2005), and 318-08 (ACI Committee 318 2008) provided provisions for a strength design method that

included consideration of anchor ductility, single anchor and group interactions, tension zone influences (cracked concrete), and seismic requirements for cast-in-place anchors and post-installed mechanical anchoring systems, it did not address provisions for adhesive anchor systems (Wollmershauser 2003).

As the popularity of mechanical anchors progressed within the construction community, so did the need to provide requisite assurance of code compliance, as well as information required for design for these anchors (ACI Committee 355 2007). To prescribe testing programs and evaluation requirements for post-installed mechanical anchors intended for use in concrete under the design provisions of ACI 318, ACI Committee 355 published ACI 355.2, *Qualification of Post-Installed Mechanical Anchors in Concrete* (ACI Committee 355 2007).

While the codification of post-installed mechanical anchors was addressed by ACI Committee 355, the post-installed adhesive anchors still remained exclusively excluded from Appendix D of the ACI 318 code until the ACI 318-11 edition (ACI Committee 318 2011). Prior to the mid-1990s, assessment of adhesive anchor systems was performed on acceptance criteria authored by the International Council of Building Officials Evaluation Service (ICBO-ES) and other evaluation agencies throughout the United States and Canada. ASTM E 1512-93 (ASTM Subcommittee E06.13 1993) published the first standardized test procedures specifically designed for adhesive anchor systems. In 1995, this standard along with a complete set of testing requirements and assessment criteria was issued by ICBO-ES as AC58, *Acceptance Criteria for Adhesive Anchors in Concrete and Masonry Elements* (ICC Evaluation Service, Inc. 1995). In 2007, AC58 was revised to address adhesive anchors in masonry only. The assessment of adhesive anchoring systems

in concrete is now exclusively covered by ICC-ES AC308, *Acceptance Criteria for Post-Installed Adhesive Anchors in Concrete Elements* (ICC Evaluation Service, Inc. 2009), which is maintained by the International Code Council's subsidiary, International Code Council Evaluation Service (ICC-ES) (Eligehausen and Silva 2008).

While ICC-ES AC308 (ICC Evaluation Service, Inc. 2009) has served as a well-accepted interim standard for code compliance of adhesive anchoring systems, ACI has developed a provisional standard similar to the qualification requirements of post-installed mechanical anchors for application to adhesive anchors with the intent of future reference into Appendix D of the ACI 318 building code requirements. This provisional standard, ACI 355.4-10, *Acceptance Criteria for Qualification of Post-Installed Adhesive Anchors in Concrete* (ACI Committee 355 2010), provides the testing programs required to qualify post-installed adhesive anchor systems for design in accordance with ACI 318 Appendix D (ACI Committee 355 2010). In the latest edition of the ACI building code requirements, ACI 318-11 Appendix D has integrated post-installed adhesive anchors per Section D2.2 (ACI Committee 318 2011). ACI 355.4-10 was not referenced by Appendix D prior to the 2011 edition of ACI 318, which implies that, adhesive anchors were not codified until referenced by Appendix D of the ACI 318-11 (Meinheit et al. 2007).

While ACI 355.4-10 closely follows the ICC-ES AC308 standards, additional research contributions have been incorporated into ACI 355.4-10, and used as interim references for adhesive anchor design. Eligehausen et al. (2006) performed extensive numerical and experimental work of adhesive bonded anchors located in groups and/or near edges to develop a bond model. This bond model is the basis for product acceptance standards. The design procedures of this work fit nicely with the current ACI 318

Appendix D procedures, as they add the additional calculation of checking the bond stress under tension, including capacity modification for anchor spacing and edge distances in almost the same manner as post-installed mechanical anchors in Appendix D (Meinheit et al. 2007).

Cook et al. (1998) performed numerical work using an international data base of 2929 adhesive anchor test results consisting of tensile and shear tests for single anchors, a pair of two anchors, and groups of four anchors. The results incorporated a variety of test conditions including confined, unconfined, close edge distance, and spacing effects. Only single anchors without edge distance and spacing affects within the database were evaluated in this research program. It concluded that single anchors subjected to tensile loading is best represented by a uniform bond stress model. This work served as a design basis for the bond model developed by Eligehausen et al. (2006).

A comprehensive test program investigating various factors' potential influence on bond strength of polymer-based adhesive anchors, which included testing of ester-based and epoxy-based adhesive anchors at elevated base material temperatures, was performed by Cook and Konz (2001). The maximum elevated base material temperature used in the testing program was 110° F (43° C), which is well below the maximum temperatures expected for welded applications to or near an adhesive anchor. The testing of these anchors at elevated temperatures produced mixed results based on average coefficients of variation greater than 20%. The ester-based products showed an increase in bond strength at the elevated temperatures, while the epoxy-based products where evenly divided among increased and decreased bond strengths. This study concluded that adhesive anchors subjected to an elevated base material temperature of 110° F (43° C) can substantially

influence the adhesive anchor bond strength. In addition to testing adhesive anchors at elevated base material temperatures, other key external factors related to the installation parameters of the adhesive anchors and suspected of influencing the bond strength of the system were examined, such as the condition of the drilled hole and the types of aggregates used in the concrete.

Bickel and Shaikh (2002) performed numerical investigations regarding the shear strength of single adhesive anchors not influenced by edge conditions, comparing both numerically adjusted Precast/Prestressed Concrete Institute (PCI) methodology of computing shear strength of HSA's and the Concrete Capacity Design (CCD) Method. This work utilized the same international database as what was used by Cook et al. (1998) for tension behavior studies, and is one of the few technical papers relating to the use of adhesive anchors in the precast industry.

Improper installation of adhesive anchors can result in a 30% reduction in bond capacity (Cook and Konz 2001). The need for proper installation and inspection of adhesive anchors has been addressed in recent works. Grosser et al. (2011) investigated 23 various construction sites in the United States to evaluate 26 adhesive anchor installation procedures. This work concluded that a large portion of the installations evaluated where performed by installers that have had no formal instruction regarding anchor installation, and that they did not fully conform to the manufacturer's printed installation instructions and/or evaluation service reports. Wollmershauser and Mattis (2008) address the influences of drilling methods, hole-cleaning, curing, and the importance of special inspection of adhesive anchor installation.

The partial collapse of the ceiling system in the Boston, MA I-90 Seaport Tunnel on July 10, 2006 acted as a catalyst and accelerated the need for additional adhesive anchoring system research pertaining to creep and sustained loads while reiterating the importance of proper installation and inspection procedures to ensure that adhesive anchors achieve their desired performance. The collapse of the concrete ceiling panels resulted in one fatality and significant traffic disruption. On July 10, 2007, the National Transportation Safety Board (NTSB) issued its final report on the partial collapse of this ceiling system, identifying the cause as a creep failure of adhesive anchors installed overhead subjected to sustained tension loading (Eligehausen and Silva 2008).

As a result of the NTSB report, the National Cooperative Highway Research Program (NCHRP) realized the specific research need for a study of the use of adhesive anchors subjected to sustained loading and in 2009, released Report 639, *Adhesive Anchors in Concrete Under Sustained Loading Conditions* (Cook et al. 2009). This work specifically developed a draft for a standard test method to determine the ability of adhesive anchors to resist sustained loads based on a stress versus time-to-failure interaction diagram for individual adhesive products (Cook et al. 2009).

In addition to addressing sustained load testing of adhesive anchors, the NTSB report also made recommendations to ACI to use its "building codes, forums, educational materials, and publications to inform design and construction agencies of the potential for gradual deformation in anchor adhesives under sustained tensile-load applications" (Cook et al. 2009). In response to the NTSB recommendations and the release of ACI 318-11, ACI and the Concrete Reinforced Steel Institute (CRSI) established an Adhesive Anchor Installer Certification (AAIC) program. ACI 318-11 revised section D.9, specifically

requiring ACI/CRSI AAIC (or equivalent) for adhesive anchors installed horizontally or upwardly inclined to support sustained tension loads (ACI Committee 318 2011).

While ACI 355.4-10 requires testing and provides assessment criteria for various conditions, including sustained and seismic loads, environmental conditions such as humidity and temperature as seen in service, and determination if anchors are acceptable for use in cracked or untracked concrete conditions, it does not address elevated temperature affects induced by welding heat after the initial installation of the anchors prior to the engagement of service level loading (ACI Committee 355 2010). ACI 355.4-10 does address reliability testing with the purpose of checking the sensitivity of the adhesive anchor system to foreseeable variations from optimal installation conditions. The reliability tests are performed to establish that the anchor is capable of safe, effective behavior under normal and adverse installation conditions (ACI Committee 355 2010). The research presented in this work would fall into this category of reliability testing.

The industry standard regarding precast concrete design briefly addresses the use of adhesive anchoring systems, and even more briefly states when welding near adhesive anchors after proper cure time be done with caution (PCI Industry Handbook Committee 2010). PCI also recommends that a certain number of anchors be proof loaded prior to acceptance, which could be interpreted as a reliability testing as outlined by ACI 355.4-10.

Hilti North America and Simpson Strong-Tie have performed limited internal testing regarding welding at or near adhesive anchors. Testing by both companies was limited and focused more on the bond strengths of the adhesives rather than the maximum temperatures incurred along the steel anchor elements. Epoxy-based adhesives tested

resulted in a 1.5% to 12% reduction in bond strength, while acrylic-based adhesives tested resulted in a 2.25% reduction in bond strength.

While there has been significant research progress to aid codification of adhesive anchoring systems to one acceptable body of building code, there has been very limited research performed on the welding effects of adhesive anchor strength and performance commonly associated with precast construction.

1.3 Background on Adhesive Anchoring Systems

Adhesive anchors are post-installed anchoring systems, typically consisting of a steel anchor element inserted into a hole drilled or cored into hardened concrete. Hole diameters are typically not greater than 1.5 times the diameter of the anchor element, which transfers loads to the concrete by bond between the steel anchor element and adhesive and bond between the adhesive and concrete. Adhesive anchors derive their resistance to applied tension though these interfaces. The steel anchor element is usually a threaded rod or reinforcing bar. Figure 6 shows a typical threaded rod used as a steel anchor element in an adhesive anchor system. The 45-degree chisel point at the end of the anchor allows for easy insertion into the adhesive-filled hole. The steel material type for the threaded rod anchor element can range from ASTM F 568M, Class 5.8 low to medium carbon steel (f_y = 58 ksi (400 MPa)) or ASTM A193, Grade B7 steel (f_y = 105 ksi (725 MPa)), to specialty stainless steels such as AISI 304/316 (f_y = 65 ksi (450 MPa)). The specific design and serviceability requirements of the load application to the threaded rod greatly affect which material is selected for use in the adhesive anchor system. Rebar used as the anchor element of the adhesive anchor system is typically ASTM A615 or ASTM

A706. The determination of the grade of rebar reinforcement depends upon the specific design and serviceability requirements for the load application to the anchor element.

Figure 6: Hilti HAS Threaded Rod

The adhesive is comprised of chemical compounds that cure when mixed together. Adhesives are formulated from organic polymers or a combination of organic polymers and inorganic materials. Organic polymers used in adhesive anchors can include, but are not limited to: epoxies, polyurethanes, polyesters, methyl methacrylates, and vinyl esters. The adhesive system addressed in this work, Hilti HIT-HY 150 MAX, is a hybrid adhesive mortar that combines urethane methacrylate resin, proprietary hardener, cement, and water. The chemical components are kept separate from the hardener and water by means of a dual-cylinder foil cartridge that is attached to a plastic manifold as seen in Figure 7. A static mixing nozzle is included with the foil cartridge package and is attached to the manifold to ensure proper mixing ratio of hardener and resin during installation.

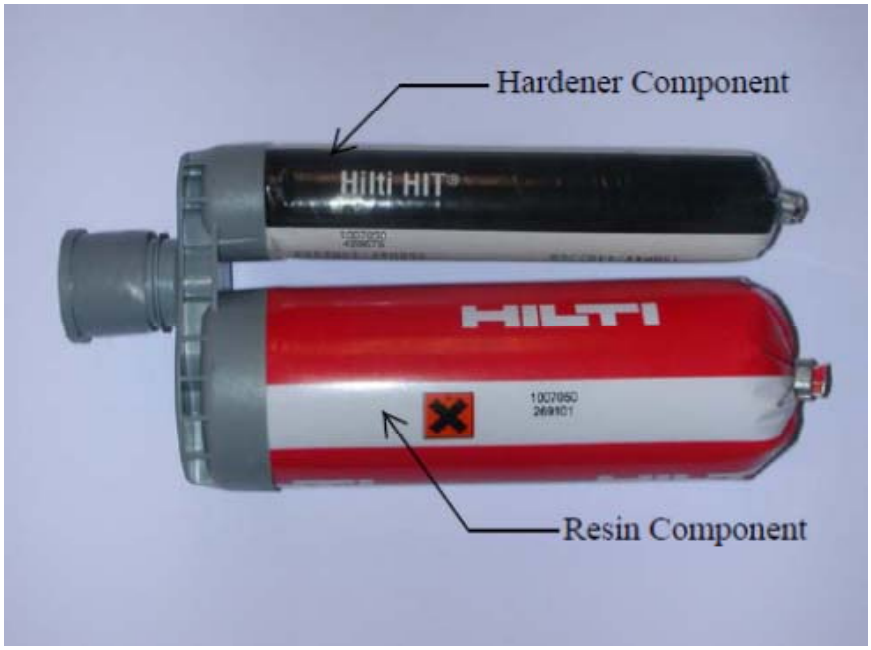

Figure 7: Hilti HIT-HY 150MAX Dual-Cylinder Foil Cartridge

Dual-cylinder foil cartridge systems such as this have become more popular on construction sites than the original glass capsule systems. This is due to the increased rugged installation delivery system. They also provide improved flexibility when adapting to various borehole geometry and are much easier to use in overhead installations.

The anchor element(s) and adhesives comprise the main components of an adhesive anchor system, however, the following components describe the entire system: proper drilling tools and drill bit sizes, adhesive anchor element, proprietary adhesive compounds in combination with the mixing and delivery system, accessories for cleaning the drilled hole, as well as ensuring proper injection of the mixed adhesive (avoiding air voids), and printed instructions for the adhesive anchor installation. Accessories of the system can include brushes, air nozzles, other items needed to complete the hole cleaning

process, and proper adhesive injection. The manufacturer's printed installation instructions provide detailed information on hole-preparation, injection, and cure for all environmental conditions permitted in the qualification. Common components that make up an adhesive anchor system, such as the typical mixing and delivery system, wire brush, and manufacturer's printed installation instructions are illustrated in Figure 8 and a basic adhesive anchor installation procedure is provided in Figure 9.

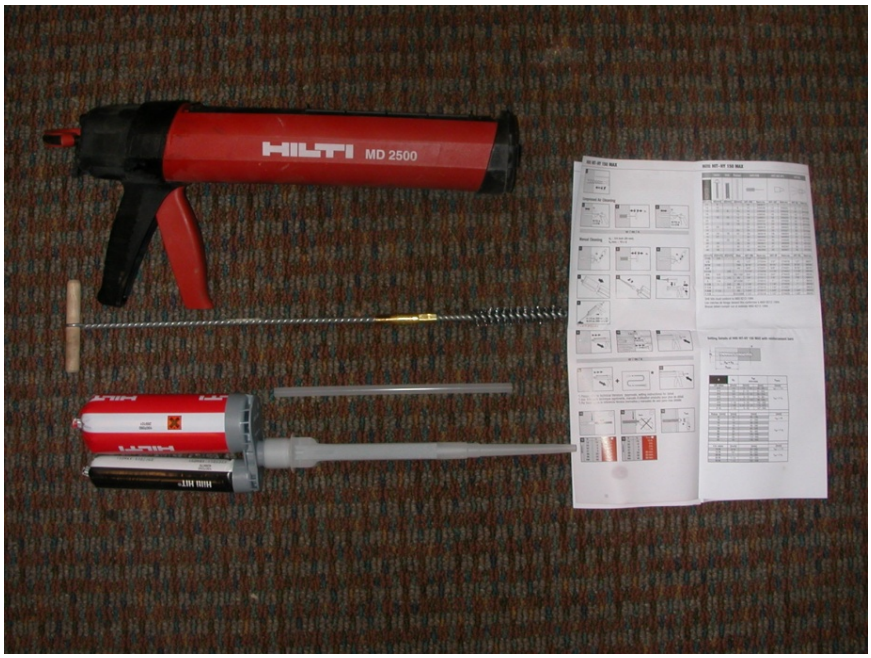

Figure 8: Common Adhesive Anchor System Components

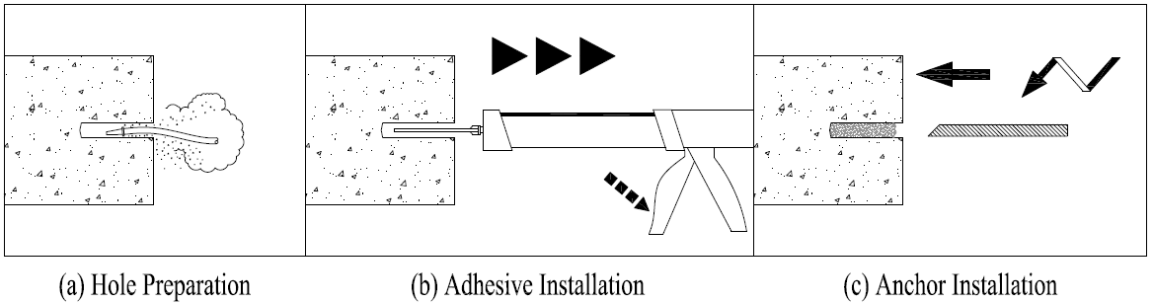

Figure 9: Basic Adhesive Anchor Installation Procedures

Adhesive anchor systems are designed to use either Allowable Stress Design (ASD) or Load and Resistance Factor Design (LRFD), also referred to as Strength Design (SD). Both methods are currently in use in the United States however, the most commonly used and accepted method is LRFD. This method is based on applying load factors to the service loads, and comparing the adhesive anchor failure mode capacities that have been reduced by the application of a resistance factor, with values varying from 0.6 to 0.75 depending on the loading condition (ACI Committee 318 2011). The adhesive anchor system failure modes must be greater than the factored service loads in order to be adequate in the design.

Appendix D of ACI 318 has incorporated the LRFD methodology into its Concrete Capacity Design (CCD) Method. The CCD Method provides relatively easy means of determining the load capacity of anchors, or groups of anchors, under concrete breakout failure conditions. It assigns resistance factors to each of the various failure modes associated with the anchor condition, and compares the controlling strength with factored loads. The CCD Method is widely used and accepted because it provides improved reliability when estimating anchor resistance compared to the ASD approach.

The CCD Method also distinguishes design based on cracked and/or uncracked concrete conditions at the anchor locations. The cracked concrete condition refers to anchors located in tensile zones of concrete members. Per ACI 318-02 Section D4.2 provisions, crack widths at the concrete surface could be expected to be as much as 0.012 to 0.16 inches for 5% fractile cracks (Wollmershauser 2003). These cracks change the distribution of stresses in the concrete and can lower the load capacity of the adhesive anchor by up to 40%. Cracked concrete condition takes this strength reduction into account in the CCD Method (Wollmershasuer 2003). It is important to note that this research focuses only on uncracked concrete conditions. Testing for this research program was performed in unreinforced, uncracked concrete.

1.4 Current Project

There has been a focus of research regarding the design and behavior of adhesive anchor systems subjected to shear and tension under normal and adverse installation and in-service conditions, but limited research regarding shear and tension testing of adhesive anchors subjected to weld effects. Since the amount of research performed on welding near and on adhesive anchors used in precast concrete repair plate applications is limited, the applicability of having reliability tests and temperature data will be useful to design professionals. By recording temperatures along the steel anchor elements, performing eccentric shear testing, and confined static tension testing on repair plates, a database can be established for designing adhesive anchoring system repairs subjected to similar conditions as those presented in this research project.

1.5 Objective

This research project will analytically predict the ultimate and design capacities of a stiffened seat repair plate utilizing a hybrid adhesive anchor system subjected to eccentric shear loads, validate the analytical predicted ultimate loads of the stiffened seat repair plate by performing eccentric shear testing, determine the temperatures along steel anchor elements subjected to welding, and determine potential bond capacity reductions in adhesive anchors subjected to welding and confined static tension testing. Analytical values will be compared to the experimental values to establish the amount of bond capacity reduction, if any, is associated with welding on or near the steel elements of the adhesive anchor system.

1.6 Scope

This research has two major components: the development of theoretical values and the analysis of experimental data. The scope of this dissertation is outlined as follows:

1. Perform sixty confined static tension tests utilizing a load cell, data acquisition instrumentation, and direct displacement LVDT and compare the results to confined static tension reference tests not subjected to welding.
2. Experimentally determine the temperature gradients along the steel anchor elements at incremental depths of anchor elements due to the welding of steel anchor elements to threaded fixtures required for confined static tension testing.

3. Predict the failure loads and determine the design load values of stiffened seat repair assemblies subjected to eccentric shear loading and fastened with nuts and washers and by directly welding the steel anchor elements to the repair assemblies utilizing Hilti HAS threaded steel anchors of different diameters and grades installed with Hilti HIT-HY 150 MAX hybrid adhesive.
4. Perform nine tensile tests of the steel anchor elements used in the eccentric shear load tests to verify the mechanical properties used to determine the ultimate loads of stiffened seat repair assemblies as described per Item 3.
5. Perform eccentric shear testing utilizing a load cell and data acquisition instrumentation to determine the actual ultimate loads of the stiffened seat repair assemblies fastened with nuts and washers and by directly welding the steel anchor elements to the repair assemblies of twenty-four test specimens consisting of three sets of eight tests and compare the capacities to the theoretical ultimate loads previously determined.
6. Determine the temperature gradients along the steel anchor elements of stiffened seat repair assemblies fastened with nuts and washers and by directly welding the steel anchor elements to the repair assemblies at incremental depths of the anchor elements due to the required welding of the stiffened seat of twenty test specimens consisting of four sets of five tests.

1.7 Dissertation Organization

This dissertation is organized into the following six chapters:

Chapter 2 discusses the theory, mechanics, and methods behind a stiffened seat connection and anchor design load data, including the basis of selection for test specimens.

Chapter 3 evaluates and discusses the load data and temperature values of the anchor specimens subjected to confined static tension loading.

Chapter 4 evaluates and discusses the load data of the anchor specimens subjected to eccentric shear loading and compares them to theoretical predictions.

Chapter 5 evaluates and discusses the temperature test data of the eccentric shear test specimens along the steel anchor elements and concrete surrounding the anchor elements.

Chapter 6 reviews the conclusions of the previous four chapters and presents recommendations for future research.

A literature review will be included where applicable in this chapter and each of the following chapters.

CHAPTER 2

EXPERIMENTAL METHODS, MATERIALS AND ANALYITCAL PREDICTIONS

2.1 Introduction

This chapter discusses various adhesive anchor failure modes, primary factors that influence the bond strength of adhesive anchoring systems, the experimental methods and materials used as the design basis used in the determination of ultimate failure loads and design level loads of eccentric shear specimens addressed in Chapter 4, and the temperature data collection of specimens discussed in Chapter 5. Confined static tension tests are a part of this experimental program, and are explicitly discussed in Chapter 3. The presentation of this chapter is structured such that adhesive anchor failure modes and accompanied influences are described prior to the experimental program design.

The experimental design and analytical predictions of this research are based on simulating conditions that commonly occur in practice. The two failure modes addressed in this research program are steel anchor element failures and bond failures. To attain these two failure modes, effective anchor embedment was determined for each group of tests addressed in the experimental design discussion.

2.2 Adhesive Anchoring System Tensile Failure Modes

Single fastening points of adhesive anchor systems not influenced by edge conditions and neighboring fasteners subjected to tensile loads in uncracked concrete can exhibit five different types of failure modes. These five different failure modes can be divided into three governing failures; concrete failure, bond failure, and steel failure. The three governing failures are primarily dependent on the effective anchor embedment.

Figure 10 illustrates the five different types of failure modes exhibited by adhesive anchor systems subjected to tensile loads.

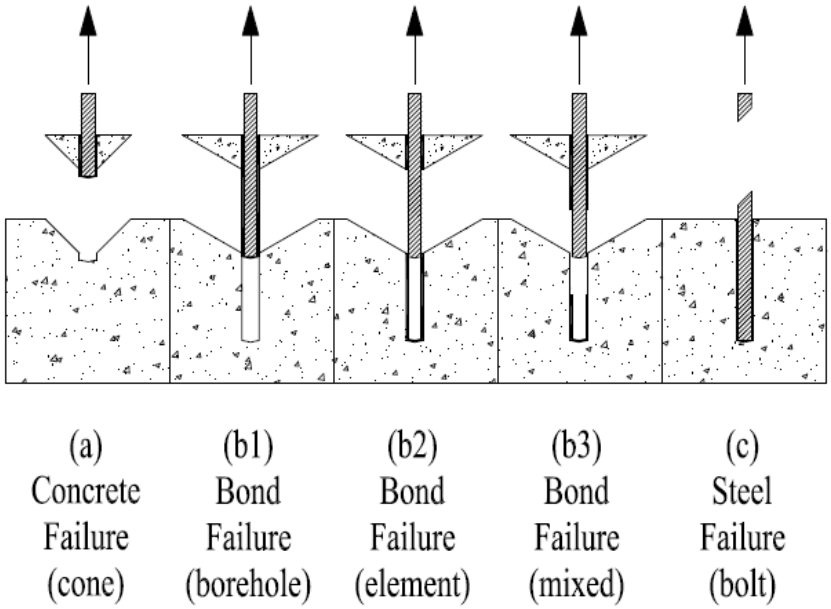

Figure 10: Common Adhesive Anchor Tensile Failure Modes

The primary mechanism for load transfer for adhesive anchor systems is a uniform bond stress model. This bond stress model is valid for adhesive anchor systems with hole diameters that do not exceed 1.5 times the anchor diameter and a ratio of embedment depth to anchor element diameter that does not exceed 20 (Cook et al. 1998). This uniform bond stress model has been shown to be both numerically and experimentally valid (National Cooperative Highway Research Program 2009). A simplified equation of the uniform bond stress model is given in Equation (1) and is illustrated in Figure 11.

$$N = \tau\pi d h_{ef} \quad (1)$$

where:

N = bond pullout strength in tension of a single anchor in uncracked concrete, lb. (N)

τ = controlling uniform bond stress between the steel anchor element and adhesive or adhesive and concrete borehole, psi (Pa)

d = diameter of the steel anchor element, inches (m)

h_{ef} = effective embedment depth of the steel anchor element, inches (m)

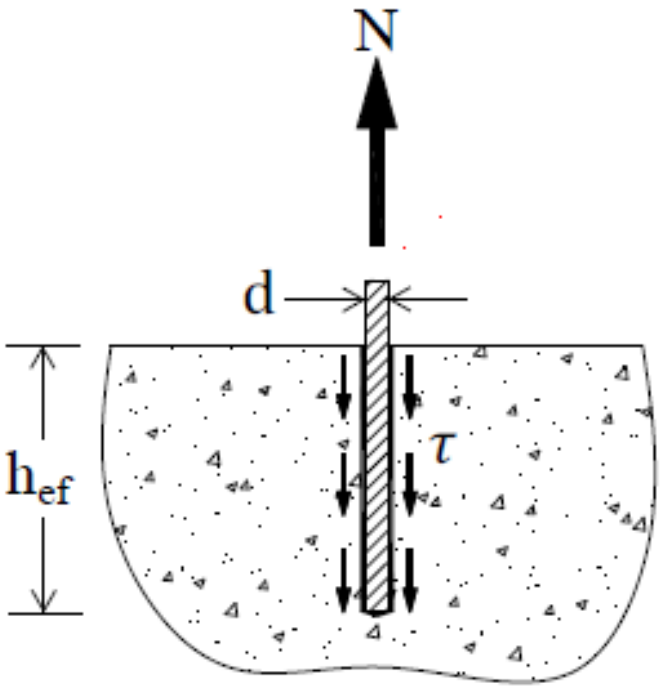

Figure 11: Uniform Bond Stress Model

2.2.1 Concrete Tensile Failure Mode

Shallow effective embedment depth typically results in a concrete cone being pulled away from the top surface of the concrete. This is due to the bond stress of the adhesive being greater than the capacity of the concrete. This type of failure is considered a concrete failure as seen per Figure 10 (a). As the effective embedment depth of the anchor is increased, the bond strength develops to a capacity less than the concrete strength. At relatively deeper effective anchor embedment depths, a bond failure will occur if the bond strength is less than the steel strength of the anchor element. If the concrete surface is unconfined, a shallow concrete cone is typically observed at the surface in combination with the predominant bond failure.

2.2.2 Bond Tensile Failure Modes

Bond failures can occur between the adhesive and the concrete borehole, between the adhesive and the steel anchor element, or a mixed combination of these two as shown in Figure 10 (b1), (b2), and (b3), respectively. The type of bond failure is dependent upon the bond stress attained between the three materials. The controlling uniform bond stress between the steel anchor element and adhesive, and the adhesive and the concrete borehole is shown in Figure 12, where “BE” designates the bond stress between the steel anchor element and the adhesive, and “BB” designates the bond stress between the adhesive and the concrete borehole.

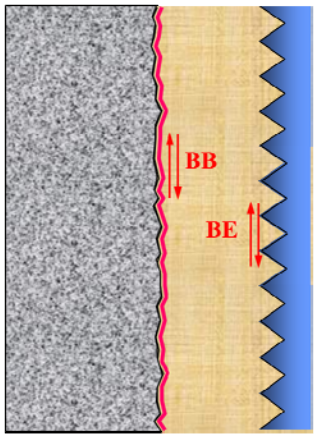

Figure 12: Bond Stresses along the Concrete Borehole and Steel Anchor Element

2.2.3 Steel Tensile Failure Mode

Relatively deep effective anchor embedment typically results in a failure of the steel anchor element, as sufficient bond strength has developed to exceed the steel's tensile capacity. The development length of the anchor is dependent upon the steel anchor element material and the properties of the adhesive.

2.2.4 Factors Influencing Bond Strength

There are four commonly accepted categories that can influence bond capacity of adhesive anchor systems (Cook et al. 2009). Each category contains several variables that affect the performance of adhesive anchors and are presented in detail. The four categories are:

1. In-service Factors
2. Factors Influencing the Adhesive
3. Installation Factors
4. Concrete Factors

It is important to reflect that these factors are commonly considered independently of one another in practice and that combinations of these factors experienced by the adhesive anchor system can have augmented effects. Minimization of these factors influencing the bond strength of the adhesive anchoring system should be paramount in order to ensure proper behavior of the system.

In-Service Factors

In-service factors include affects due to elevated temperatures, reduced temperatures, moisture in service, and freeze-thaw. Elevated temperature factors address temperatures at installation, temperature variations during the life of the adhesive anchor system, and the effects of sustained elevated temperatures. Adhesives exposed to elevated temperatures can become more susceptible to creep and experience significant reductions in bond strength (Messler 2004).

Reduced temperature factors address installation temperature and brittleness associated with the reduced temperature. Reduced temperature factors are not as significant as elevated temperature factors, but can stimulate brittleness in the adhesive (Cognard 2005). Reduced temperatures can increase the adhesive viscosity and reduce cure times during installation (ACI Committee 355 2010).

Moisture in service addresses the moisture conditions of the base material and its effect on the adhesive anchor system during the service life of the anchor. These conditions can include dry, damp, or immersed conditions. The presence of absorbed moisture after the adhesive has cured has produced test results akin to creep behavior in adhesive anchor systems subjected to elevated temperatures (Chin et al. 2009). Moisture can degrade an adhesive through three mechanisms: softening of the adhesive through

absorption, destruction of adhesion by penetration between the adhesive and substrate, and detrimental movement by swelling due to absorption by porous substrates (Cognard 2005).

Freeze-thaw factors address the degree and frequency of freeze-thaw cycles experienced by the adhesive anchor system. The natural expansion and contraction of adhesive anchor system materials due to temperature variance can alter the structural performance of the system by the disruption of equilibrium (Cook et al. 2009).

Factors Influencing the Adhesive

Adhesive factors that influence the bond strength can include the type of adhesive, mixing effort, curing time prior to loading, annular gap, fiber content and chemical resistance. The chemical compositions of different adhesives vary, even among same chemical types. The type of adhesive affects the bond strength exhibited by the adhesive anchor system. It has generally been observed that epoxy-based adhesives have higher bond strengths than ester-based adhesives (Cook and Konz 2001).

The bond strength attained by the adhesive is dependent upon proper chemical composition and mixing of the chemicals. The mixing effort is a measure of how well the adhesive components are mixed prior to injection into the borehole, and is a significant factor of importance. Some adhesive anchor systems ensure proper mixing through mechanical means built into the design of the system, while others are purely reliant upon the installer to properly proportion and mix the adhesive components. These types of adhesive anchor systems are discussed in Section 1.3 of this work. The mixed adhesive must be of a consistency such that all voids between the steel anchor element and the concrete borehole are filled, as voids reduce the effective area used to develop bond stress.

Curing time of the adhesive prior to loading can significantly affect the bond strength. Cook and Konz (2001) tested adhesives with 24 hour and 7 day cure times, observing that the bond strength for the 24 hour cure time was 81% of the bond strength for the 7 day cure time.

Annular gap is the space between the steel anchor element and the sides of the concrete borehole. According to Colak (2007), reduced annular gaps can lower the potential for creep. However, work done by Krishnamurthy (1996) suggests the annular gap does not significantly affect the bond capacity of adhesive anchor systems. Current data regarding the influence of the annular gap is inconclusive.

The fiber content of an adhesive pertains to the type and proportion of the fillers in the adhesive. Colak (2001) states that creep resistance can be increased by increasing the volume of fibers in an adhesive.

Chemical resistance of an adhesive refers to its resistance against alkalis, sulfurs, and other deleterious compounds exposed to the adhesive anchor system. Similar to the moisture in service mechanisms previously described, these compounds can infiltrate into the adhesive and degrade the adhesive bond strength (Cognard 2005).

Installation Factors

Typical installation factors include concrete borehole orientation, drilling, and cleaning and moisture conditions of the base material during installation. Adhesive anchoring systems should be installed per the manufacturer's printed installation instructions in order to minimize reductions in bond strength during installation. Concrete borehole orientation can be positioned downward, horizontal, or vertical. Vertical and vertically inclined concrete boreholes tend to prove difficult in installation, as gravity can

pull the adhesive from out of the borehole causing voids between the borehole and steel anchor element and reduce the adhesive quantity. These voids can reduce bond strength due to the reduction in effective area/volume of adhesive.

Concrete borehole drilling consists of two common methods. One method uses a diamond-core drill bit while the other uses a carbide-tipped drill bit in conjunction with a rotary hammer drill. Concrete boreholes drilled with a diamond-core bit produce a smooth-surface borehole. Concrete boreholes drilled using a rotary hammer drill and carbide-tipped bit produce a rough-surface borehole. Adhesive bond strengths have been determined to be higher with increased surface roughness along the concrete borehole (Cook and Jain 2005).

The cleanliness of the concrete borehole can considerably affect bond capacity. Cook and Konz (2001) concluded from their testing program that the average bond stress was reduced by 29% for adhesive anchors installed in uncleaned concrete boreholes. The fine concrete dust created from the drilling of the concrete borehole can inhibit the bond between the adhesive and the concrete.

Moisture during installation addresses the moisture conditions of the base material during the installation of the anchor, including the cure time. Similar to moisture in service, base material moisture conditions during installation can vary between dry, damp, water filled, or submerged. Base material moisture during installation can reduce the bond strength of the adhesive by two mechanisms. One mechanism is the moisture in the concrete borehole restricts the adhesive from entering pores along the borehole. The second mechanism is a chemical mechanism in which the moisture alters the chemical reaction between the resin and hardener components of the adhesive. The manufacturer's

printed installation instructions provide moisture limitations for their specific adhesive anchor systems. Anchor systems installed in conditions that exceed the recommended moisture limitations can experience reductions in bond strength. Cook and Konz (2001) have performed extensive testing considering moisture in installation effects on the bond strength of adhesive anchors.

Concrete Factors

Factors that influence the bond strength of adhesive anchors relating to concrete include the concrete mix design, type of coarse aggregate, and the condition of concrete being cracked or uncracked. The concrete mix design can include factors such as the type of cement used, the type of fine aggregate used, as well as admixtures such as air entrainment, plasticizers, and pozzolans. These factors are not as influential in affecting the bond strength as the coarse aggregate used in the concrete mix.

The type of coarse aggregate and its mineralogy used in the concrete mix can significantly reduce the bond strength capacity of the adhesive. Cook and Jain (2005) observed adhesive anchor systems installed in concrete mixes containing harder coarse aggregates resulted in higher bond strength due to the harder coarse aggregates producing a rougher surface along the concrete borehole.

A cracked concrete condition considers the effect of cracks around, near, and/or through the annular gap of the adhesive anchor. These cracks can significantly reduce the bond strength of the adhesive. It has been observed through testing that the adhesive anchors and/or the concrete boreholes can attract or induce cracking in the concrete at the borehole location (Eligehausen and Balogh 1995). Extensive research by Eligehausen and Balogh (1995), Fuchs et al. (1995), and Meszaros (1999) have concluded that bond

strength in cracked concrete can vary by 33% to 70% compared to bond strengths in uncracked concrete.

2.3 Adhesive Anchoring System Shear Failure Modes

Shear failures associated with adhesive anchor systems typically exhibit three controlled failure modes; (a) concrete breakout, (b) concrete pryout, and (c) steel failure. The controlled failure modes are dependent upon the relation of the anchor to free edges and the configuration of the applied shear load. Figure 13 illustrates the three controlled failure modes exhibited by adhesive anchor systems subjected to shear loads.

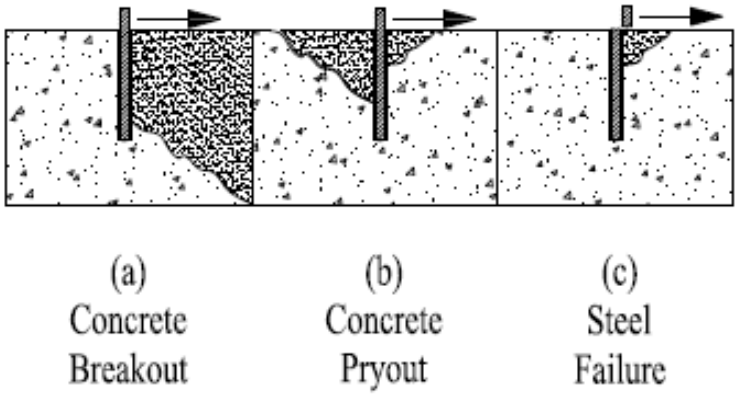

Figure 13: Common Adhesive Anchor Shear Failure Modes

2.3.1 Concrete Breakout

For adhesive anchors loaded in shear directed toward a free edge, a concrete breakout failure typically occurs as shown in Figure 13 (a). Concrete breakout shear capacities are determined from the CCD Method assuming a breakout cone angle of 35 degrees, and considers fracture mechanics theory (ACI Committee 318 2011). In cases

where the shear is directed away from the free edge, the concrete breakout strength in shear need not be considered.

2.3.2 Concrete Pryout

A concrete pryout failure mode, as shown in Figure 13 (b), may govern when a steel anchor element is both short and relatively stiff. Concrete pryout failure modes typically occur with steel anchor elements having shallow effective embedment depths and shear loads applied at relatively large distance above the concrete surface. The shear load acting above the concrete surface in conjunction with a stiff steel anchor element cause the anchor to "pryout" of the concrete.

2.3.3 Steel Shear Failure Mode

A steel failure mode exhibited by an adhesive anchor system is controlled by the shear strength of the steel anchor element, as shown in Figure 13 (c). This type of failure mode occurs when free edges, effective embedment depth, and anchor stiffness do not control the shear capacity. The nominal shear strength of the steel anchor element is based on the tensile strength of the steel anchor element and considers the effective cross-sectional area of threaded elements and is expressed in the simplified form of Equation (2).

$$V = 0.6A_e f_u \tag{2}$$

where:

V = ultimate shear strength of a single anchor in uncracked concrete, lb. (N)

A_e = effective cross-sectional area of an anchor in shear, in^2 (m^2)

f_u = specified ultimate tensile strength of anchor steel, psi (Pa)

Section D.6.1.2 of ACI 318-11 Appendix D limits the design tensile strength of the anchor steel to the lesser of 1.9 times the specified yield strength or 125,000 psi (860

MPa) (ACI Committee 318 2011). The limit of the lesser value of 1.9 times the specified yield strength or 125,000 psi (860 MPa) is to ensure that under service conditions, the steel anchor stress does not exceed the specified yield strength and is based on the conversion of LRFD provisions (ACI Committee 318 2011).

2.4 Steel Component Failure Modes

Steel component failure modes are often desired in higher seismic areas to protect against nonductile failures. Adhesive anchor systems requiring ductile failure modes typically use steel anchor elements and/or their attachments to attain this behavior as they provide the best locations for energy dissipation in the nonlinear range of response (ACI Committee 318 2011). If properly designed, ductile steel anchor elements are capable of providing sufficient elongation such that desired system displacements are achieved.

Section D.1 of ACI 318-11 defines a ductile steel element as "an element with a tensile test elongation of at least 14 percent and reduction in area of at least 30 percent" (ACI Committee 318 2011). The main design intent of using the steel anchor elements as ductile steel elements is to provide a less brittle failure mechanism than that exhibited by concrete and bond failures.

2.5 Eccentric Shear Behavior Study

The experimental basis of testing eccentric shear specimens is to calculate the predicted capacity of the stiffened seats in uncracked concrete, controlled by the steel anchor element shear and tension interaction capacity, and compare these values to the welded eccentric shear specimens to determine if capacity reductions are present due to the influence of welding on and/or near the steel anchor elements.

Edge distance and spacing factors were not considered in the testing program presented in this work in order to minimize bond strength influences. To further minimize bond strength influences and circumscribe the welding influence, additional parameters discussed per Section 2.2.4 were not considered. The hybrid adhesive anchor system used for both the temperature gradient tests and eccentric shear tests were installed per the manufacturer's printed installation instructions. The anchoring system was installed in dry hole conditions in a downward direction. The adhesive gel and cure times were attained prior the installation of the base plates and stiffened seats.

The test slabs used in the testing measured 12 inches (304.8 mm) in thickness consisting of unreinforced normal weight concrete and designated as high-strength concrete per Section 5.2.5 of ICC-ES AC308. The test slabs measured approximately 10 feet x 10 feet (3.05 m x 3.05 m), and used aggregates meeting ASTM C 33 requirements. All test surfaces replicated a smooth trowel finish. Concrete test cylinders were prepared, cured, and stored in accordance with ASTM C 31. The concrete compressive strengths at the time of testing were determined and are provided with the eccentric shear test results presented in Chapter 4.

The failure modes of the eccentric shear tests were designed to be controlled by the shear capacity of steel anchor element. It is common practice that when designing similar repairs to the eccentric shear test specimens tested, the overall design is controlled by the steel capacity of the anchors to avoid brittle failures. An investigation of welding influences on bond strength for tensile load applications is presented in Chapter 3 because steel failures will not fully represent the loss of bond strength for similar welded applications applied by eccentric shear loading.

The other steel components included in the eccentric shear test specimen were designed such that all limit state capacities are greater than the steel capacity of the anchor to ensure the steel failure of the anchors. The controlling limit states of the other steel components of the test specimens are shear and bending of the base plate, shear and bending of the stiffened seat, weld failure between the stiffened seat and the base plate, and weld failure between the steel anchor elements and the base plate.

Two steel anchor element diameters were considered in the experimental program of this research, 0.5 inch (12.7 mm) and 0.625 inch (15.9 mm) diameters. Two material types were also considered due to chemical composition compatibility with welding, ASTM F 568M Class 5.8 and ASTM A 193 B7. The ASTM F 568M Class 5.8 anchors will be used when fillet welding the steel anchor elements to the base plate due to lower carbon content than the ASTM A 193 B7 material. The ASTM A 193 B7 anchors will use standard compatible fasteners (nuts and washers) provided with the adhesive anchor system to attach the steel anchor elements to the base plate of the test specimen. Though the 0.625 inch (59.9 mm) diameter ASTM A 193 B7 steel anchor elements were included in the temperature gradient tests, they will not be included in the eccentric shear tests due to the material capacity exceeding the hydraulic pump capacity available for this testing.

Ancillary testing was performed to confirm the tensile and yield stresses of each diameter anchor and corresponding material type used in the eccentric shear tests. The tensile stress values determined from the ancillary testing were used in the analytical predictions given per Section 2.5.1. Details of the ancillary testing determining the tensile strength of the material types is given in Section 2.6.

A total of twenty-four eccentric shear load tests were performed. Eight tests of each test group were selected thus, exceeding the number of test samples required for reliability testing requirement addressed in ICC-ES AC308 and ACI 355.4-10 and to aid in providing a suitable database of tested load values. Table 1 outlines the eccentric shear test program. The eccentric shear load test results and observations are presented in Chapter 4.

Table 1: Test Matrix for Number of Eccentric Shear Specimens

Fastening Condition of Anchors Applied to Eccentric Shear Specimens →				Nut and Washer	Fillet Weld
Steel Anchor Element Diameter, in. (mm)	Anchor Embedment, in. (mm)	Steel Anchor Element Material	Test Group	Number of Tests	Number of Tests
0.5 (12.7)	6.0 (152)	ASTM F 568M Class 5.8	A	0	8
		ASTM A 193 Grade B7	B	8	0
0.625 (15.9)	7.5 (191)	ASTM F 568M Class 5.8	C	0	8

2.5.1 Analytical Predictions of Eccentric Shear Specimens

This section describes the mechanics used to develop the predicted load capacities of the eccentric shear test specimens. The predicted load capacities of the test specimens are based upon the assumption that the welding procedure does not influence the capacity of the system. The predicted values will be compared to the actual load test results to determine if welding procedures reduced the capacity of the test specimens.

The equations of the predicted load capacities will be derived and presented in this section as well as the predicted load values. Step-by-step quantitative calculations for each anchor group will be excluded. A sample step-by-step quantitative calculation of a predicted load value is presented in the Appendix A.

The general assumptions used in predicting the eccentric shear load capacities are:

- Shear distribution to each anchor is equal;
- Tension in the top two anchors is distributed equally;
- Shear and tension interaction at the top two anchors control the steel capacity of the specimen;
- Whitney stress block approximation is applicable;
- Compression block is distributed across the width of the stiffened seat.

An average concrete compressive strength value of 7,805 psi (53.8 MPa), as given per Chapter 4, will be used in the predicted failure load values. Tensile stresses presented in Section 2.6 will also be considered in the predicted values.

Figure 14 illustrates the Free Body Diagram (FBD) acting upon the eccentric shear test specimen, and forms the basis of the derivation of the steel and tension interaction capacity for a single anchor subjected to eccentric shear loading.

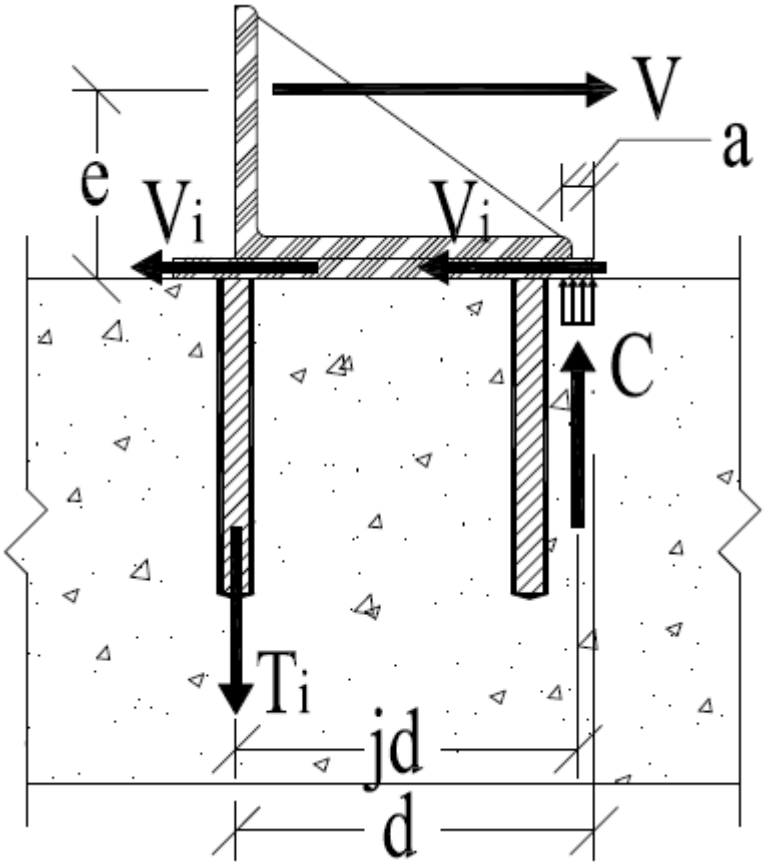

Figure 14: Free Body Diagram of Eccentrically Loaded Repair Plate

Considering the tension component of the eccentric shear load, the moment induced on the repair plate due to the eccentric shear loading can be written as Equation (3):

$$\mathrm{M} = \mathrm{Ve} \tag{3}$$

Using static equilibrium, the tension resultant can be written as Equation (4):

$$\mathrm{T_i} = \frac{T}{2} = \mathrm{C} = \frac{\mathrm{Ve}}{2\mathrm{jd}} \tag{4}$$

Considering equal shear distribution based on anchor stiffness, the shear component of each anchor can be determined by Equation (5):

$$V_i = \frac{V}{4} \tag{5}$$

Limiting a single steel anchor element to its shear and tension interaction capacity, the interaction equation can be expressed in terms of the applied eccentric shear load in Equation (6):

$$\frac{Ve}{2A_e f_u jd} + \frac{V}{4(0.6)A_e f_u} = 1.0 \tag{6}$$

where:

V = applied shear load of a single steel anchor element, lb. (N)

A_e = effective cross-sectional area of an anchor in shear, in^2 (m^2)

f_u = specified tensile strength of anchor steel as determined per Section 2.6, psi (Pa)

e = eccentricity of the applied shear load = 4.5 inches (114.3 mm)

jd = effective depth from the centroid of tension anchorage to the bottom of the base plate, inches (m)

Using the Whitney stress block approximation, the effective depth can be determined using Equation (7):

$$jd \approx d - \frac{A_e f_u}{2(0.85)f'_c b} \tag{7}$$

where:

d = depth of the centroid of the tension anchorage to the bottom of the base plate = 8.5 inches (215.9 mm)

f'_c = average concrete compressive strength at the time of testing = 7,805 psi (53.8 MPa)

b = width of the compression block = 7 inches (177.8 mm)

Using the approximated effective depth represented by Equation (7), the shear and tension interaction can be derived through the Equations (8) and (9) to solve for the applied shear load of a single steel anchor element, as given per Equation (10):

$$\frac{Ve}{2A_e f_u \left[d - \frac{A_e f_u}{2(0.85)f'_c b}\right]} + \frac{V}{4(0.6)A_e f_u} = 1.0 \tag{8}$$

$$\frac{Ve}{2A_e f_u d - \frac{A_e^2 f_u^2}{(0.85)f'_c b}} + \frac{V}{2.4A_e f_u} = 1.0 \tag{9}$$

$$V_i = \left[\frac{1}{\frac{e}{2A_e f_u d - \frac{A_e^2 f_u^2}{(0.85)f'_c b}} + \frac{1}{2.4A_e f_u}}\right] \tag{10}$$

Considering the shear and tension interaction of the top two anchors controls the capacity of the eccentric shear test specimen, the predicted failure load for each test group can be determined using Equation (11):

$$V = \left[\frac{2}{\frac{e}{2A_e f_u d - \frac{A_e^2 f_u^2}{(0.85)f'_c b}} + \frac{1}{2.4A_e f_u}}\right] \tag{11}$$

Table 2 presents the predicted eccentric shear values using Equation (11) for the testing matrix outlined per Table 1.

Table 2: Predicted Eccentric Shear Failure Loads

Steel Anchor Element Diameter, in. (mm)	Anchor Embedment, in. (mm)	Steel Anchor Element Material	Test Group	Predicted Failure Load, lb. (kN)
0.5 (12.7)	6.0 (152)	ASTM F 568M Class 5.8	A	45,267 (201.4)
		ASTM A 193 Grade B7	B	65,754 (292.5)
0.625 (15.9)	7.5 (191)	ASTM F 568M Class 5.8	C	69,141 (307.6)

In addition to the predicted eccentric shear failure loads, factored nominal design strengths will also be considered to compare the tested failure loads. In considering the design strengths of the eccentric shear test specimens, ACI 318-11 Section D.4.3 defines the strength reduction factors for brittle steel elements as being 0.65 for tension and 0.6 for shear. ACI 318-11 Sections D.5.1.2 and D.6.1.2 limit the tensile strength of the anchors to the smaller of 125,000 psi (862.1 MPa) or 1.9 times the yield strength of the anchor. Anchor materials tested per Section 2.4 that exceed the criteria of Sections D.5.1.2 and D.6.1.2 of ACI 318-11 will be limited to these specified design provisions. Incorporating

the design provisions into the previously derived failure load prediction equation, the following factored nominal design load derivation is expressed as Equation (12):

$$\varphi V_n = \left[\frac{2}{\frac{e}{0.65\left[2A_e f_u d - \frac{A_e^2 f_u^2}{(0.85) f_c' b}\right]} + \frac{1}{0.6[2.4 A_e f_u]}} \right] \quad (12)$$

Table 3 presents the factored nominal design load values using Equation (12) for the testing matrix outlined in Table 2.

Table 3: Factored Nominal Design Loads of Eccentric Shear Tests

Steel Anchor Element Diameter, in. (mm)	Anchor Embedment, in. (mm)	Steel Anchor Element Material	Test Group	φV_n, lb. (kN)
0.5 (12.7)	6.0 (152)	ASTM F 568M Class 5.8	A	28,007 (124.6)
		ASTM A 193 Grade B7	B	29,608 (131.7)
0.625 (15.9)	7.5 (191)	ASTM F 568M Class 5.8	C	42,787 (190.3)

2.5.2 Eccentric Shear Specimen Configurations

The base plate components (sometimes referred to in industry as receiver plates) were fabricated from 0.5 inch (12.7 mm) thick ASTM A 36 flat bar stock and measured 10

inches x 12 inches (250 mm x 300 mm). Standard oversized diameter holes were punched into the base plates corresponding to the diameters of the two steel anchor elements used. Base plates with 0.625 inch (15.9 mm) and 0.75 inch (19.1 mm) diameter holes were used with 0.5 inch (12.7 mm) and 0.625 inch (15.9 mm) holes, respectively.

Stiffened seat components were fabricated from ASTM A 36 L6x6x1/2 (150 mm x 150mm x 12mm) angle material and cut to 7 inches (177.8 mm) in length. Three 0.5 inch (12.7 mm) thick gusset plates were added to the angle to ensure the shear and bending capacity of the stiffened seat did not control the failure mode of the test specimens. The stiffened seat were installed horizontally centered on the base plate and the top of the stiffened seat was aligned vertically with the centroid of the top two tension anchors as shown per Figure 15 (a).

The stiffened seats and steel anchor elements were welded to the base plate as illustrated per Figure 15 (b). Welding of the eccentric shear test specimens was performed by an American Welding Society (AWS) certified welder using a Miller Bobcat 225 amp DC arc welder. MG-7018 0.125 inch (3.2 mm) and 0.15625 inch (4.0 mm) diameter welding rods were used to weld the stiffened seat to the base plate and the steel anchor elements to the base plate for test groups A and C indicated per Table 1. All welds were designed at higher capacities than the steel anchor elements.

The eccentric shear test specimens were tested in two concrete slabs. Sixteen test specimens were tested in the first slab and eight were tested in the second slab. Figure 16 shows the general specimen layout used during testing. Figure 17 shows the layout of specimens prior to installation.

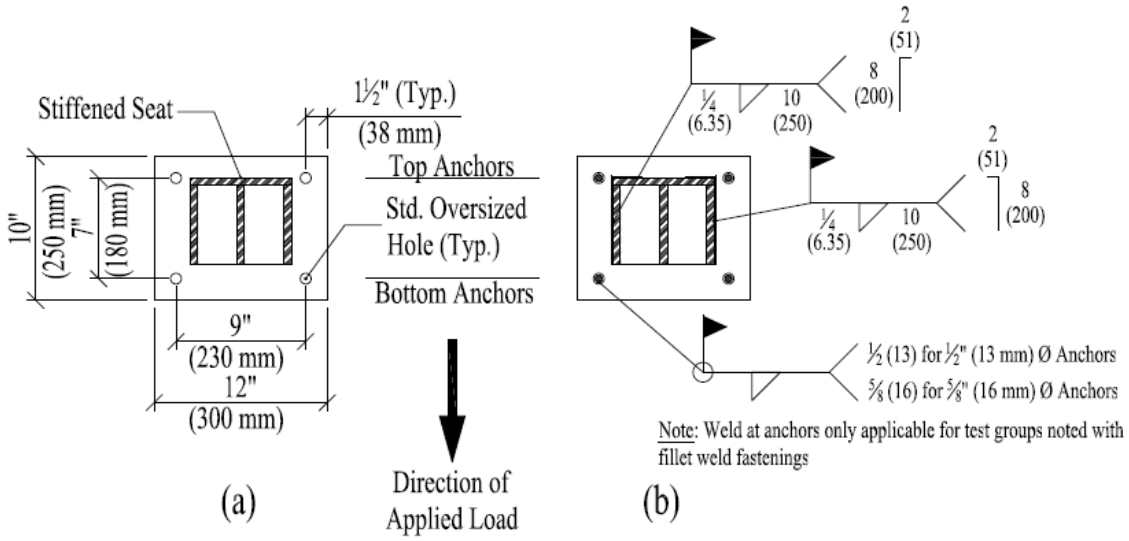

Figure 15: Configuration of Eccentric Shear Test Specimen Components

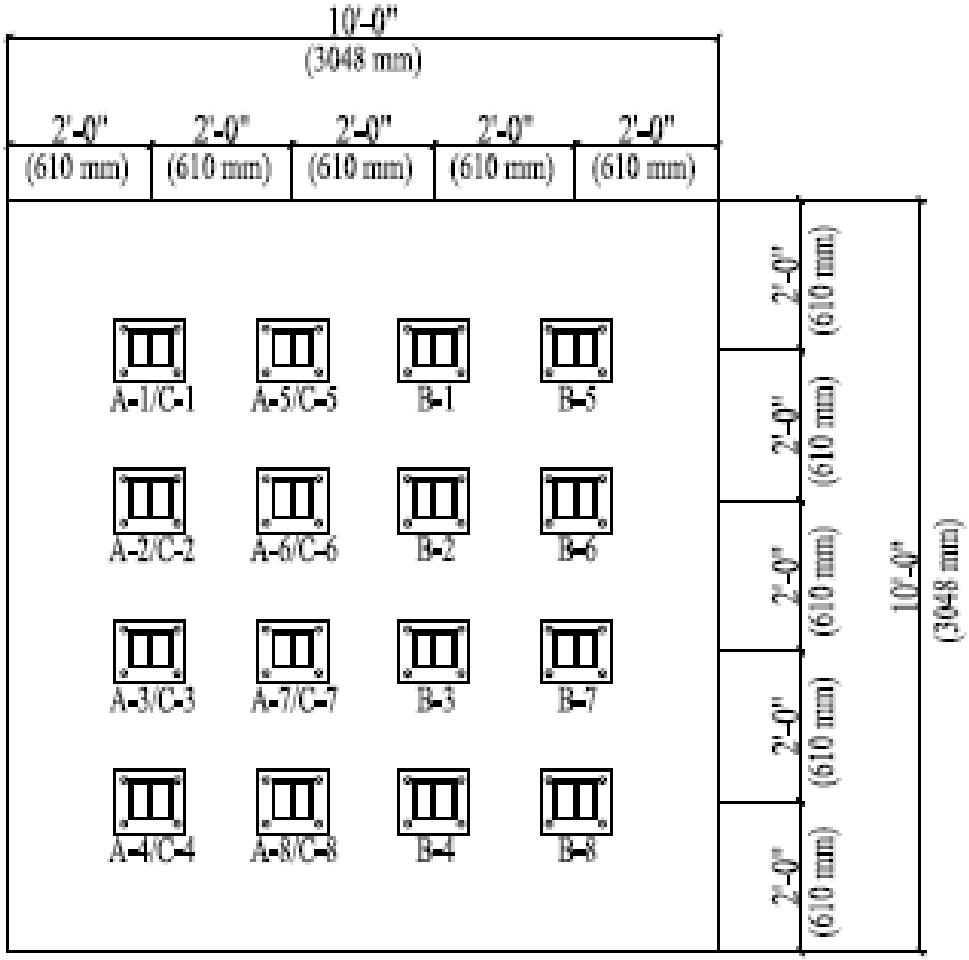

Figure 16: Eccentric Shear Test Specimen Layout

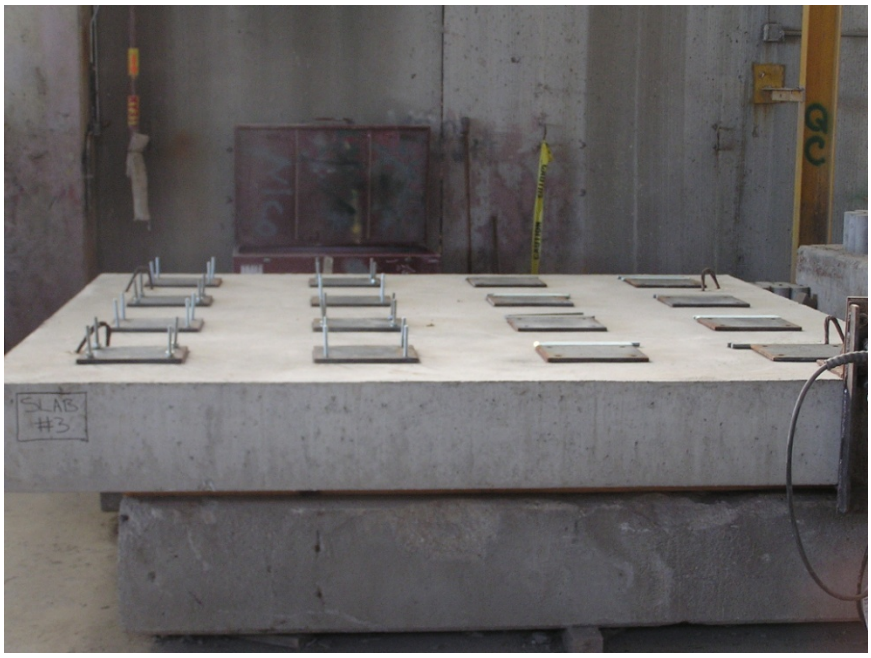

Figure 17: Layout of Eccentric Shear Test Specimens Prior to Stiffened Seat Installation

Loads were applied to the eccentric shear test specimens through a system of high-strength steel rods loaded by an Enerpac P-842 lightweight hand pump and RRH-3010 30 ton (267 kN) double-acting hollow plunger cylinder. The high-strength rods were threaded through two holes fabricated in stiffened seat components. The two high-strength rods were fastened to the stiffened seats using nuts and plate washers.

A large plate washer element was used to transition the two high-strength rods to a larger diameter single high-strength rod which attached through the hollow plunger cylinder. Nuts and plate washers were used at the back side of the hollow plunger cylinder to attach the single high-strength rod and load cell. Figure 18 shows the configuration and attachment of the high-strength rods to the test specimens. The height of the high-strength rods and the hollow plunger cylinder with relation to the top surface

of the concrete slab was set to establish the 4.5 inch (114.3 mm) eccentricity applied to the test specimens.

Figure 18: Configuration of High-strength Rods and Hollow Plunger Cylinder

The cylinder was held in place by a steel-jawed frame that attached to the concrete slabs. To minimize movement in the frame, a neoprene bearing pad was placed between the vertical edge of the slab and frame. Three concrete screw anchors were also used to fasten the bottom jaw of the frame to the underside side of the concrete slabs to further restrain rotational movement in the testing set-up.

Load data was acquired continuously using a data acquisition instrument (SCXI-1000) manufactured by Vishay Measurements. This instrument is capable of both acquisition and signal conditioning. The acquired and conditioned data was transferred to a laptop computer using a PCIMCI card to be read by Labview 7.1, software supplied by Vishay Measurements. A simulator was specifically written for this project to record the

loads using Labview 7.1 such that the data could be written directly to a file for further analysis. Figure 19 shows the picture of the front panel of the software written for this project. Figure 20 shows an overall view of the testing configuration used in the testing of the eccentric shear specimens.

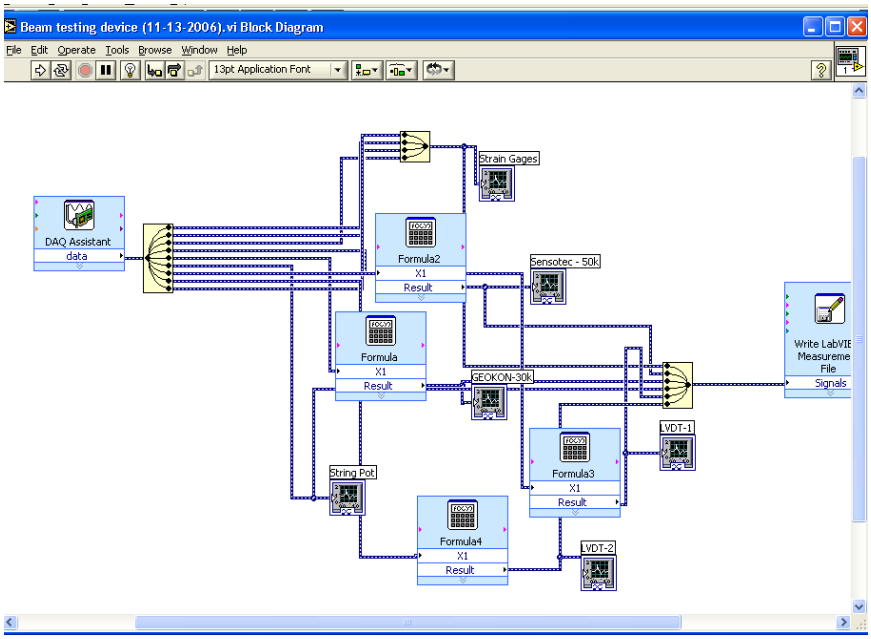

Figure 19: Front Panel of the Simulator Using Labview 7.1

Figure 20: Overall Testing Configuration of Eccentric Shear Tests

2.6 Ancillary Tensile Tests of Steel Anchor Elements

Tensile tests were performed on the HAS steel anchor elements used in the eccentric shear tests to establish the actual material strengths. Testing was performed at the University of Missouri-Kansas City. Figure 21 shows the typical testing configuration for the tensile tests. Three samples of each material type and diameter were tested, as grouped per Table 1. Results of the tensile tests are presented in Tables 4 through 6. A 0.2% offset method was used to determine the yield strength of each material. Figure 22 depicts the typical failure observed with the tensile test specimens. Stress versus elongation plots for these tests is included in Appendix B.

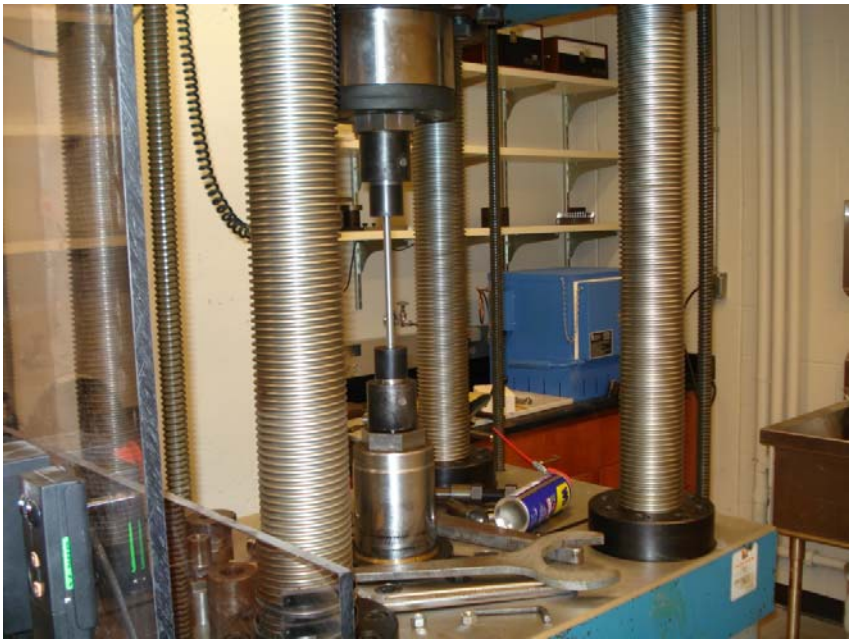

Figure 21: Typical Test Configuration of Tensile Tests

Table 4: Test Group A Threaded Rod Tensile Test Results

	Tensile Strength, ksi (MPa)	Yield Strength, ksi (MPa)	Tensile/Yield Ratio
Test 1	115.7 (798.2)	87.7 (604.5)	1.32
Test 2	116.9 (805.9)	89.7 (618.5)	1.30
Test 3	115.4 (795.7)	87.1 (600.5)	1.33
Average	116.0 (799.9)	88.1 (607.8)	1.32
COV	0.66%	1.56%	1.69%

Table 5: Test Group B Threaded Rod Tensile Test Results

	Tensile Strength, ksi (MPa)	Yield Strength, ksi (MPa)	Tensile/Yield Ratio
Test 1	169.4 (1168.1)	141.7 (977.2)	1.20
Test 2	175.5 (1210.5)	140.3 (967.2)	1.25
Test 3	172.0 (1186.4)	139.7 (963.5)	1.23
Average	172.3 (1188.3)	140.6 (969.3)	1.23
COV	1.79%	0.74%	2.05%

Table 6: Test Group C Threaded Rod Tensile Test Results

	Tensile Strength, ksi (MPa)	Yield Strength, ksi (MPa)	Tensile/Yield Ratio
Test 1	112.0 (772.1)	89.5 (617.5)	1.25
Test 2	113.5 (782.6)	90.1 (621.4)	1.26
Test 3	109.2 (753.3)	86.6 (597.1)	1.26
Average	111.6 (769.4)	88.7 (612.0)	1.26
COV	1.93%	2.13%	0.46%

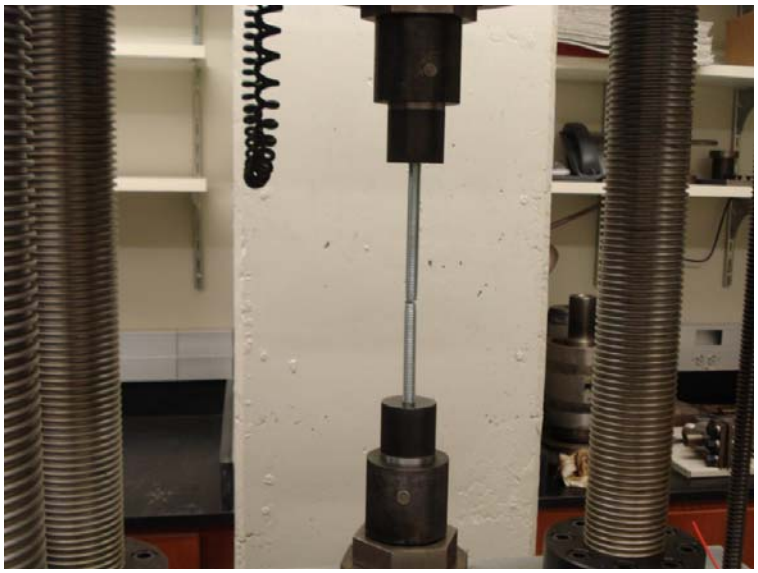

Figure 22: Typical Observed Failure of Tensile Test Specimen

2.7 Experimental Design of Temperature Gradient Test Specimens

The primary experimental design intent of the temperature gradient test specimens is to determine the maximum temperatures along the steel anchor elements of the eccentric shear test specimens. The temperature gradient specimens were separated from the eccentric shear tests on the basis that the volume of thermocouple wires protruding to the surface along the annular gap would not accurately represent the actual capacity of the eccentric shear tests. The temperature specimens are identical to the eccentric shear specimens described in Section 2.5.2 of this chapter and subjected to similar welding on and/or near the steel anchor elements in order to correlate the experienced temperature gradients to any potential detriment to bond or steel anchor element performance.

The temperature gradient test specimens were installed per the manufacturer's printed installation instructions in 12 inch (305 mm) high-strength concrete slabs similar to the slabs used for the eccentric shear test specimens. The material specifications, steel anchor element sizes, effective embedment depths, weld and stiffened seat design used in the temperature gradient test specimens are addressed in Section 2.5.2 and are based on the design predictions of Section 2.5.1.

Thermocouples were placed in relatively symmetric locations along the steel anchor elements in order to capture the temperature gradient along the anchor embedment. A total of ten thermocouples per test specimen were used. One group of five thermocouples was attached to a top tension (load side) anchor and one group of five thermocouples was attached to a bottom shear (rear) anchor as related to the eccentric shear test specimens. The five thermocouples per anchor were arranged such that temperatures at the bottom, midpoint, top intermediate point, and surface of the anchor

length were recorded as well as the top of the anchor projecting out into free air above the surface of the concrete slab. Figure 23 illustrates the steel anchor element thermocouple group locations with relation to the test specimen configuration.

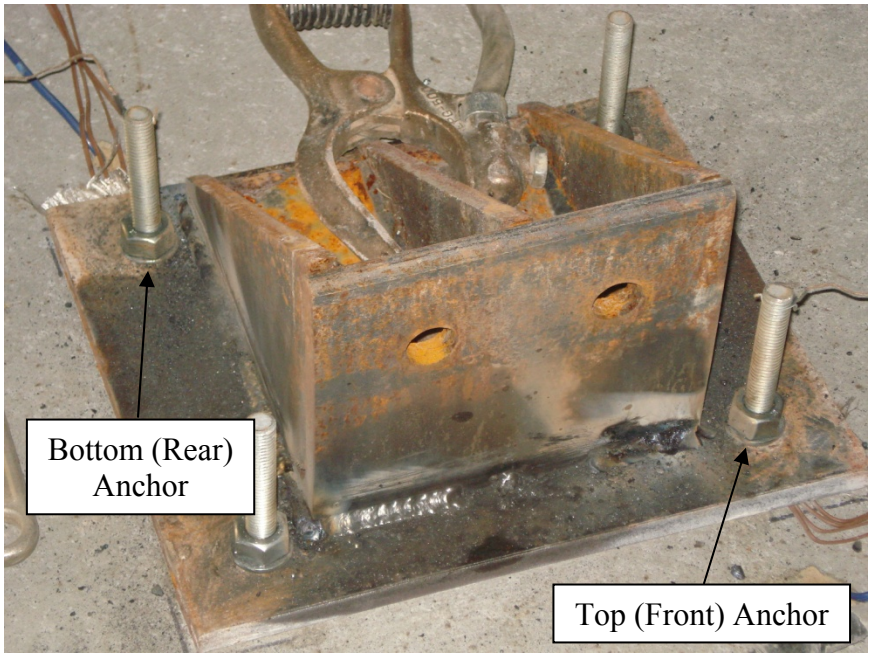

Figure 23: Temperature Gradient Test Specimen Showing Thermocouple Group Locations

Type-K thermocouples were used to record temperatures along the steel anchor elements during welding. Calibrated handheld thermocouple thermometers were used to record maximum temperatures. The ends of the thermocouple wires were protected by a thermal conductive heat-shrink membrane to protect the handheld thermometers from any current overload generated by the welder. The thermocouples were attached to the anchors by means of a thin wire to hold them in the proper location with respect to the embedment depth.

In addition to recording temperatures along the steel anchor element, additional thermocouples were installed in the concrete slab adjacent to the adhesive anchor system. These additional concrete thermocouples were located at a horizontal distance of 3 inches (76.2 mm) from the adhesive anchors and set at vertical distances corresponding to the bottom, midpoint, and top surface of the anchor embedment. The temperature readings taken in the concrete slab concurrently with the steel anchor element temperatures should confirm if the concrete acts as a heat sink for the test specimens.

While not specifically addressed in ICC-ES AC308 and ACI 355.4-10, the temperature gradient tests and eccentric shear tests can be considered reliability tests per the purpose outlined by these provisions. The purpose of reliability tests for the qualification of adhesive anchoring systems is to "establish that the anchor is capable of safe, effective behavior under normal and adverse conditions, both during installation and service" (ACI Committee 355 2010). Five tests of each test group as defined per Table 7 was selected to correspond with the number of tests required for reliability testing requirement addressed in ICC-ES AC308 and ACI 355.4-10. Test groups are organized by anchor diameters, material type, and fastening condition of the anchors to the base plate. Table 7 outlines the temperature gradient test program. The temperature gradient results and observations are presented in Chapter 5.

Four split core cylinder samples were cored after the welding procedures were completed on the test specimens. The split cores cylinders were taken from one test specimen from each test group to perform a visual observation of the adhesive material along the steel anchor element and the concrete borehole to confirm if visible charring or

discoloration of the adhesive occurred. These observations are also presented in Chapter 5.

Table 7: Test Matrix for Number of Temperature Gradient Specimens

Fastening Condition of Anchors Applied to Temperature Specimens →				Nut and Washer	Fillet Weld
Steel Anchor Element Diameter, in. (mm)	Anchor Embedment, in. (mm)	Steel Anchor Element Material	Test Group	Number of Tests	Number of Tests
0.5 (12.7)	6.0 (152)	ASTM F 568M Class 5.8	D	0	5
		ASTM A 193 Grade B7	E	5	0
0.625 (15.9)	7.5 (191)	ASTM F 568M Class 5.8	F	0	5
		ASTM A 193 Grade B7	G	5	0

2.7.1 Temperature Gradient Test Specimen Configurations

For all 0.5 inch (12.7 mm) diameter HAS steel anchor elements tested per Table 7, thermocouples were installed on the anchors per Figure 24 (a). For all 0.625 inch (15.9 mm) diameter HAS steel anchor elements tester per Table 7, thermocouples were installed

per Figure 24 (b). Thermocouples one through five were attached directly to the steel anchor elements while six through eight were installed into the concrete slab. Figure 24 shows an installed single anchor with thermocouples.

Temperature gradient test specimens were oriented and installed in the concrete slab in a similar manner to the eccentric shear test configurations and is shown per Figure 25. Test specimens were tested one group (five specimens) at a time as categorized by Table 7 and tested in the sequential order as marked per Figure 26.

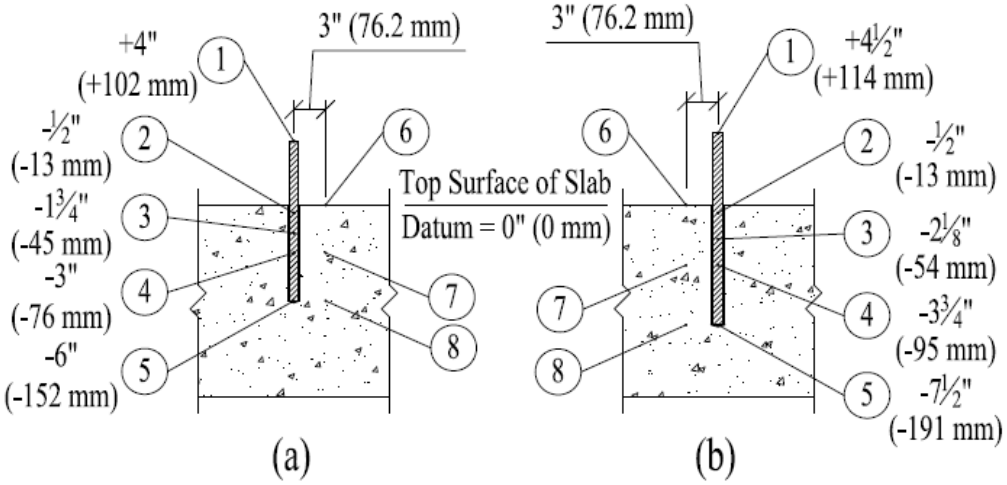

Figure 24: Thermocouple Distribution along Anchor Embedment

Figure 25: Installed Thermocouples for Single Anchor of Temperature Gradient Test

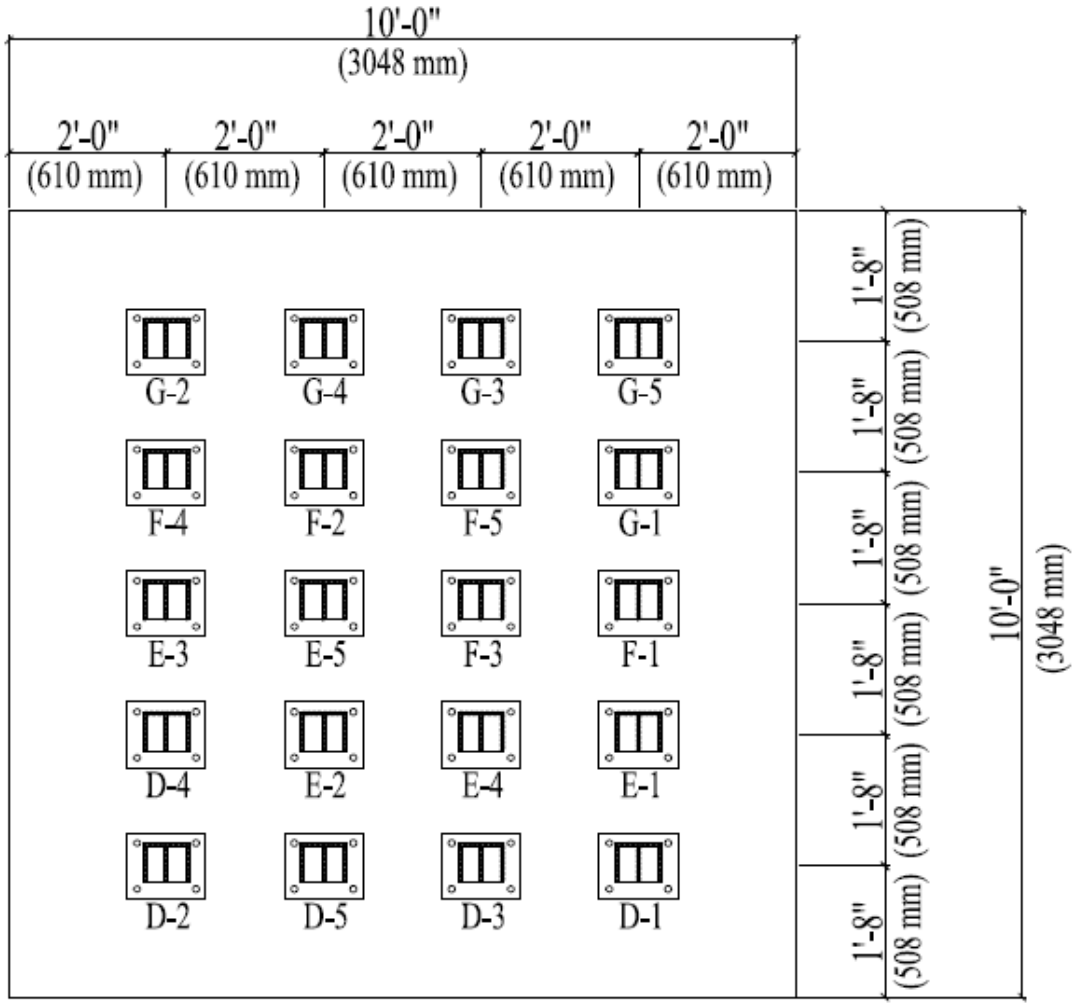

Figure 26: Temperature Gradient Test Specimen Layout

Four, calibrated four-channel Omega Engineering HH501DK handheld thermocouple thermometers were used to record the temperatures experienced by the steel anchor elements during welding. Temperatures at each thermocouple location were recorded every minute until each location started to decrease. Quick-connect terminal installed at the ends of the installed thermocouples allowed for relatively simple transitions of the thermometers after each test. Thermocouple wires were marked per Figure 24 to allow for the correct coordination between individual thermocouple wires and

the channel inputs on the thermometers. Figure 27 shows the handheld thermocouple thermometers used to record temperatures during testing.

Figure 27: Handheld Thermocouple Thermometers used to Record Weld Temperatures

Welding of the temperature gradient test specimens was performed by an American Welding Society (AWS) certified welder using a Miller Bobcat 225 amp DC arc welder. MG-7018 0.125 inch (3.2 mm) and 0.15625 inch (4.0 mm) diameter welding rods were used to weld the stiffened seat to the base plate and the steel anchor elements to the base plate for test groups D and F indicated per Table 7. A flame and heat retardant material was placed between the base plate and the thermocouple wires projecting from the annular gap to protect the wires from excessive heat induced by welding procedures of the tests. Figure 28 shows the protective material placed between the base plate and the thermocouple wires projecting out the top of the concrete slab.

Figure 28: Protective Material Placed between Base Plate and Thermocouple Wires

2.8 Discussion

Though the ASTM A 193 B7 test specimens utilize nut and washer fastenings, the adhesive anchor system is still exposed to considerable amounts of welding near the anchors due to the attachment of the stiffened seat component.

The published tensile and yield strengths of the two materials tested were considerably less than the actual values determined by the ancillary testing. Per the manufacturer's published data, the tensile strengths for both ASTM F 568M Class 5.8 and ASTM A 193 B7 materials are 72.5 ksi (500 MPa) and 125 ksi (860 MPa), respectively (Hilti 2011). Published yield strengths for both ASTM F 568M Class 5.8 and ASTM A 193 B7 materials are 58.0 ksi (400 MPa) and 105 ksi (725 MPa), respectively (Hilti 2011). A comparison of the average tested and published values are presented in Table 8.

Table 8: Comparison of Tensile Test Results to Published Values

	Published Values		Average Tested Values		Percent Difference from Published Loads	
Material	Tensile, ksi (MPa)	Yield, ksi (MPa)	Tensile, ksi (MPa)	Yield, ksi (MPa)	Tensile, ksi (MPa)	Yield, ksi (MPa)
ASTM F 568M Class 5.8	72.5 (500)	58.0 (400)	113.8 (785)	88.4 (610)	+57.0%	+52.4%
ASTM A 193 B7	125.0 (860)	105.0 (725)	172.3 (1188)	140.6 (970)	+37.8%	+33.9%

CHAPTER 3

EVALUATION OF CONFINED STATIC TENSION TESTS

3.1 Introduction

Confined static tension tests were performed to evaluate a tension induced bond failure of the anchor system. This was performed in order to determine any reduction of bond capacity due to welding influences and to provide additional verification of the temperature gradient of the anchor system when subjected to welding. The steel anchor elements were welded to tensile inserts by a certified welder using standard welding practices. The anchor systems were tension tested to failure and results were compared to non-welded reference tests for performance comparisons of the anchor system subjected to heat induced by welding.

This chapter discusses the experimental basis, instrumentation and data collection, test results and observations, comparisons and discussion of sixty individual confined static tension tests. The entire testing presented in this chapter was performed at Hilti's North America Testing Laboratory in Tulsa, Oklahoma. The testing performed at this facility used equipment and restraints designed to confine the base material failure surrounding the anchors, in compliance with ASTM E 488-96.

3.2 Basis of Experimental Design for Confined Static Tension Tests

The experimental basis of design for the confined static tension tests is to focus on bond performance of the adhesive anchor systems when subjected to welding influences. In order to ensure the bond strength is the controlling failure of the confined static tension tests, the proper anchor embedment must be determined. The steel anchor element

embedment depth influences the type of failure exhibited by the adhesive anchor system. Figure 29 shows the influence of embedment depth on the design capacity of adhesive anchor systems and the failure mode associated with each design capacity region.

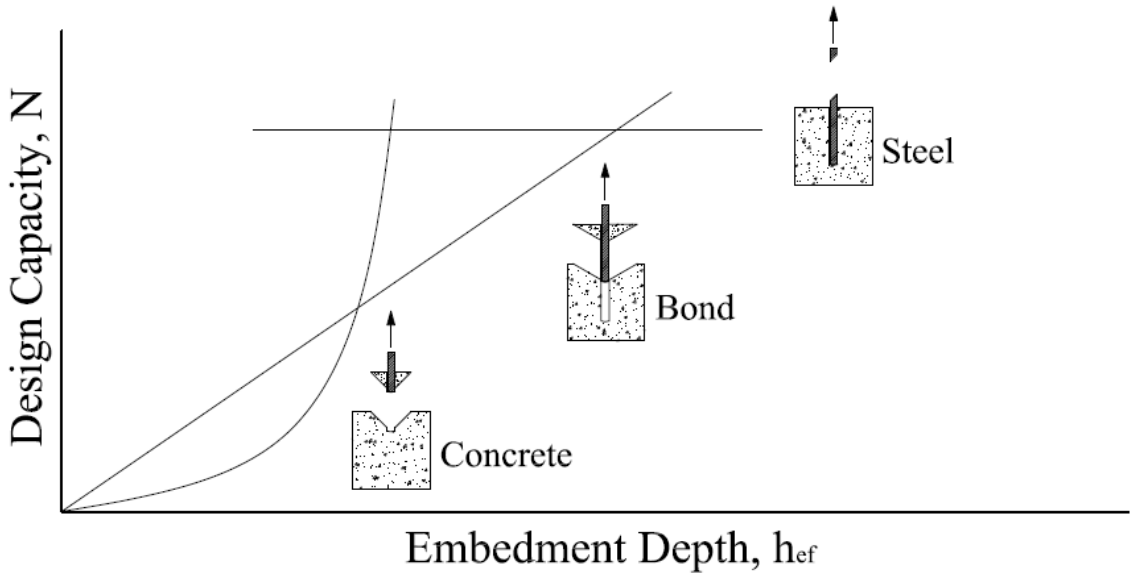

Figure 29: Embedment Depth Influence on Anchor System Design Capacity

For shallow embedment depths less than about six times the steel anchor element diameter, the nominal concrete capacity of a single anchor in tension in uncracked concrete is limited by the concrete cone breakout. Equation (D-3) of ACI 318-11 equates the nominal concrete capacity of a single anchor in tension, and is represented by Equation (13) (ACI Committee 318 2011):

$$N_{cb} = \frac{A_{Nc}}{A_{Nco}} \psi_{ec,N} \psi_{ed,N} \psi_{c,N} \psi_{cp,N} N_b \tag{13}$$

where:

N_{cb} = nominal concrete breakout strength of a single anchor in tension, lb. (N)

A_{Nc} = projected concrete failure area of a single anchor or group of anchors, in^2 (m^2)

A_{Nco} = projected concrete failure area of a single anchor if not limited by edge distance or spacing, in^2 (m^2)

$\Psi_{ec,N}$ = factor used to modify tensile strength of anchors based on eccentricity of applied loads

$\Psi_{ed,N}$ = factor used to modify tensile strength of anchors based on proximity to edges of concrete members

$\Psi_{c,N}$ = factor used to modify tensile strength of anchors based on presence of absence of cracks in concrete

$\Psi_{cp,N}$ = factor used to modify tensile strength of post-installed anchors intended for use in uncracked concrete without supplementary reinforcement to account for the splitting tensile stresses due to installation

N_b = basic concrete breakout strength in tension of a single anchor in cracked concrete, lb. (N)

The basic concrete breakout strength is defined per Equation (D-6) of ACI 318-11 and is expressed as Equation (14) (ACI Committee 318 2011):

$$N_b = k_c \lambda_a \sqrt{f'_c} h_{ef}^{1.5} \tag{14}$$

where:

k_c = coefficient of basic concrete breakout strength in tension

λ_a = modification factor reflecting the reduced mechanical properties of lightweight concrete in certain concrete anchorage applications

f'_c = specified compressive strength of concrete, psi (Pa)

h_{ef} = effective embedment depth of steel anchor element, inches (m)

For single anchors not subjected to edge distances and load eccentricity in normal weight unreinforced uncracked concrete specimens, as used in this research program, we can set the modification factors to unity, simplifying the nominal concrete capacity of a single anchor in tension by the concrete cone breakout as shown in Equation (15):

$$N_{cb} = k_c \sqrt{f'_c} h_{ef}^{1.5} \tag{15}$$

For embedment depths between about six to eight times the steel anchor element diameters, the nominal concrete strength exceeds the nominal bond strength of a single anchor in tension and shifts the failure mode of the system from a concrete failure to an adhesive bond failure. The nominal bond strength in tension of a single adhesive anchor in both cracked and uncracked concrete is represented by Equation (D-18) of ACI 318-11 and is expressed by Equation (16) (ACI Committee 318 2011):

$$N_a = \frac{A_{Na}}{A_{Nao}} \psi_{ed,Na} \psi_{cp,Na} N_{ba} \tag{16}$$

where:

N_a = nominal bond strength of a single adhesive anchor in tension, lb. (N)

A_{Na} = projected influence area of a single adhesive anchor or group of adhesive anchors, in^2 (m^2)

A_{Nao} = projected influence area of a single adhesive anchor if not limited to edge distance or spacing, in^2 (m^2)

$\Psi_{ed,Na}$ = factor used to modify tensile strength of adhesive anchors based on the proximity of edges of concrete member

$\Psi_{cp,Na}$ = factor used to modify the tensile strength of adhesive anchors intended for use in uncracked concrete without supplementary reinforcement to account for the splitting tensile stresses due to installation

N_{ba} = basic bond strength of a single adhesive anchor in tension, lb. (N)

The basic bond tension capacity of a single adhesive anchor in uncracked concrete is determined by Equation (D-22) of ACI 318-11 and is presented in Equation (17) (ACI Committee 318 2011):

$$N_{ba} = \lambda_a \tau_{uncr} \pi d_a h_{ef} \tag{17}$$

where:

λ_a = modification factor reflecting the reduced mechanical properties of lightweight concrete in certain concrete anchorage applications

τ_{uncr} = characteristic bond stress of adhesive anchor in uncracked concrete, psi (Pa)

d_a = outside diameter of steel anchor element, inches (m)

h_{ef} = effective embedment depth of steel anchor element, inches (m)

For single anchors not subjected to edge distances in normal weight unreinforced uncracked concrete specimens, as used in this research program, the modification factors are set to unity, simplifying the nominal bond strength capacity of a single anchor in tension to Equation (18):

$$N_a = \tau_{uncr} \pi d_a h_{ef} \tag{18}$$

For embedment depths greater than about eight times the steel anchor element diameter, the nominal bond strength exceeds the nominal steel strength of a single anchor in tension, and shifts the failure mode of the system from a bond failure to a steel anchor element failure. The nominal steel strength in tension of a single adhesive anchor is represented by Equation (19):

$$N_{sa} = A_{se,N} f_{uta} \tag{19}$$

where:

N_{sa} = nominal strength of a single anchor or individual anchor in a tension group of anchors in tension as governed by the steel strength, lb. (N)

$A_{se,N}$ = effective cross-sectional area of steel anchor element, in^2 (m^2)

f_{uta} = specified tensile strength of steel anchor element, psi (Pa)

Using the nominal design capacities, a minimum and maximum effective embedment depth of the steel anchor elements can be used to determine the bond failure region of the adhesive anchor systems. The minimum effective embedment depth for bond failure to occur is attained by setting the nominal concrete breakout strength equal to the nominal bond strength. Equations (20) and (21) derive the minimum effective embedment depth presented in Equation (22).

$$N_{cb} = N_a \tag{20}$$

$$k_c \sqrt{f_c'} h_{ef}^{1.5} = \tau_{uncr} \pi d_a h_{ef} \tag{21}$$

$$h_{ef} \geq \left(\frac{\tau_{uncr} \pi d_a}{k_c \sqrt{f_c'}} \right)^2 \tag{22}$$

The maximum effective embedment depth for bond failure to occur is determined by setting the nominal bond strength equal to the nominal tensile strength of the steel anchor element. Equations (23) and (24) derive the maximum effective embedment depth presented in Equation (25).

$$N_a = N_{sa} \tag{23}$$

$$\tau_{uncr}\pi d_a h_{ef} = A_{se,N} f_{uta} \tag{24}$$

$$h_{ef} \leq \frac{A_{se,N} f_{uta}}{\tau_{uncr}\pi d_a} \tag{25}$$

Using proprietary data provided by Hilti, effective embedment depths for each steel anchor element were determined based on the adhesive anchoring system to produce bond controlled failures of the static tension tests. The determined embedment depths for each anchor diameter and corresponding adhesive anchor system is shown in Table 10 of Section 3.3.

3.3 Specimen Parameters and Testing Matrix

Two types of adhesive anchoring systems were evaluated during the confined static tension testing portion of this research. The primary adhesive anchoring system tested was Hilti HIT-HY 150MAX with HAS threaded steel anchor elements, while additional testing was performed using Hilti HIT-RE 500-SD with HAS threaded steel anchor elements. The HIT-HY 150MAX is a hybrid adhesive as defined in Chapter 1, while the HIT-RE 500-SD adhesive anchoring system is an injectable two-component epoxy adhesive. The components are kept separate from the hardener and water by means of a dual-cylinder foil cartridge attached to a manifold. Applications and installation

procedures for the HIT-RE 500SD are very similar to the HIT-HY 150MAX system. It is important to reiterate that the embedment depths of the confined static tension specimens were designed such that a bond failure mode would occur as discussed per Section 3.2. Concrete and steel failure modes would not provide adequate data for determining true bond capacity of the adhesive anchor system.

All adhesive anchor systems were installed in two, 12 inch (304.8 mm) thick unreinforced normal weight concrete slabs. One slab being designated as a high-strength concrete slab, and the other being a low-strength concrete slab, as defined per Section 5.2.5 of ICC-ES AC308. Both slabs measured 7 feet x 9 feet (2.1 m x 2.7 m), and used aggregates meeting ASTM C 33. All test surfaces replicated a smooth trowel finish. Concrete test cylinders were prepared, cured, and stored in accordance with ASTM C 31. The concrete compressive strengths at the time of testing were determined and recorded, and are shown in Table 9. Figure 30 shows the typical slab profile used for the confined static tension tests.

Table 9: Concrete Compressive Strengths of Test Slabs

Concrete Type	Compressive Strength, psi (MPa)
Low-strength	3,950 (27.24)
High-strength	8,040 (55.45)

Figure 30: Typical Slab Profile used for Confined Static Tension Tests

In order to best match the concrete strengths of the slabs used for the eccentric shear loading per Chapter 5, the fillet weld applications of the HIT-HY 150MAX were performed in the high-strength concrete slab, while all plug weld testing of both the HIT-HY 150MAX and HIT-RE 500-SD were performed in the low-strength slab. Steel plates in compliance with ASTM E 488-96 were used for both reference and welded tests to confine the base material failure surrounding the anchors. All installation of the anchoring systems was per the manufacturer's printed installation instructions. The general test conditions were for a single anchor away from edges under dry base material conditions. Drilling and installation directions were vertical downward.

Prior to performing any welded tests, reference tests were performed to establish baseline bond capacities of each type of anchoring system in the concrete slabs not subjected to welding influences. Figure 31 shows reference test specimens installed in

one of the concrete slabs prior to testing. These baseline bond strengths will be used to compare the tests performed where welding was applied to the anchoring systems.

Figure 31: Reference Test Specimens Installed Prior to Testing

Fillet and plug weld influences were considered in the confined static tension tests. The HAS steel anchor elements were welded to threaded fixtures which attached directly to the data collection system. The threaded fixtures were machined from AISI/SAE 4340 steel specifically for these confined static tension tests. Internal hole diameters and thicknesses for each steel anchor element type were set to meet the testing requirements per section 5.4 of ASTM E 488-96. The external threads on the fixtures were machined to match the testing equipment used by Hilti. Welding was performed by an AWS certified welder using a Multiquip Whisper Weld 300 amp DC arc welder. MG-7018 0.125 inch (3.2 mm) and 0.15625 inch (4.0 mm) diameter welding rods were used to weld the steel

anchor elements to the tensile fixtures. The confined static tension tests were performed immediately after the anchors were welded to the tensile fixtures. Figures 32 and 33 illustrates a typical HAS steel anchor element plug welded and fillet welded, respectively, to a tensile fixture prior to load testing.

Figure 32: Plug Welded Test Specimen

Figure 33: Fillet Welded Test Specimen

In accordance with Table 4.1, test numbers 1a and 1b of the ICC-ES AC308 (ICC Evaluation Service, Inc. 2009), five separate tests of each test configuration were

performed to ensure the test results satisfied the requirements for test specimens, anchor installation, and testing. Table 10 summarizes the test matrix performed for the sixty confined static tension tests.

Table 10: Test Matrix for Number of Confined Static Tension Tests

			High-strength Concrete		Low-strength Concrete	
Adhesive Type	Steel Anchor Element Diameter, in. (mm)	Anchor Embedment, in. (mm)	Number of Reference Tests	Number of Fillet Weld Tests	Number of Reference Tests	Number of Plug Weld Tests
HIT-HY 150 MAX	0.5 (12.7)	2.75 (69.9)	Group H: 5	Group H: 5	Group J: 5	Group J: 5
	0.625 (15.9)	3.5 (88.9)	Group I: 5	Group I: 5	Group K: 5	Group K: 5
HIT-RE 500-SD	0.5 (12.7)	2.75 (69.9)	0	0	Group L: 5	Group L: 5
	0.75 (19.1)	4.25 (108.0)	0	0	Group M: 5	Group M: 5

3.4 Instrumentation and Data Collection of Tension Test Specimens

The HAS steel anchor elements were wired with Type-K thermocouples located at the bottom, middle, and top of the embedded depth as shown per Figure 34. The ends of the thermocouple wires were protected by a thermal conductive heat-shrink membrane to protect the handheld thermometers from any current overload generated by the welder. The thermocouples were attached to the anchors by means of a thin wire to stabilize in the proper location with respect to the embedment depth. Once the thermocouples were attached to the anchors, the anchors were installed into the concrete slabs leaving access to the ends of the thermocouples as shown per Figure 35.

Figure 34: Thermocouple Attachment to HAS Steel Element

Figure 35: Installed Anchor with Thermocouples

Steel plates were placed around the installed anchors for purposes of confining the concrete around the anchor during load testing. The tensile fixtures were then placed on top of the steel confining plates as shown per Figure 36. During the welding of the anchors, temperatures at various locations along the anchor element were recorded using calibrated handheld thermocouple thermometers as illustrated per Figure 37. Maximum temperature data recording features were used on the thermocouple thermometers to record the maximum temperatures experienced by the steel anchor elements during the welding process.

Figure 36: Welding of Anchor to Tensile Fixture

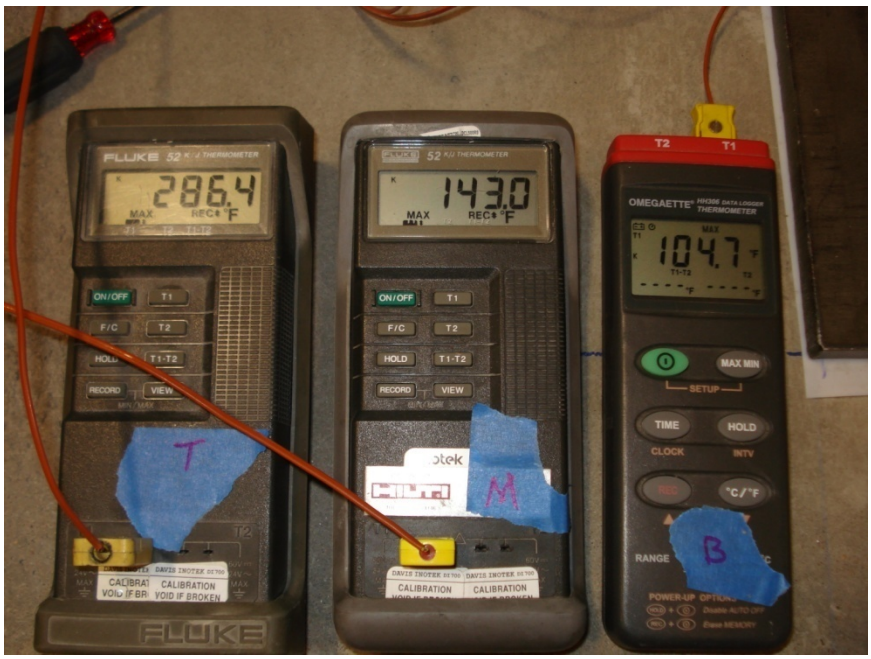

Figure 37: Handheld Thermometers used to Record Temperature during Welding

For data collection of the reference tests, a single-acting hollow core hydraulic ram was mounted on top of a test support. A calibrated compression style through-hole load cell was positioned with spherical washers on top of the hydraulic ram. A M30 threaded rod, having an internally threaded coupler, was inserted through the ram and load cell and attached to the test sample as seen in Figure 38. The M30 threaded rod that extended through the hydraulic ram and load cell was affixed with a M30 nut. A manual valve controlled the hydraulic pump supplied loading pressures.

Figure 38: Data Collection Configuration for Reference Tests

For data collection of the welded tests, a single-acting hollow core hydraulic ram was mounted on top of a test support. A calibrated compression style through-hole load cell was positioned with spherical washers on top of the hydraulic ram. A M30 threaded

rod, with a tensile bell, was inserted through the ram and load cell and attached to a tensile insert having an external threading of M58 as shown per Figure 39. The M30 threaded rod that extended through the hydraulic ram and load cell was affixed to the reaction frame with a M30 nut. A manual valve controlled hydraulic pump supplied loading pressures.

Figure 39: Data Collection Configuration for Welded Tests

For both reference and welded tests, a calibrated load cell and direct displacement LVDT were attached to proprietary data acquisition instrumentation and data was recorded and saved to data files. Printouts of the load versus displacement plots from the data files can be found in the Appendix C of this dissertation.

3.5 Tension Test Results and Observations

Confined static tension tests were performed per the testing matrix shown in Table 10 of Section 3.3, and recorded. The results of each set of tests are presented in this section. Failure modes, as discussed per Chapter 2, are noted in the tables for each set of tests, and defined in Table 11. The bond stress for each test was based on a uniform bond stress model, and was determined by taking the maximum load divided by the surface area of adhesive between the adhesive-steel interfaces as expressed by Equation (26):

$$\sigma_{bond} = \frac{P_{max}}{\pi d h_{ef}} \tag{26}$$

Table 11: Definition of Observed Confined Static Tension Failure Modes

C (Concrete Failure)	S (Steel Failure)	B (Bond Failure)
C_C = Cone	S_B = Bolt	B_B = Bond/Borehole
C_E = Edge	S_T = Thread	B_E = Bond/Element
C_{Sp} = Spall	S_X = Weld	B_{BE} = Bond/Borehole/Element (mixed bond failure)

Table 12 – Test Group H Reference Tests Results

	Test 1	Test 2	Test 3	Test 4	Test 5
Maximum Load, lb. (kN)	14,052 (62.51)	14,101 (62.72)	14,475 (64.39)	13,396 (59.59)	14,192 (63.13)
Maximum Displacement, in. (mm)	0.172 (4.37)	0.157 (3.99)	0.181 (4.60)	0.133 (3.38)	0.149 (3.79)
Bond Stress, psi (MPa)	3,253 (22.43)	3,264 (22.51)	3,351 (23.11)	3,101 (21.39)	3,285 (22.66)
Failure Mode	B_E	B_E	B_{BE} /C_C	B_{BE} /C_C	B_E
Average Maximum Load, lb. (kN)	14,043 (62.47)				
COV	2.83%				

The reference tests of Test Group H typically produced failure modes between the adhesive and the steel anchor element as shown in Figure 40. The two tests producing mixed bond failure modes were predominantly a bond failure between the steel anchor elements and the adhesive, and produced a minimal amount of borehole bond failure as seen per Figure 41. The bond strength of these five reference tests were averaged, producing average bond strength of 14,043 lb. (62.47 kN) and a coefficient of variation of 2.83%.

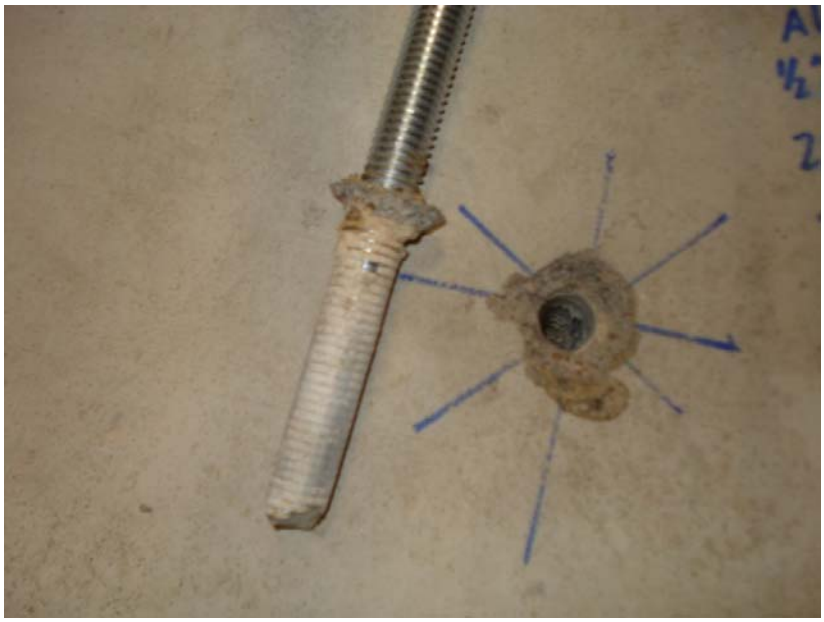

Figure 40: Bond/Element Failure of Test Group H Reference Test

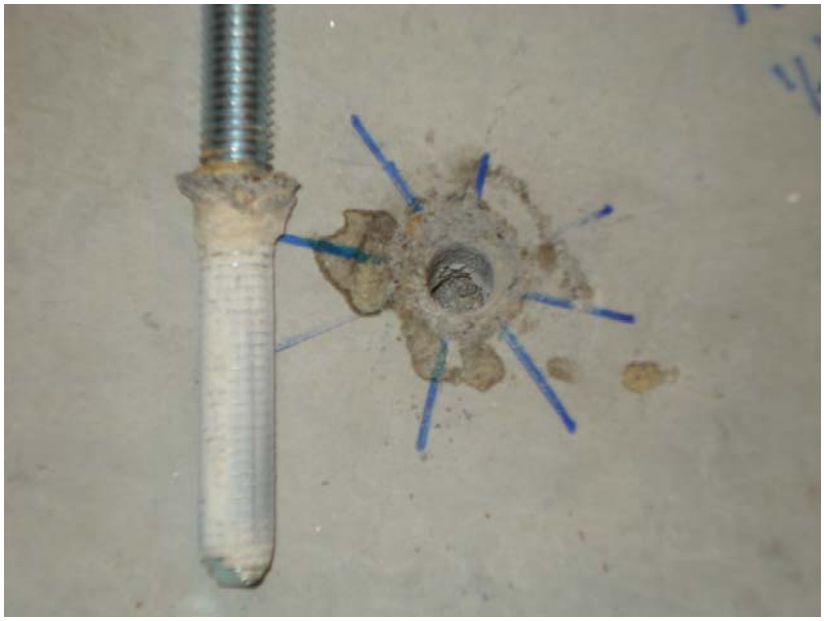

Figure 41: Mixed Bond Failure of Test Group H Reference Test

Table 13 – Test Group H Welded Tests Results

	Test 1	Test 2	Test 3	Test 4	Test 5
Maximum Load, lb. (kN)	11,111 (49.42)	10,700 (47.60)	10,738 (47.77)	11,524 (51.26)	10,322 (45.92)
Maximum Displacement, in. (mm)	0.110 (2.79)	0.091 (2.31)	0.094 (2.39)	0.097 (2.46)	0.092 (2.34)
Bond Stress, psi (MPa)	2,572 (17.74)	2,477 (17.08)	2,486 (17.15)	2,668 (18.40)	2,390 (16.48)
Failure Mode	B_E/C_C	B_{BE}/C_C	B_E/C_C	B_E/C_C	B_E/C_C
Average Maximum Load, lb. (kN)	10,879 (48.39)				
COV	4.19%				

The fillet weld tests of Test Group H typically produced failure modes between the adhesive and the steel anchor element. One test produced mixed bond failure modes, but was minimal on the amount of borehole bond failure as seen per Figure 42. The dominant failure mode for these mixed bond failure tests was a bond failure between the steel anchor element and the adhesive. The bond stresses of these five reference tests were averaged, producing average bond strength of 10,879 lb. (48.39 kN) and a coefficient of variation of 4.19%.

Figure 42: Mixed Bond Failure of Test Group H Welded Test

The average value of the bond strength for the welded tests was 3,164 lb. (14.07 kN) less than the reference tests. The coefficient of variation for the welded tests was 1.36% higher than the reference test. The observed failure modes of the reference and welded tests were very similar. The common failure mode for both tests was bond failure between the steel anchor element and the adhesive.

Table 14 – Test Group I Reference Tests Results

	Test 1	Test 2	Test 3	Test 4	Test 5
Maximum Load, lb. (kN)	19,093 (84.93)	20,880 (92.88)	18,578 (82.64)	19,426 (86.41)	21,631 (96.22)
Maximum Displacement, in. (mm)	0.116 (2.95)	0.129 (3.28)	0.137 (3.48)	0.118 (3.0)	0.139 (3.53)
Bond Stress, psi (MPa)	2,778 (19.16)	3,038 (21.95)	2,703 (18.64)	2,827 (19.50)	3,148 (21.71)
Failure Mode	B_E /C_C	B_{BE}	B_E	B_E	B_E
Average Maximum Load, lb. (kN)	19,922 (88.62)				
COV	6.44%				

The reference tests of Test Group I typically produced failure modes between the adhesive and the steel anchor element. The mixed failure modes of Test Group I reference tests one and two were similar to those exhibited by Test Group H reference tests presented in Table 12. Figure 43 shows the mixed bond failure mode for test two. The bond strength of these five reference tests was averaged, resulting in an average bond stress of 19,922 lb. (88.62 kN) and a coefficient of variation of 6.44%.

Figure 43: Mixed Bond Failure of Test Group I Reference Test

Table 15 – Test Group I Welded Tests Results

	Test 1	Test 2	Test 3	Test 4	Test 5
Maximum Load, lb. (kN)	19,192 (85.37)	15,246 (67.82)	16,102 (71.63)	18,877 (83.97)	17,138 (76.23)
Maximum Displacement, in. (mm)	0.154 (3.91)	0.125 (3.18)	0.106 (2.69)	0.137 (3.48)	0.110 (2.79)
Bond Stress, psi (MPa)	2,793 (19.26)	2,219 (15.30)	2,343 (16.16)	2,747 (18.95)	2,494 (17.20)
Failure Mode	B_E	B_E	B_{BE} /C_C	B_E	B_E
Average Maximum Load, lb. (kN)	17,311 (77.0)				
COV	9.9%				

The fillet weld tests of Test Group I produced similar failure modes to all of the previous tests. The dominant failure mode for these mixed bond failure tests was a bond failure between the steel anchor element and the adhesive. The bond strength of these five reference tests was averaged, producing average bond strength of 17,311 lb. (77.0 kN) and a coefficient of variation of 9.9%. Figure 44 shows the common failure mode between the adhesive and the anchor.

Figure 44: Bond/Element Failure of Test Group I Welded Test

The average bond strength of the welded tests was 2,611 lb. (11.61 kN) less than the reference tests. The welded tests produced a 3.46% higher coefficient of variation than that of the reference tests. Both the reference and welded tests produced similar failure modes. The common failure mode of both the welded and reference tests was bond failure between the steel anchor element and the adhesive.

Table 16 – Test Group J Reference Tests Results

	Test 1	Test 2	Test 3	Test 4	Test 5
Maximum Load, lb. (kN)	13,284 (59.10)	13,876 (61.72)	14,023 (62.38)	13,618 (60.58)	13,774 (61.14)
Maximum Displacement, in. (mm)	0.091 (2.31)	0.126 (3.20)	0.141 (3.58)	0.136 (3.45)	0.120 (3.05)
Bond Stress, psi (MPa)	3,075 (21.21)	3,212 (22.15)	3,246 (22.39)	3,153 (21.75)	3,189 (21.99)
Failure Mode	B_E	B_E	B_E	B_E	B_E
Average Maximum Load, lb. (kN)	13,715 (61.01)				
COV	2.06%				

All five of the reference tests for Test Group J resulted in bond failure between the adhesive and the steel anchor element. The average bond strength for the five tests was 13,715 lb. (61.01 kN) with a coefficient of variation of 2.06%.

Table 17 – Test Group J Welded Tests Results

	Test 1	Test 2	Test 3	Test 4	Test 5
Maximum Load, lb. (kN)	8,829 (39.27)	10,158 (45.19)	9,576 (42.60)	10,789 (48.99)	9,771 (43.46)
Maximum Displacement, in. (mm)	0.118 (3.0)	0.106 (2.69)	0.094 (2.39)	0.098 (2.49)	0.117 (2.97)
Bond Stress, psi (MPa)	2,044 (14.10)	2,352 (16.22)	2,217 (15.29)	2,498 (17.23)	2,262 (15.60)
Failure Mode	S_X	$B_{E/}C_C$	$B_{E/}C_C$	B_{BE}	$B_{E/}C_C$
Average Maximum Load, lb. (kN)	9,825 (43.70)				
COV	7.37%				

Though test one was controlled by a weld failure between the steel anchor element and the tensile fixture as shown in Figure 45, the dominant failure mode for the five plug weld tests of Test Group J was bond failure between the adhesive and the steel anchor element. Tests two, three, and five were total bond failures between the adhesive and the steel anchor element, while test four was a mixed bond failure between the adhesive and steel anchor element and the adhesive and borehole. Bond failure between the adhesive

and the steel anchor element occurred over a large portion of the anchor embedment as provided per Figure 46. The weld failure of test one was only one of two weld failures that occurred for all of the welded test samples. The portion of the anchor that remained embedded in the slab was cored and split to visually examine the condition of the adhesive prior to welding, and is addressed in Section 3.8 of this chapter. The average bond strength for these tests is 9,825 lb. (43.70 kN) with a coefficient of variation of 7.37%.

Figure 45: Weld Failure of Test Group J Welded Test

Figure 46: Bond/Element Failure of Test Group J Welded Test

The plug weld applications of the steel anchor elements produced a larger drop in bond strength than the fillet weld tests. The average bond strength of the welded tests was 3,890 lb. (17.31 kN) lower than the reference tests of Test Group J. The difference of the coefficient of variation between the welded and reference tests of Test Group J was 5.31%, which is slightly higher than Test Group H. The common failure mode of both the reference and welded tests was bond failure between the steel anchor element and the adhesive, which is consistent with the previous test groups.

Table 18 – Test Group K Reference Tests Results

	Test 1	Test 2	Test 3	Test 4	Test 5
Maximum Load, lb. (kN)	19,879 (88.43)	20,650 (91.86)	20,163 (89.69)	20,264 (90.14)	20,923 (93.07)
Maximum Displacement, in. (mm)	0.128 (3.25)	0.149 (3.79)	0.117 (2.97)	0.133 (3.38)	0.106 (2.69)
Bond Stress, psi (MPa)	2,893 (19.95)	3,005 (20.72)	2,934 (20.23)	2,949 (20.34)	3,045 (21.00)
Failure Mode	B_E	B_E	B_E	B_E	B_E
Average Maximum Load, lb. (kN)	20,376 (90.64)				
COV	2.02%				

All five of the reference tests of Test Group K resulted in bond failure between the adhesive and the steel anchor element. The average bond strength for the five tests is 20,376 lb. (90.64 kN) with a coefficient of variation of 2.02%.

Table 19 – Test Group K Welded Tests Results

	Test 1	Test 2	Test 3	Test 4	Test 5
Maximum Load, lb. (kN)	11,917 (53.01)	16,923 (75.28)	16,466 (73.24)	17,509 (77.88)	15,438 (68.67)
Maximum Displacement, in. (mm)	0.280 (7.11)	0.133 (3.38)	0.125 (3.18)	0.153 (3.89)	0.129 (3.28)
Bond Stress, psi (MPa)	1,734 (11.96)	2,463 (16.99)	2,396 (16.52)	2,548 (17.57)	2,246 (15.49)
Failure Mode	B_E/C_C	B_E	B_E/C_C	B_E	B_E
Average Maximum Load, lb. (kN)	15,651 (69.62)				
COV	14.19%				

All five of the plug weld tests of Test Group K resulted in bond failure between the adhesive and the steel anchor element as seen in Figure 47. The average bond strength for the five tests is 15,651 lb. (69.62 kN) with a coefficient of variation of 14.19%.

Figure 47: Bond/Element Failure of Test Group K Welded Test

Test one of Test Group K resulted in a significantly lower maximum load and higher displacement than the other four tests in the group as shown in Appendix C. A visual inspection of the test specimen revealed no air voids along the annular gap, and the adhesive material appeared to be uniform along the embedment of the anchor. The failure mode of test one is consistent with the other bond/element failures of the other four tests in the group. Figure 48 shows the test one specimen of Test Group K.

Figure 48: Test Group K Test One Welded Test

Test five of the welded tests of Test Group K slightly skewed the data for the group. The average bond strength of the welded tests of this group was 4,726 lb. (21.02 kN) less than the average bond strength of the reference tests. The difference in the coefficient of variation of the welded tests and the reference tests was 12.17%. Even though the difference in the coefficient of variance was slightly large, the difference in bond strength between the welded tests and reference tests was still less than that exhibited by Test Group H. The common failure mode of both the reference and welded tests of Test Group K was bond failure between the steel anchor elements and the adhesive.

Table 20 – Test Group L Reference Tests Results

	Test 1	Test 2	Test 3	Test 4	Test 5
Maximum Load, lb. (kN)	13,439 (59.78)	14,151 (62.95)	15,656 (69.64)	15,709 (69.88)	15,415 (68.57)
Maximum Displacement, in. (mm)	0.162 (4.12)	0.158 (4.01)	0.279 (7.09)	0.295 (7.49)	0.249 (6.33)
Bond Stress, psi (MPa)	3,111 (21.46)	3,276 (22.59)	3,624 (24.99)	3,637 (25.09)	3,569 (24.61)
Failure Mode	B_{BE}/C_C	B_{BE}/C_C	S_B	S_B	S_B
Average Maximum Load, lb. (kN)	14,874 (66.16)				
COV	6.88%				

For the HIT-RE 500-SD system reference tests using 0.5 inch (12.7 mm) diameter anchors, Test Group L, two of the tests resulted in mixed bond failures while three of the reference tests resulted in steel element failures. Figure 49 shows the typical mixed bond failure exhibited for two of the tests. For the three tests resulting in a steel failure mode the adhesive bond exceeded the expected value, shifting the failure mode from a bond controlled failure to a steel controlled failure. The displacements for these three tests exhibited a more ductile behavior than those of test one and two. Figure 50 illustrates the

typical steel failure mode experienced by tests three, four, and five. The average bond strength for these five reference tests is 14,874 lb. (66.16 kN) with a coefficient of variation of 6.88%.

Figure 49: Mixed Bond Failure of Test Group L Reference Test

Figure 50: Steel Anchor Element Failure of Test Group L Reference Test

Table 21 – Test Group L Welded Tests Results

	Test 1	Test 2	Test 3	Test 4	Test 5
Maximum Load, lb. (kN)	12,647 (56.26)	13,872 (61.71)	13,018 (5.91)	13,723 (61.04)	13,537 (60.22)
Maximum Displacement, in. (mm)	0.122 (3.10)	0.149 (3.79)	0.150 (3.81)	0.180 (4.57)	0.138 (3.51)
Bond Stress, psi (MPa)	2,929 (20.20)	3,211 (22.15)	3,014 (20.79)	3,177 (21.91)	3,134 (21.61)
Failure Mode	S_X	B_B	B_B	B_B	B_B
Average Maximum Load, lb. (kN)	13,359 (59.43)				
COV	3.83%				

For the plug weld tests of Test Group L, one test resulted in a steel weld failure while the other four tests resulted in bond failures between the adhesive and the borehole. The steel weld failure that occurred is the second of two steel weld failures that occurred out all the welded tests. Per visual observations, it appeared the failure plane occurred along the plane of the root weld pass between the steel anchor element and the tensile fixture. Figure 51 shows the steel weld failure that occurred for test one. Figure 52 illustrates the typical bond failure mode experienced by tests two through five. The

average bond strength for these five reference tests is 13,359 lb. (59.43 kN) with a coefficient of variation of 3.83%.

Figure 51: Weld Failure of Test Group L Welded Test

Figure 52: Bond/Borehole Failure of Test Group L Welded Test

For Test Group L, the average bond strength of the welded test specimens was 1,515 lb. (6.74 kN) less than the reference tests. The coefficient of variation of the reference test was 3.05% higher than the welded tests of this group. The higher coefficient of variation exhibited by the reference tests was due to the three steel anchor element failures experienced by tests three, four, and five.

Table 22 – Test Group M Reference Tests Results

	Test 1	Test 2	Test 3	Test 4	Test 5
Maximum Load, lb. (kN)	35,868 (159.55)	37,151 (165.26)	34,859 (155.10)	35,474 (157.80)	33,289 (148.08)
Maximum Displacement, in. (mm)	0.375 (9.53)	0.359 (9.12)	0.214 (5.44)	0.256 (6.50)	0.437 (11.1)
Bond Stress, psi (MPa)	3,582 (24.70)	3,710 (25.59)	3,481 (24.01)	3,543 (24.43)	3,324 (22.92)
Failure Mode	S_B	S_B	B_{BE}	B_B/C_C	B_B/C_C
Average Maximum Load, lb. (kN)	35,328 (157.15)				
COV	4.0%				

For the reference tests of Test Group M, test one and two exhibited steel element failures. As previously seen with the 0.5 inch (12.7 mm) diameter reference tests for the HIT-RE 500-SD system, the bond strength of the adhesive exceeded the steel strength of the anchor element for these two tests. Figure 53 shows the steel element failure mode exhibited by tests one and two. Test three experienced a mixed bond failure between the adhesive and the borehole, and the adhesive and the steel anchor element as shown in Figure 54. Tests four and five of Test Group M exhibited bond failure between the

adhesive and the borehole as shown in Figure 55. The average bond strength for these five reference tests was 35,328 lb. (157.15 kN) and the coefficient of variation is 4.0%.

Figure 53: Steel Anchor Element Failure of Test Group M Reference Test

Figure 54: Mixed Bond Failure of Test Group M Reference Test

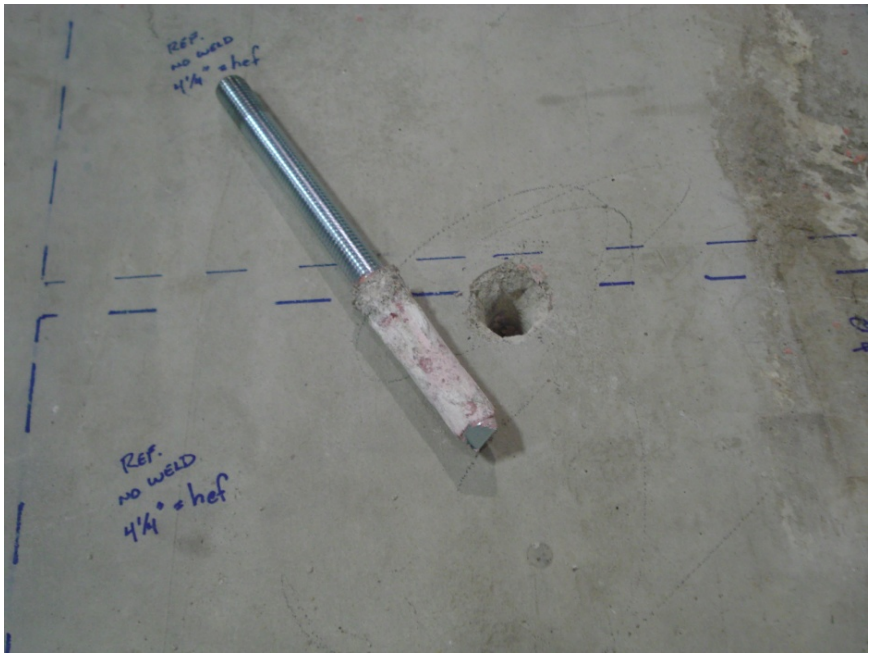

Figure 55: Bond/Borehole Failure of Test Group M Reference Test

Table 23 – Test Group M Welded Tests Results

	Test 1	Test 2	Test 3	Test 4	Test 5
Maximum Load, lb. (kN)	25,084 (111.58)	31,030 (138.03)	35,344 (157.22)	33,470 (148.88)	35,207 (156.61)
Maximum Displacement, in. (mm)	0.201 (5.11)	0.201 (5.11)	0.277 (7.04)	0.253 (6.43)	0.293 (7.44)
Bond Stress, psi (MPa)	2,505 (17.28)	3,099 (21.37)	3,530 (24.35)	3,342 (23.05)	3,516 (24.25)
Failure Mode	B_B/C_C	B_B/C_C	S_B	S_B	B_B
Average Maximum Load, lb. (kN)	32,027 (142.46)				
COV	13.28%				

Tests three and four of Test Group M welded tests experienced steel element failure modes as seen per Figure 56. The dominant failure modes for tests one, two, and five were bond failures between the adhesive and the borehole as shown in Figure 57. The average bond strength of the five tests was 32,027 lb. (142.46 kN) with a coefficient of variation of 13.28%.

Figure 56: Steel Anchor Element Failure of Test Group M Welded Test

Figure 57: Bond/Borehole Failure of Test Group M Welded Test

The average bond strength of the welded tests of Test Group M was 3,301 lb. (14.68 kN) less than the average bond stress of the reference tests. The coefficient of variation was 9.28% higher for the welded tests compared to the reference tests of this test group. The large coefficient of variation for the welded tests was due to test one. Though test one of the welded tests exhibited a maximum load of 6,943 lb. (30,884 N) below the

average load and exhibited similar behavior to test one of test group K, the 330 psi (2.28 MPa) difference between the welded and reference tests of Test Group M is comparable to the 350 psi (2.41 MPa) difference exhibited by Test Group L. A visual inspection of test one revealed no air voids along the annular gap, and the adhesive material appeared to be uniform along the embedment of the anchor. This load deflection plot is referenced in Appendix C.

Section 3.6 Collection of Temperature Data

Maximum temperatures were recorded during the welding of the steel anchor elements to the tensile fixtures prior to performing the confined static tension tests. The results for each set of tests are presented in Tables 24 through 29 of this section. Figures 58 through 63 are also presented in this section and combine the maximum temperatures recorded at each thermocouple location to produce a maximum temperature gradient experienced by the steel anchor element during the welding process. Figures 58 through 63 use 2D scatter line plots with mean temperature values fitted with a linear trend line to illustrate the variance in recorded maximum temperatures at each thermocouple location and the temperature gradient profile experienced by the steel anchor elements during the welding process.

Table 24 –Maximum Recorded Temperatures for Test Group H Welded Tests

	Maximum Recorded Temperatures, °F (°C)				
Thermocouple Location, in. (mm)	Test 1	Test 2	Test 3	Test 4	Test 5
Surface (0.0)	388.0 (197.8)	289.0 (142.8)	371.8 (188.8)	321.4 (160.8)	318.8 (159.3)
-1.375 (-34.9)	138.6 (59.2)	144.0 (62.2)	148.4 (64.7)	124.4 (51.3)	123.6 (50.9)
-2.75 (-69.9)	100.2 (37.9)	102.2 (39.0)	108.4 (42.4)	99.3 (37.4)	95.2 (35.1)
Initial Base Material Temperature, °F (°C)	72 (22.2)				

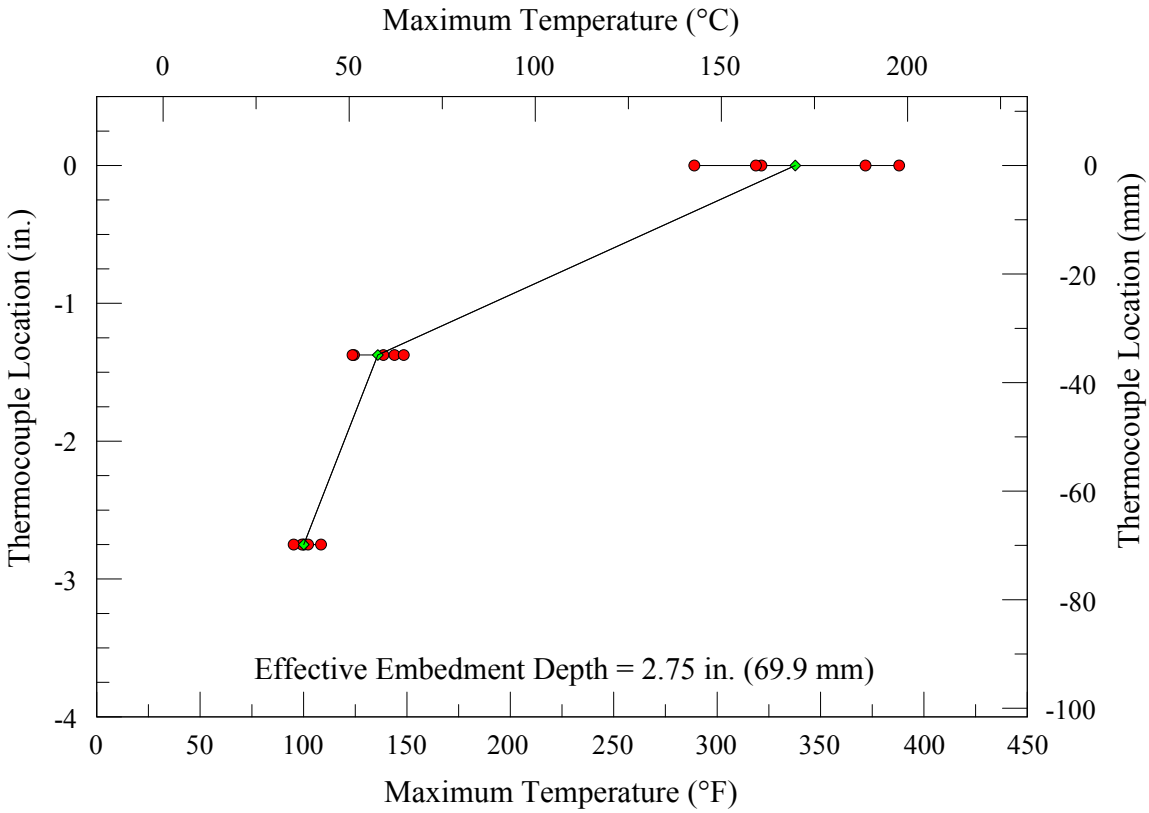

Figure 58: Weld Temperature Gradient for Test Group H

Table 25 –Maximum Recorded Temperatures for Test Group I Welded Tests

	Maximum Recorded Temperatures, °F (°C)				
Thermocouple Location, in. (mm)	Test 1	Test 2	Test 3	Test 4	Test 5
Surface (0.0)	249.0 (120.6)	315.0 (157.2)	331.2 (166.2)	263.0 (128.3)	386.2 (196.8)
-1.75 (-44.5)	133.4 (56.3)	131.0 (55.0)	136.2 (57.9)	155.6 (68.7)	134.0 (56.7)
-3.5 (-88.9)	92.6 (33.7)	92.3 (33.5)	128.2 (53.4)	114.4 (45.8)	92.7 (33.7)
Initial Base Material Temperature, °F (°C)	71 (21.7)				

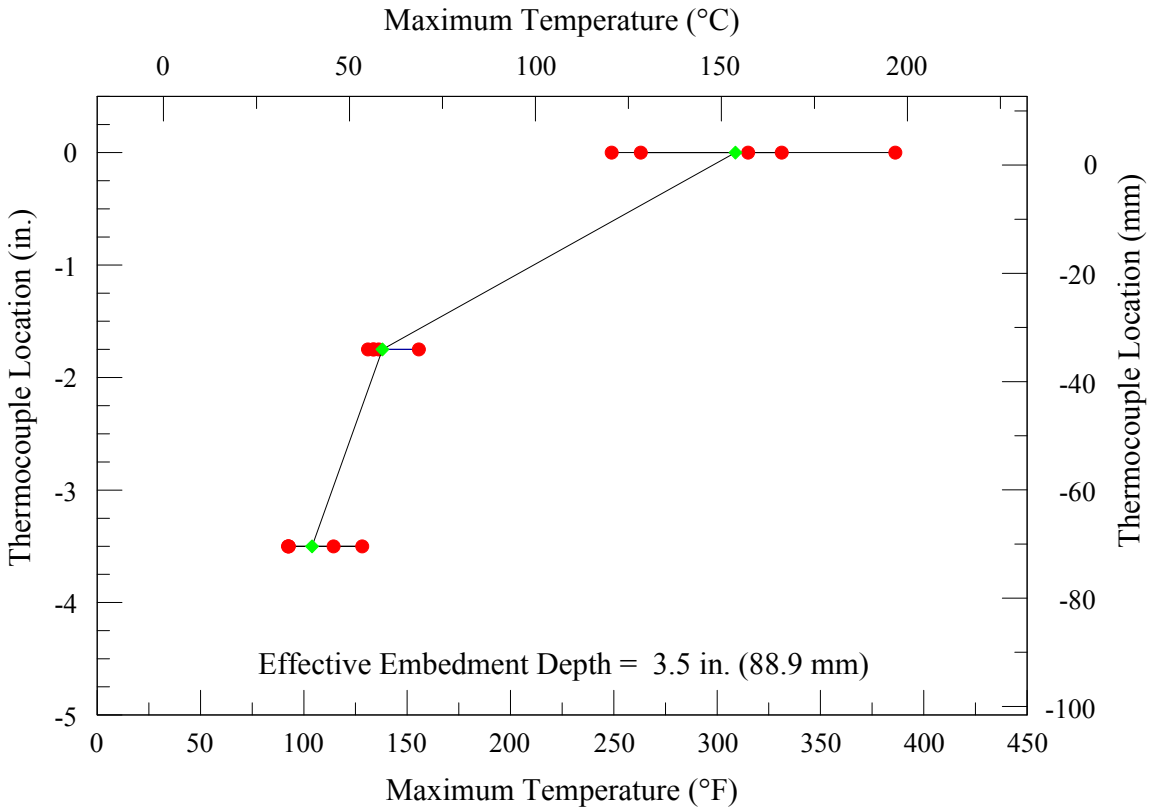

Figure 59: Weld Temperature Gradient for Test Group I

Table 26 –Maximum Recorded Temperatures for Test Group J Welded Tests

	Maximum Recorded Temperatures, °F (°C)				
Thermocouple Location, in. (mm)	Test 1	Test 2	Test 3	Test 4	Test 5
Surface (0.0)	576.2 (302.3)	501.4 (260.8)	519.4 (270.8)	535.8 (279.9)	398.8 (203.8)
-1.375 (-34.9)	163.6 (73.1)	171.4 (77.4)	170.6 (77.0)	163.8 (73.2)	164.6 (73.7)
-2.75 (-69.9)	102.5 (39.2)	125.7 (52.1)	113.5 (45.3)	112.6 (44.8)	110.9 (43.8)
Initial Base Material Temperature, °F (°C)	70 (21.1)				

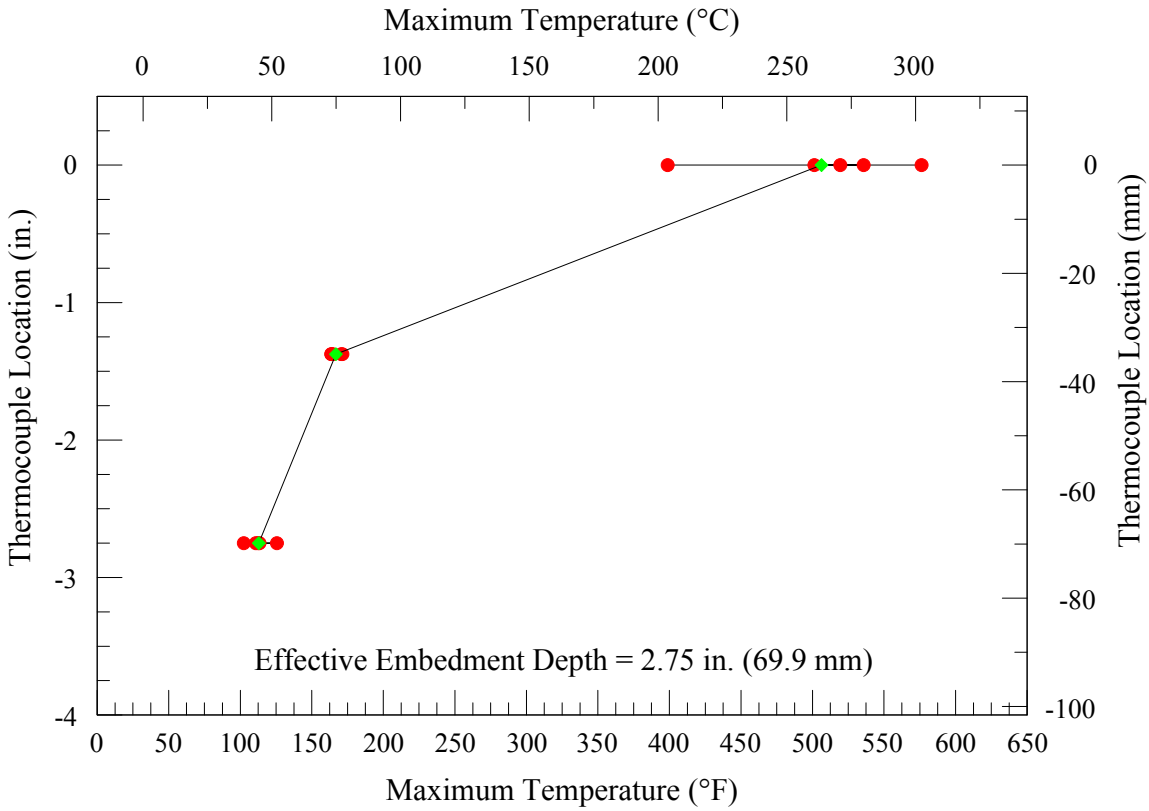

Figure 60: Weld Temperature Gradient for Test Group J

Table 27 –Maximum Recorded Temperatures for Test Group K Welded Tests

	Maximum Recorded Temperatures, °F (°C)				
Thermocouple Location, in. (mm)	Test 1	Test 2	Test 3	Test 4	Test 5
Surface (0.0)	388.0 (197.8)	371.6 (188.7)	407.2 (208.4)	478.4 (248.0)	390.4 (199.1)
-1.75 (-44.5)	174.0 (78.9)	152.6 (67.0)	147.8 (64.3)	159.4 (70.8)	132.4 (55.8)
-3.5 (-88.9)	102.5 (39.2)	100.5 (38.1)	99.5 (37.5)	109.0 (42.8)	92.0 (33.3)
Initial Base Material Temperature, °F (°C)	72 (22.2)				

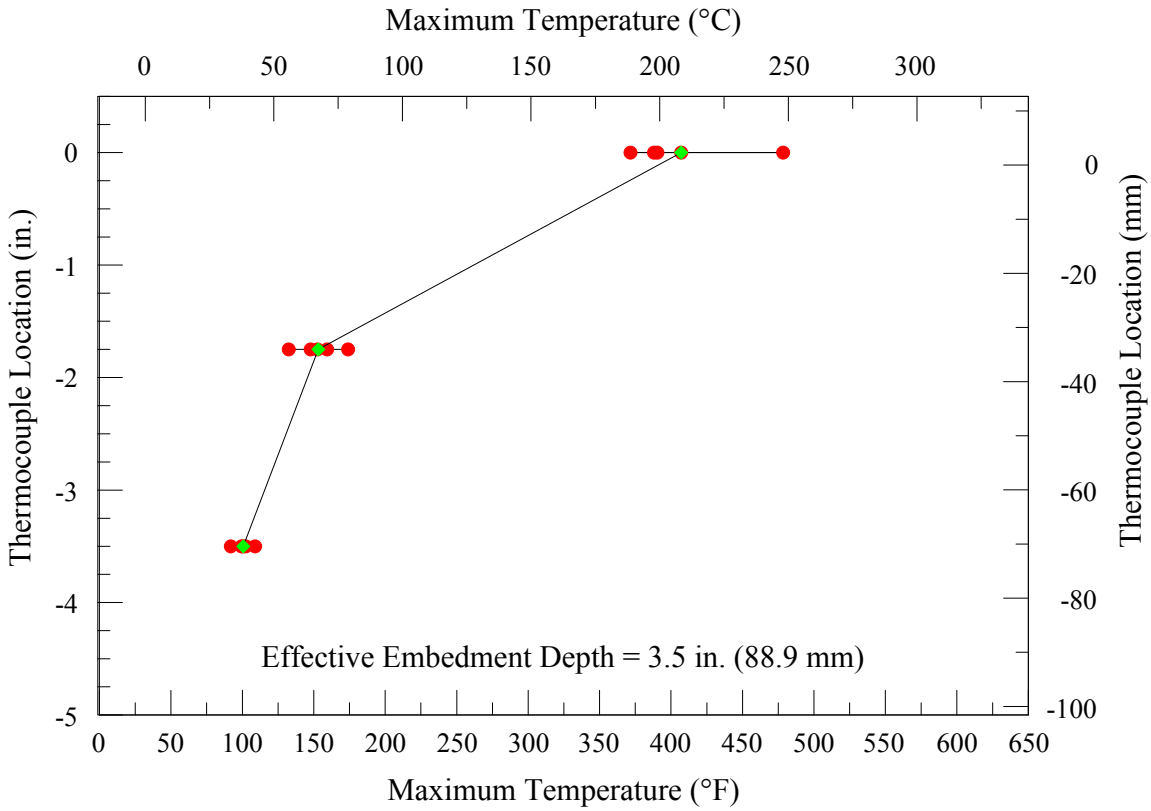

Figure 61: Weld Temperature Gradient for Test Group K

Table 28 –Maximum Recorded Temperatures for Test Group L Welded Tests

	Maximum Recorded Temperatures, °F (°C)				
Thermocouple Location, in. (mm)	Test 1	Test 2	Test 3	Test 4	Test 5
Surface (0.0)	257.2 (125.1)	262.6 (128.1)	286.4 (141.3)	303.0 (150.6)	313.8 (156.6)
-1.375 (-34.9)	116.2 (46.8)	127.2 (52.9)	143.0 (61.7)	140.0 (60.0)	155.0 (68.3)
-2.75 (-69.9)	87.7 (30.9)	96.3 (35.7)	104.7 (40.4)	99.4 (37.4)	108.6 (42.6)
Initial Base Material Temperature, °F (°C)	74 (23.3)				

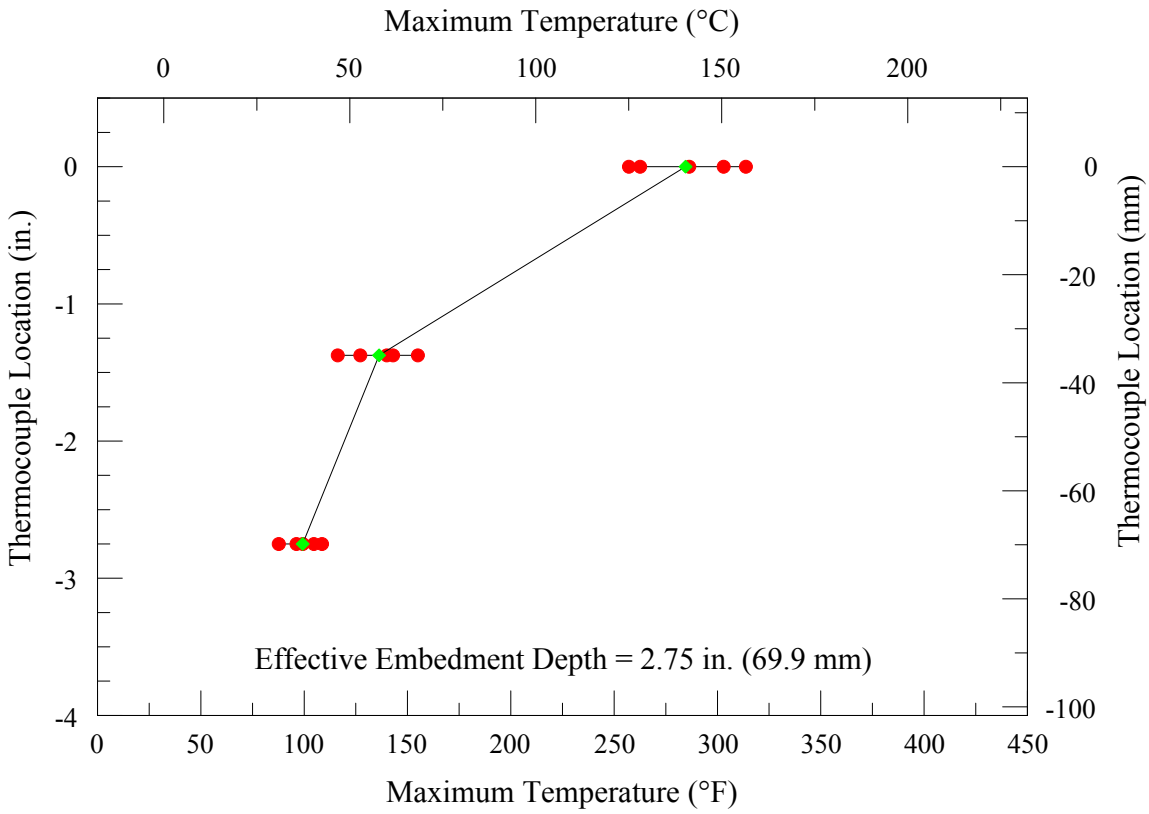

Figure 62: Weld Temperature Gradient for Test Group L

Table 29 –Maximum Recorded Temperatures for Test Group M Welded Tests

	Maximum Recorded Temperatures, °F (°C)				
Thermocouple Location, in. (mm)	Test 1	Test 2	Test 3	Test 4	Test 5
Surface (0.0)	395.8 (202.1)	341.2 (171.8)	404.2 (206.8)	344.2 (173.4)	359.2 (181.8)
-2.125 (-53.9)	140.4 (60.2)	149.2 (65.1)	140.2 (60.1)	136.6 (58.1)	152.2 (66.8)
-4.25 (-107.9)	106.3 (41.3)	112.0 (44.4)	119.0 (48.3)	118.3 (47.9)	115.0 (46.1)
Initial Base Material Temperature, °F (°C)	70 (21.1)				

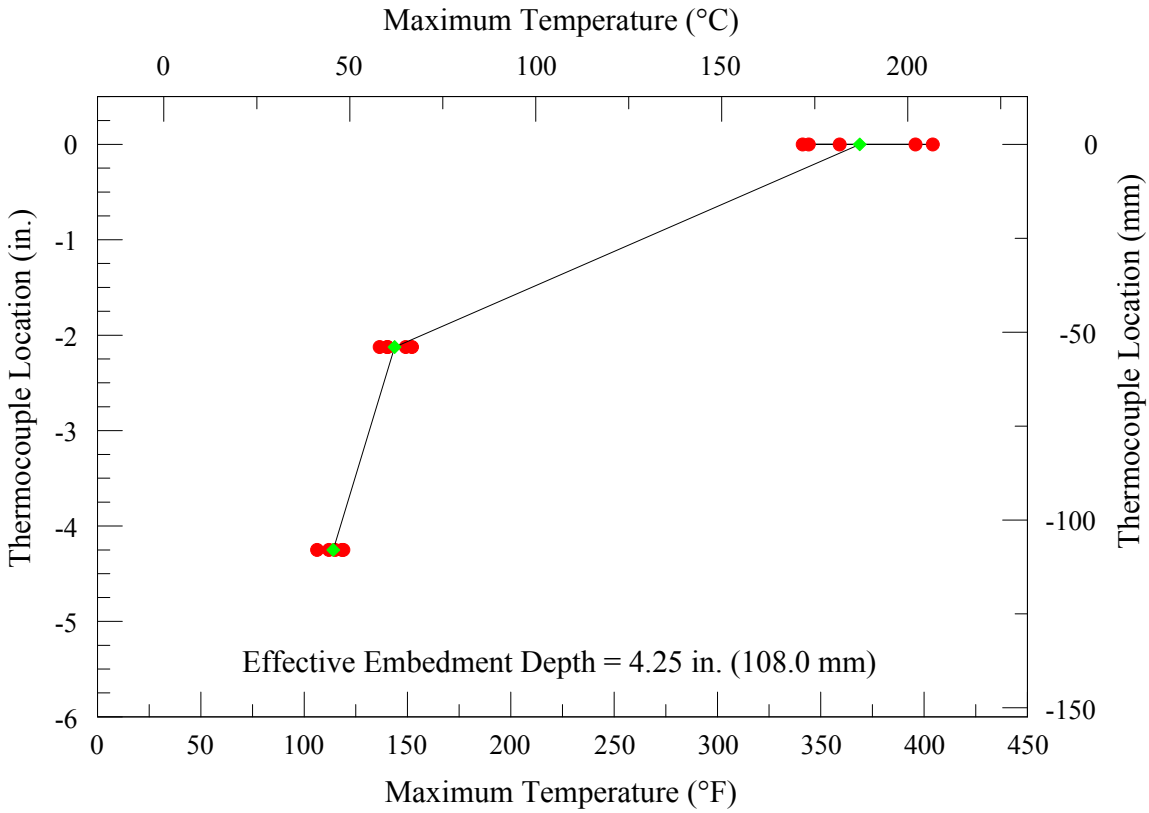

Figure 63: Weld Temperature Gradient for Test Group M

3.7 Comparison of Reference and Welded Tests

In order to compare the influence of the welding exposure to the adhesive anchoring system between the ultimate capacities of the reference and the welded Tables 12 through 23 of Section 3.5 can be grouped by test type and plotted as a vertical bar chart. Figure 64 compares the average reference tests bond capacity to the average welded tests bond capacity. It can be observed from Figure 64 that a reduction of bond capacity on the adhesive anchor systems exposed to welding exists. For the HIT-HY 150MAX adhesive anchor system, it can be seen that the reduction in bond capacity varies for the type of welding experienced. Greater bond capacity reductions were observed for plug

welded tests over the fillet welded tests. Based on the temperature gradient data from Section 3.6, higher temperature values were experienced for the plug welded tests than the fillet welded tests. For the HIT-RE 500-SD adhesive anchor systems subjected to plug welding, the reduction in ultimate capacity was less than that experienced by the HIT-HY 150MAX system which could suggest that high-strength, two-part epoxy adhesive systems have better bond capacity performance when subjected to welding influences.

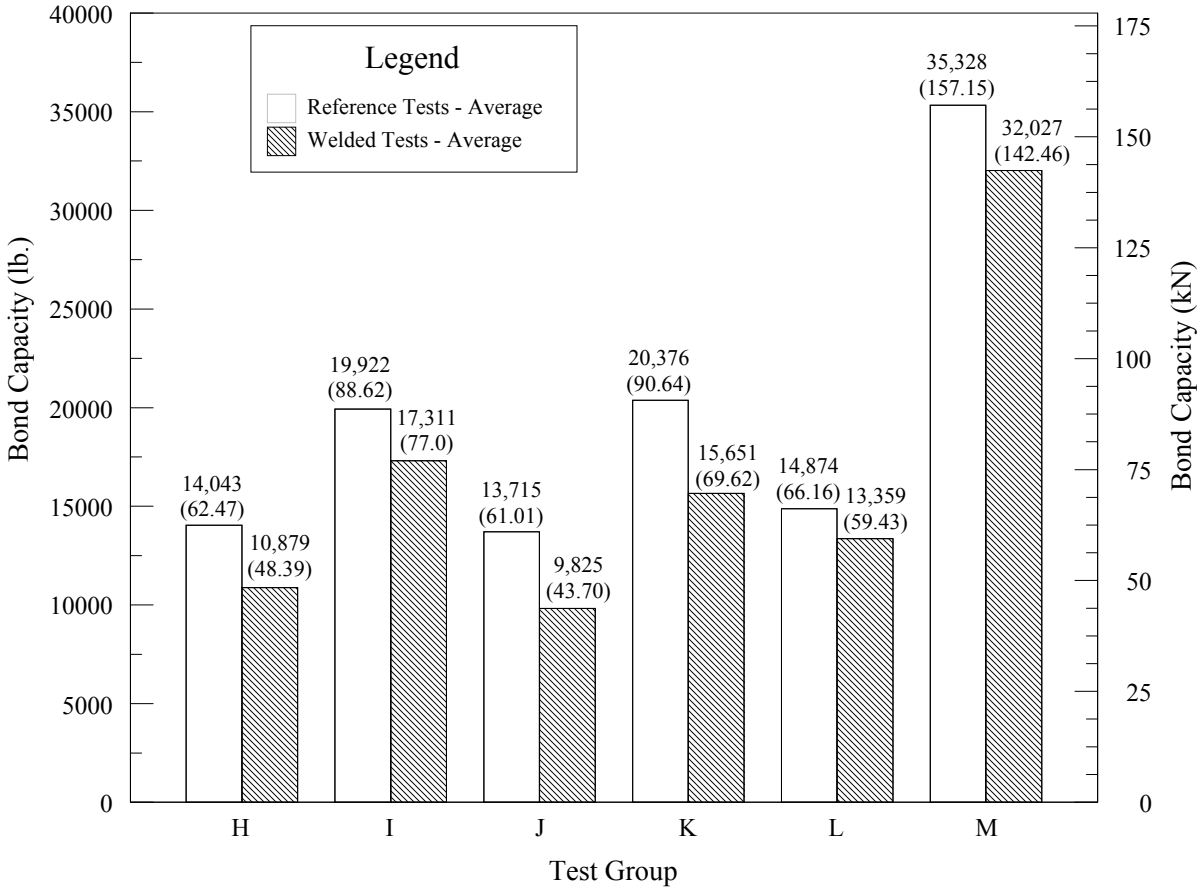

Figure 64: Comparison of Average Reference and Welded Tests Bond Capacity Values

To correlate the maximum temperatures experienced during welding to the reductions of the average bond capacity of the welded test specimens, Table 30 is presented. From Table 30, it is observed that the maximum reduction in average bond capacity occurs with the maximum recorded temperatures in Test Group J. These maximum temperatures and reduction of average bond capacity is the largest for all of the test groups of the confined static tension tests.

Table 30: Comparison of Average Bond Capacity Reductions and Maximum Recorded Temperatures

Test Group	Maximum Recorded Temperature, °F (°C)		Reduction in Average Bond Capacity, lb. (kN)
H	Surface	388.0 (197.8)	3,164 (14.07)
	Middle	148.4 (64.7)	
	Bottom	108.4 (42.4)	
I	Surface	386.2 (196.8)	2,611 (11.61)
	Middle	155.6 (68.7)	
	Bottom	128.2 (53.4)	
J	Surface	501.4 (260.8)	3,890 (17.30)
	Middle	171.4 (77.4)	
	Bottom	125.7 (52.1)	
K	Surface	478.4 (248.0)	4,725 (21.02)
	Middle	174.0 (78.9)	
	Bottom	109.0 (42.8)	
L	Surface	313.8 (156.6)	1,515 (6.74)
	Middle	155.0 (68.3)	
	Bottom	108.6 (42.6)	
M	Surface	404.2 (206.8)	3,301 (14.68)
	Middle	152.2 (66.8)	
	Bottom	119.0 (48.3)	

It is also observed from Table 30 that the test groups using the HIT-HY 150MAX hybrid adhesive anchoring system, Test Groups H, I, J, and K, experienced larger reductions in average bond capacity with the 0.5 inch (12.7 mm) diameter steel anchor elements than with the 0.625 inch (15.9 mm) diameter steel anchor elements. In addition, when comparing the weld condition of the steel anchor elements to the tensile fixtures (plug weld versus fillet weld) regardless of the anchor diameter, the plug welded conditions (Test Groups J and K) experience a higher average reduction of bond capacity compared to the fillet welded conditions (Test Groups H and I). Test Groups J and K have an average bond capacity reduction of 4,308 lb. (19.16 kN) versus 2,888 lb. (12.84 kN) exhibited by Test Groups H and I.

3.8 Discussion

As seen in Tables 12 through 23 presented in Section 3.5, the primary type of failure exhibited by the confined static tension tests were bond failures which correlate to the basis of experimental design as discussed per Section 3.2. Based on these observed bond failures, it can be concluded that the test results are representative of the bond strength of the adhesive anchor systems tested. Based on Table 30 in Section 3.7, it can also be concluded from the bond strength and temperature data collected, during the confined static tension tests, that welding does influence the ultimate capacity of the adhesive anchor system.

To further investigate the welding influence on the confined static tension welded test specimens, a single split core encasing a 0.5 inch (12.7 mm) diameter anchor using the HIT-HY 150MAX system was taken from the low-strength concrete test slab. This

anchor was taken from Test 1 of Test Group J referenced in Table 17 of Section 3.5. Based on physical observations, there were no visual signs of charring or adhesive discoloration near the point of welding. The split core visually appeared similar in condition as those split cores presented in Chapter 4 of this dissertation. Figure 65 shows the split core sample taken from the welded confined statistic tension tests.

Figure 65: Split Core Sample from Welded Confined Static Tension Test

The temperature gradients experienced by each welded test are similar in behavior as seen per Section 3.6. To compare the overall temperature gradient regardless of weld type, the temperature gradients for all welded tests are combined and shown in Figure 66. For all tests, it is observed that the experienced temperature range decreases along the

embedment depth of the steel anchor elements. It is also observed that at about 2 inches (50.8 mm) below the concrete surface (point of welding) for the two adhesive anchoring systems tested, the maximum experienced temperatures fall below the maximum short-term temperatures defined for "Temperature Range B" of each system's ICC–ES Evaluation Service Report (ESR).

The maximum short-term temperature for the HIT-HY 150MAX adhesive anchoring system in "Temperature Range B" is 176° F (80° C) (ICC Evaluation Service, Inc. 2010). The maximum short-term temperature for the HIT-RE 500-SD adhesive anchoring system in "Temperature Range B" is 162° F (72° C) (ICC Evaluation Service, Inc. 2012). Based on this observation it is proposed that by disregarding the top 2 inches (50.8 mm) in the upper temperature gradient and adding this disregarded embedment as additional overall anchor embedment will provide bond capacities that exceed the reference test bond capacities.

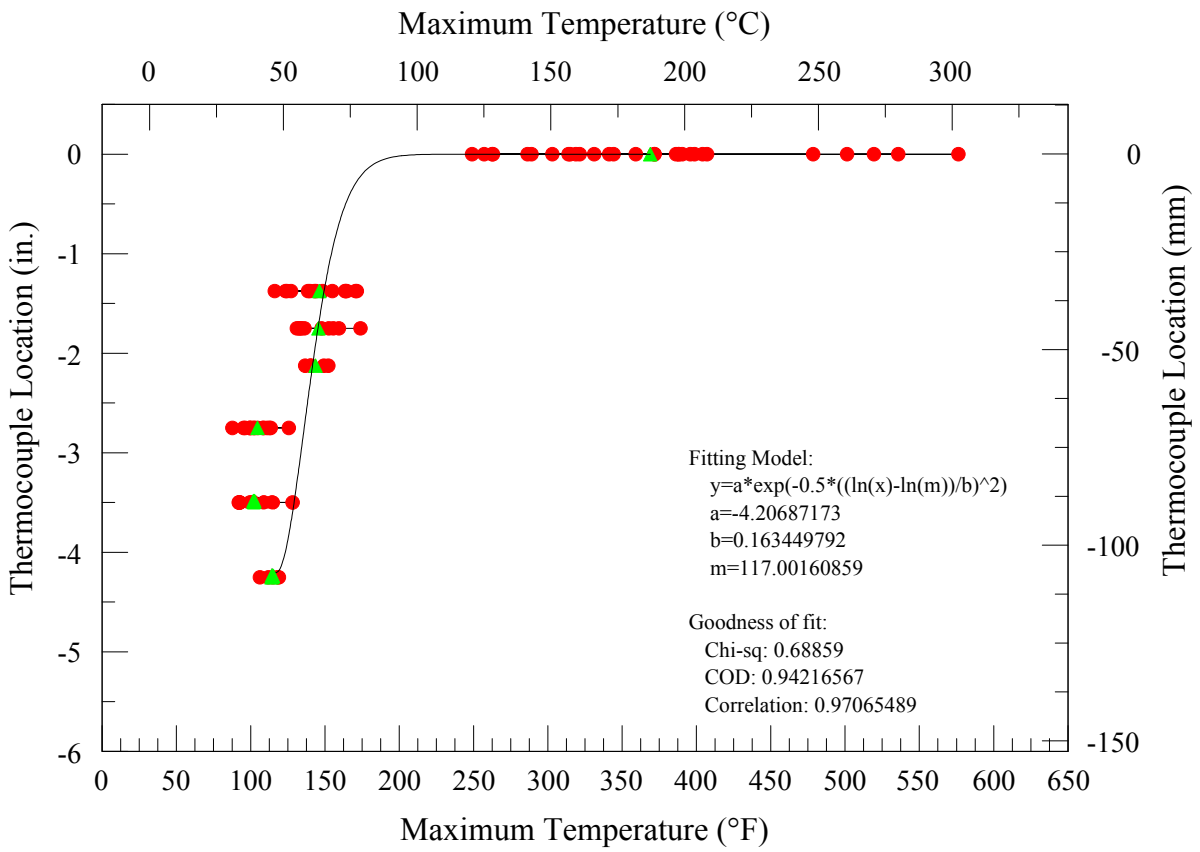

Figure 66: Combined Maximum Temperature Gradient for all Welded Confined Static Tension Tests

To predict ultimate capacities for these systems at the specific embedment depths chosen for this research program, the reference bond capacity values may be used with an additional 2 inches (50.8 mm) of embedment depth added to the required embedment depth calculated for non–welded. This logic is rooted in the fact that temperatures experienced in the additional anchor embedment region are lower than the lowest maximum temperature values experienced during the collection of temperature gradient data. The additional capacity due to additional anchor embedment can be expressed by Equation (27):

$$P_{\Delta h_{ef}} = \pi d \Delta_{h_{ef}} \tau_{ref} \quad (27)$$

where:

$P_{\Delta hef}$ = additional nominal bond strength due to additional anchor embedment compensating for adhesive exposed to short-term temperatures which exceed the manufacturer's maximum values, lb. (N)

d = diameter of the steel anchor element, inches (m)

Δ_{hef} = additional anchor embedment used to compensate for adhesive exposed to short-term temperatures that exceed the manufacturer's maximum values, inches (m)

τ_{ref} = nominal bond stress value of adhesive anchor system not subjected to welding influence, psi (Pa)

Using the additional nominal bond strength from Equation (27) and the nominal reference bond strength value presented in Section 3.5, the maximum nominal temperature compensation capacity can be determined per Equation (28):

$$P_{comp} = P'_{ref} + P_{\Delta h_{ef}} \quad (28)$$

where:

P_{comp} = nominal compensated capacity allowing for adhesive exposed to temperatures that exceed the manufacturer's maximum values, lb. (N)

P'_{ref} = nominal reference bond strength of an adhesive anchor system exposed to welding influences that neglects the portion of effective anchor embedment exposed to short-term temperatures that exceed the manufacturer's maximum values, lb. (N)

The nominal reference bond strength of an adhesive anchor system exposed to welding influences that neglects the portion of effective anchor embedment exposed to

short-term temperatures that exceed the manufacturer's maximum values is determined by Equation (29):

$$P'_{ref} = \pi d\left(h_{ef} - h_{T,max}\right)\tau_{ref} \quad (29)$$

where:

$h_{T,max}$ = anchor embedment distance of adhesive exposed to temperatures that exceed the manufacturer's maximum values, inches (m)

To illustrate that disregarding the top 2 inches (50.8 mm) in the upper temperature gradient and adding this disregarded embedment as additional overall anchor embedment does provide nominal capacities which meet the nominal reference capacities values, Table 31 is presented. The nominal compensated capacities are plotted in comparison to the nominal reference tests capacities in Figure 67. As seen per Figure 67, the nominal compensated welded test capacities do match the nominal reference test capacities, which would suggest that compensating for the adhesive exposed to maximum short-term temperatures beyond the manufacturer's maximum values, design values can be attained for adhesive anchor systems subjected to welding influences. However it should be noted, that determination of design capacity required the use of characteristic bonds stresses provided by the Manufacturer's ICC-ESRs in the relevant temperature ranges.

Table 31 – Nominal Compensated Capacities of Welded Tension Test Specimens

	Test Group					
	H	I	J	K	L	M
P_{ref}, lb. (kN)	14,043 (62.47)	19,921 (88.61)	13,715 (61.01)	20,376 (90.64)	14,874 (66.16)	35,328 (157.16)
τ_{ref}, psi (MPa)	3,251 (22.42)	2,899 (19.99)	3,175 (21.90)	2,965 (20.45)	3,443 (23.75)	3,528 (24.33)
$P_{\Delta hef}$, lb. (kN)	10,213 (45.43)	11,384 (50.64)	9,975 (44.37)	11,644 (51.79)	10,817 (48.11)	16,625 (73.96)
P'_{ref}, lb. (kN)	3,830 (17.04)	8,538 (37.98)	3,741 (16.64)	8,733 (38.85)	4,056 (18.04)	18,703 (83.20)
P_{comp}, lb. (kN)	14,043 (62.47)	19,922 (88.62)	13,716 (61.01)	20,377 (90.64)	14,873 (66.15)	35,328 (157.16)

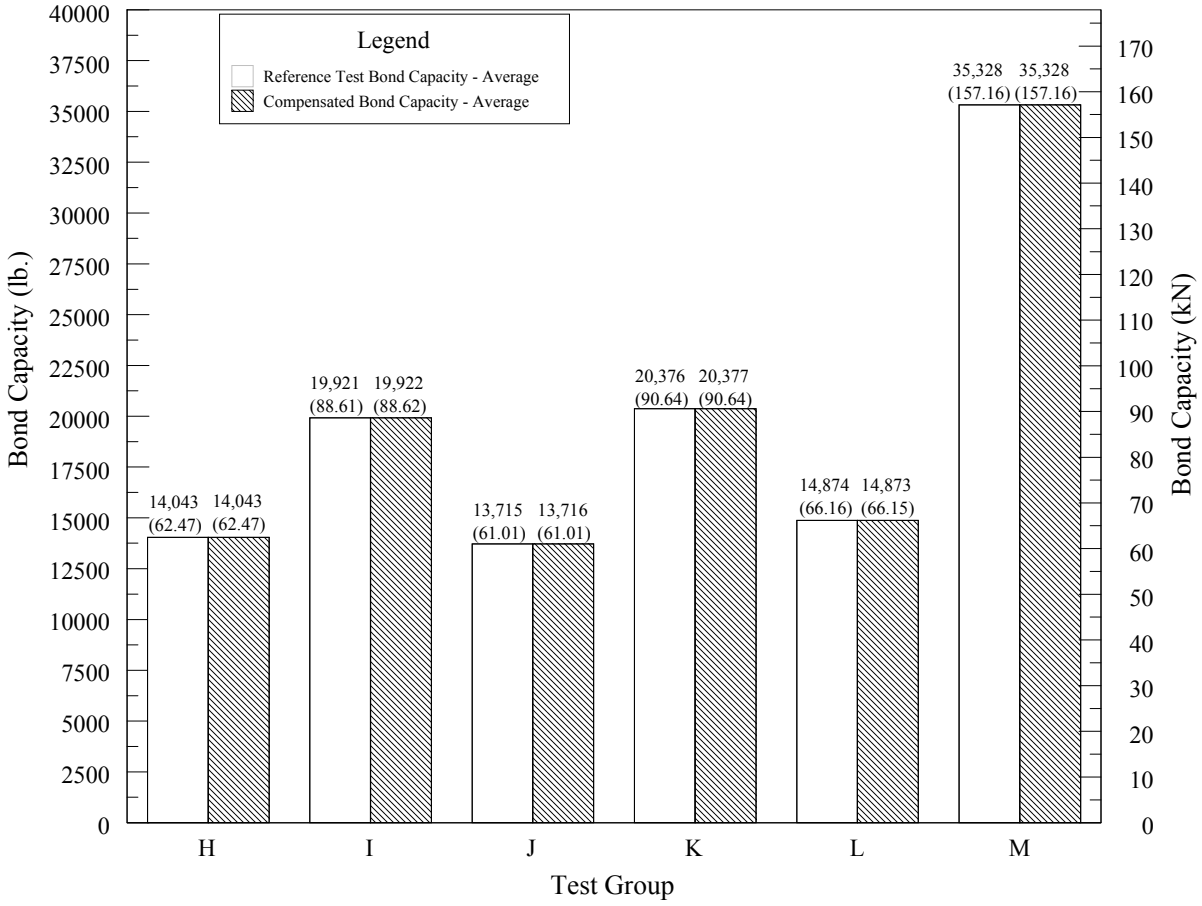

Figure 67: Comparison of Nominal Compensated Welded Test Bond Capacity Values to Nominal Reference Bond Capacity Values

Based on this suggested design philosophy, it is proposed that the temperature gradient presented in Figure 66 be used in conjunction with the adhesive manufacturer's published temperature data to establish the maximum short-term temperature range allowed for that specific adhesive anchor system. The maximum short-term temperature can be plotted as a vertical line intersecting the temperature gradient. At this intersection point, a horizontal line can be drawn to determine the amount of anchor embedment that should be disregarded at the top of the effective embedment depth. The anchor

embedment should be added as additional anchor embedment below the established horizontal line, as presented in Equation (28). It is important to note that ICC-ES ESR reports were used for the adhesive anchor systems tested in this research program; however it is critical that the manufacturer's published technical data be used that is specific to the adhesive anchoring system being considered.

The coefficient of variation for all confined static tension tests performed in this research program resulted in values of less than 15%. Per ICC-ES AC308, Sections 11.3.2.1 and 11.3.2.3 (ICC Evaluation Service, Inc. 2009), additional reduction factors are not required for the compensated welded bond stress values presented. In addition, coefficients of variation less than 15% for adhesive anchors in concrete elements are considered to be acceptable by current experience (European Organization for Technical Approvals 1997). Based on these acceptance criteria, it is suggested that current design practices apply to the adhesive anchor systems tested in this research program, even when subjected to welding influences such as those presented in this work.

CHAPTER 4

EVALUATION OF ECCETNRIC SHEAR LOAD TEST SPECIMENS

4.1 Introduction

This chapter discusses the testing procedure, collection of data, test results, and observations of the twenty four eccentric shear tests defined per Table 1 in Chapter 2. The failure loads presented in Section 4.3 are compared to the predicted failure loads and design failure loads presented in Tables 2 and 3, respectively, in Chapter 2. In addition, four core samples encompassing single steel anchor elements of the eccentric shear tests were taken. These cores were split along a diametrical axis exposing the adhesive and visually examined for any charring or discoloration experienced by the adhesive material. A discussion of the testing results and observations concludes this chapter.

4.2 Testing Procedure and Collection of Data

The eccentric shear test specimens were installed and welded as described per Section 2.5.2. Prior to testing, 4 inch x 8 inch (102 mm x 203 mm) concrete cylinders were tested to determine the compressive strength of the concrete slabs. An average 28-day compressive strength of 7,805 psi (53.83 MPa) was attained for the concrete strength at the time of testing.

Load was continuously applied to the test specimens until a failure occurred as shown in Figure 20 of Section 2.5.2. Loads for each test were recorded and saved using a data acquisition system as described in Section 2.5.2. Visual observations of the testing procedure and failure modes were recorded in a field log. The results and observed

failures as well as testing observations of the eccentric shear tests are presented in Tables 32, 33, and 34 of Section 4.3.

4.3 Results of Eccentric Shear Tests and Observations

The load test results and observed failure modes for Test Groups A, B, and C eccentric shear tests are presented in Table 32, 33, and 34, respectively. Detailed descriptions of the failure and testing observations are presented subsequent to Tables 32, 33, and 34.

Table 32: Test Group A Failure Load Values and Observed Failures

Test Number	Load at Failure, lb. (kN)	Description of Observed Failure
1	31,148 (138.6)	weld failure between the steel anchor elements and the base plate with excessive rotational displacement – no anchors fractured
2	39,115 (174.0)	weld failure between the steel anchor elements and the base plate with excessive rotational displacement – no anchors fractured
3	37,377 (166.3)	shear and tension interaction failure of top two anchors – two top anchors and one bottom anchor fractured – one bottom anchor remained in place
4	33,466 (148.9)	weld failure between the steel anchor elements and the base plate with excessive rotational displacement – no anchors fractured
5	31,144 (138.5)	shear and tension interaction failure of top two anchors – two top anchors fractured – bottom anchors remained in place
6	24,914 (110.8)	shear and tension interaction failure of top two anchors – two top anchors fractured – bottom anchors remained in place
7	25,059 (111.5)	shear and tension interaction failure of top two anchors – two top anchors fractured – bottom anchors remained in place
8	22,017 (97.9)	shear and tension interaction failure of top two anchors – two top anchors fractured – bottom anchors remained in place
	COV = 20.11%	

The load test results for Group A show a large degree of variation in load test values. The coefficient of variation for this group of tests is 20.11%, which was due to the two different types of failure modes. The first type of failure mode observed, as seen with tests one, two, and four, was a failure of the weld between the steel anchor elements and the base plate. The top (load side) portion of the base plate pulled through the welds along the steel anchor elements as seen in Figure 68. As load was continuously applied to the specimens, the base plate continued to rotate about its bottom edge, as illustrated by Figure 69. Testing was stopped when the specimens would no longer withstand an increase in applied load due to excessive rotational deformation.

Figure 68: Typical Weld Failure between Test Group A Steel Anchor Elements and Base Plate

Figure 69: Test Group A Rotational Displacement Due to Weld Failures at Steel Anchor Elements

The second type of failure mode observed was a shear and tension failure of the two load side steel anchor elements. This type of failure was observed in tests three, five, six, seven, and eight. For these five tests, the two load side anchors fractured, but the bottom (rear) anchors remained in place preventing separation of the test specimen and the concrete slab. Figure 70 shows the fracturing of the top two anchors.

Figure 70: Test Group A Shear and Tension Failure of Two Top (Load Side) Steel Anchor Elements

Though a shear and tension interaction failure of the two load side anchors occurred, the tested load values were significantly lower compared to other load test values of the test group. Projections of the two load side anchors from the concrete test slab were relatively larger compared to those of Test Group B failures, where nuts and washers were used to fasten the steel anchor elements to the base plates. Figure 71 shows the projection of a load side anchor with relation to the top surface of the concrete slab.

Figure 71: Test Group A Projection of Top (Load Side) Steel Anchor Element from Concrete Surface

Observations after testing showed the failure plane of the fractured anchors occurred near the plane of the root weld between the anchors and base plates. Specimens were removed from the slabs to examine the two fractured load side anchors. For tests three, five, six, seven, and eight, the failure planes of the anchors were located at about the midpoint of the base plate thickness, which is near the root weld applied to the steel anchor elements. Figures 72 and 73 illustrate the typical failure plane locations observed in relation to the bottom side of the base plate.

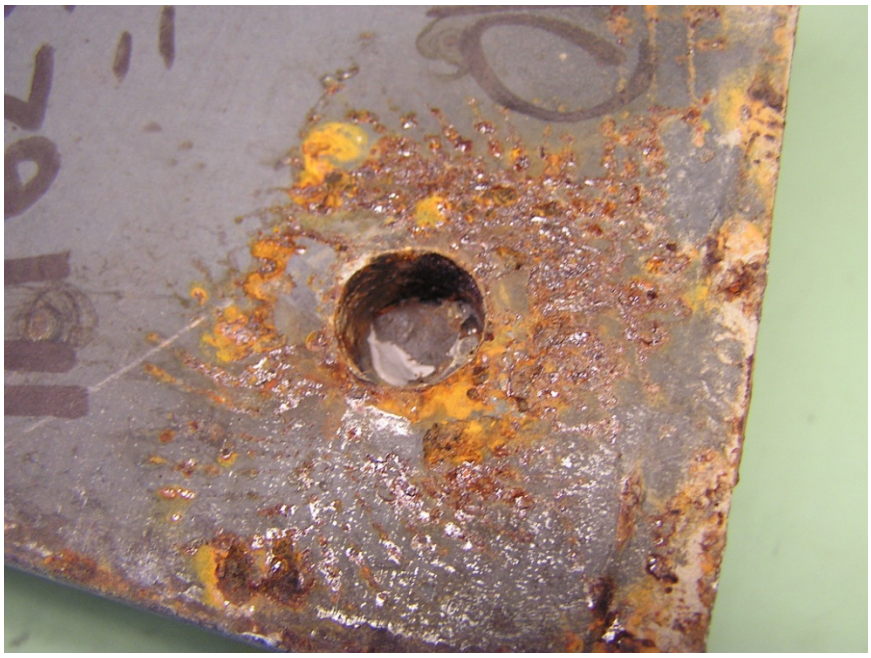

Figure 72: View of Bottom of Base Plate Showing Steel Anchor Element Failure Plane of Test Group A

Figure 73: Test Group A Steel Anchor Element Failure Plane near the Root Weld Plane

For all eight tests performed, no visual signs of any adhesive bond performance issues were present. There were no apparent displacements between the anchor system and the concrete slab. All observed failure loads were steel related, specifically regarding the weld performance, which suggests welding compatibility issues with the steel anchor elements.

Table 33: Test Group B Failure Load Values and Observed Failures

Test Number	Load at Failure, lb. (kN)	Description of Observed Failure
1	66,640 (296.4)	shear and tension interaction failure of top two anchors – all four anchors fractured – complete detachment of specimen from slab
2	63,743 (283.5)	shear and tension interaction failure of top two anchors – all four anchors fractured – complete detachment of specimen from slab
3	65,916 (293.2)	shear and tension interaction failure of top two anchors – all four anchors fractured – complete detachment of specimen from slab
4	62,873 (279.7)	weld failure between the stiffened seat and base plate – no anchors fractured
5	65,384 (290.8)	shear and tension interaction failure of top two anchors – all four anchors fractured – complete detachment of specimen from slab
6	61,031 (271.5)	shear and tension interaction failure of top two anchors – all four anchors fractured – complete detachment of specimen from slab
7	64,318 (286.1)	shear and tension interaction failure of top two anchors – all four anchors fractured – complete detachment of specimen from slab
8	65,042 (289.3)	shear and tension interaction failure of top two anchors – two top anchors fractured – bottom two anchors remained in place

COV = 2.80%

Test results for Group B were very consistent in both tested load values and observed failure modes, as the coefficient of variation of the group is 2.80%. Seven of the eight tests produced very similar failure mode behavior. Test four exhibited a weld failure between the stiffened seat and base plate, as seen in Figure 74, and is an exception to the group. Though test four resulted in a different failure mode displayed by the other seven tests of the test group, the failure load for this test was close to the other failure loads values of the group. No adhesive bond failures or bond displacements were observed during testing. The overall performance of these test specimens was controlled by the steel behavior the steel anchor elements, which was the design basis of the eccentric shear testing program.

The typical failure mode observed was a shear and tension interaction failure of the two load side anchors. Tests one, two, three, five, six, and seven all resulted in the complete detachment of the test specimen from the concrete slab. The number eight test specimen did not detach from the concrete slab, but did produce excessive bending in the two rear anchors as seen in Figure 75.

Figure 74: Test Group B Weld Failure between the Stiffened Seat and Base Plate

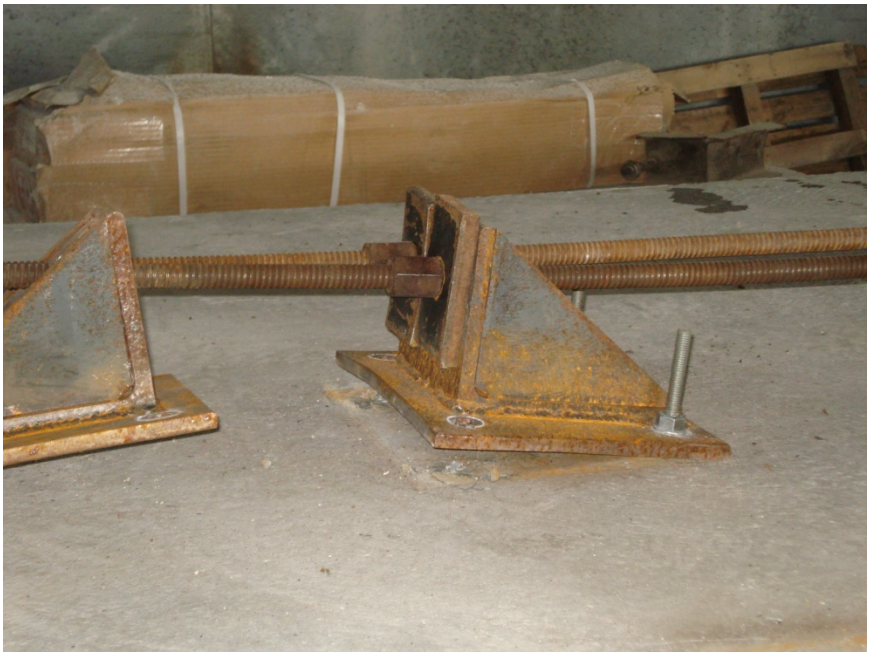

Figure 75: Observed Failure of Test Eight Specimen of Test Group B

For the common failure mode where all four anchors fractured and the specimens detached from the concrete slab, consistent anchor behavior was observed at the top

surface of the concrete slab. Top steel anchor elements exhibited cup and cone characteristics along the failure plane as well as large bending deformations near the top surface of the concrete slab as shown in Figure 76. Shallow surface concrete cone spalls due to the applied tension were also commonly observed as shown in Figure 77.

Figure 76: Typical Shear and Tension Failure Experienced by Test Group B Steel Anchor Elements

Figure 77: Concrete Cone and Spalling Observed around Top (Load Side) Steel Anchor Elements of Test Group B

Rear anchors of the common observed failure mode typically produced shear failure planes of 90 degrees to the longitudinal axis of the steel anchor elements. Since the load side anchor's shear and tension interaction capacity were the controlling component of the system, as soon as the load side anchors fractured, the entire remaining applied load on the system is transferred to the two rear anchors. The transfer of the remaining applied load then overloads the bottom two anchors, forcing a catastrophic shear failure of the two rear anchors. Figure 78 shows the shear plane exhibited by the bottom anchors of the Group B tests. Figure 79 shows a comparison of the shear and tension failure exhibited by the load side steel anchor elements and the shear failure exhibited by the rear steel anchor elements. Figure 80 summarizes the load side and rear anchor behavior of test Group B along the concrete slab surface.

Figure 78: Typical Shear Failure Experienced by Bottom (Rear) Steel Anchor Elements of Test Group B

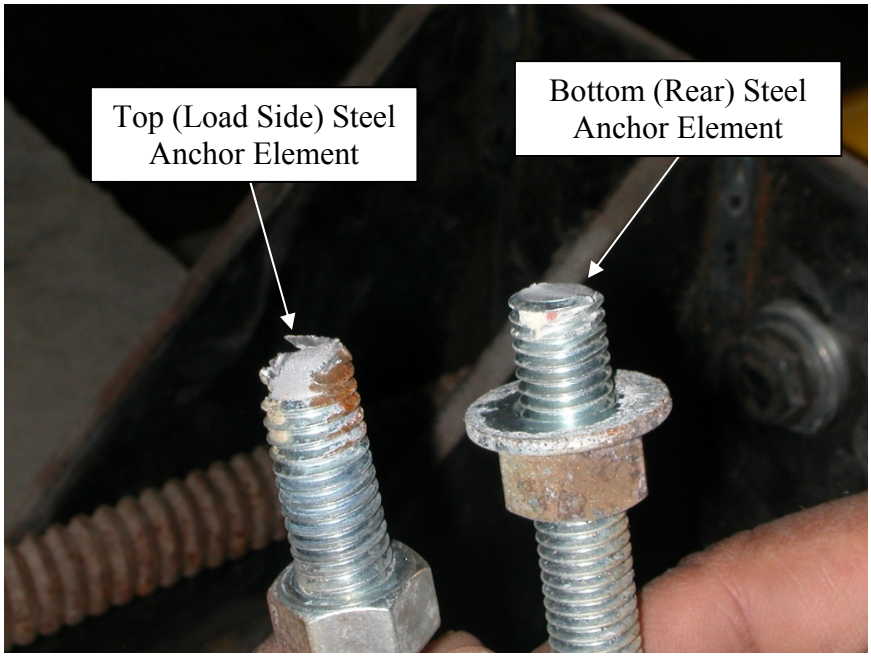

Figure 79: Comparison of Top (Load Side) and Bottom (Rear) Steel Anchor Element Failures of Test Group B

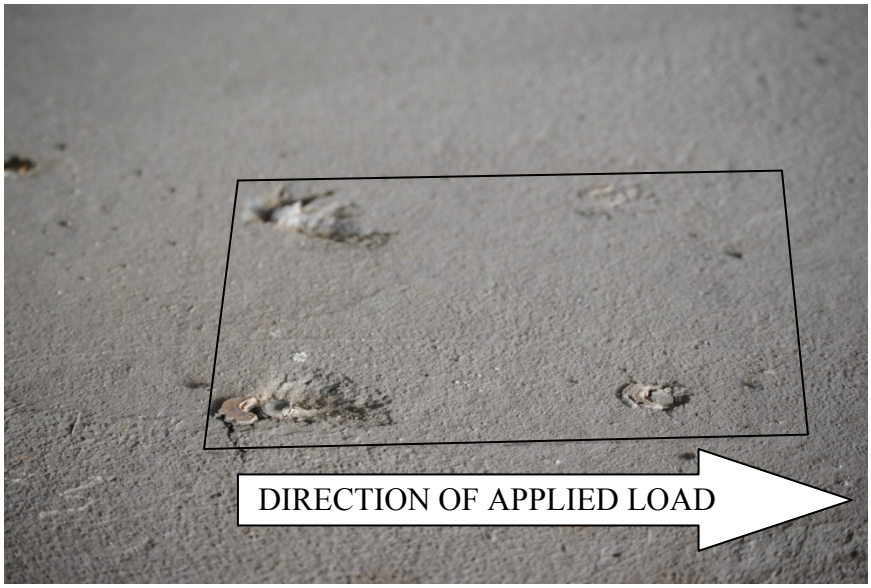

Figure 80: Typical Test Group B Steel Anchor Element Profiles at Concrete Slab Surface after Failure

Table 34: Test Group C Failure Load Values and Observed Failures

Test Number	Load at Failure, lb. (kN)	Description of Observed Failure
1	49,835 (221.7)	test stopped due to spalling of concrete between the edge of the test slab and the reaction frame – no anchors fractured
2	46,938 (208.8)	shear and tension interaction failure of top two anchors – two top anchors and one bottom anchor fractured – one bottom anchor remained in place
3	62,873 (279.7)	shear and tension interaction failure of top two anchors – all four anchors fractured – complete detachment of specimen from slab
4	57,513 (255.8)	shear and tension interaction failure of top two anchors – two top anchors fractured – two bottom anchor remained in place
5	33,755 (150.1)	shear and tension interaction failure of one top anchor – one top anchor fractured – load stopped due to inability of test specimen to take any more applied load
6	41,723 (185.6)	shear and tension interaction failure of top two anchors – two top anchors fractured – two bottom anchor remained in place
7	35,349 (157.2)	shear and tension interaction failure of one top anchor – one top anchor fractured – load stopped due to inability of test specimen to take any more applied load
8	35,783 (159.2)	shear and tension interaction failure of one top anchor – one top anchor fractured – load stopped due to inability of test specimen to take any more applied load

COV = 23.75%

The load test results for Test Group C show a large degree of variation in load test values very similar to Test Group A. The coefficient of variation for this group of tests was 23.75%, which was due to multiple types of observed failure modes. One type of failure mode observed, as seen with test one, was excessive spalling of the concrete test slab between the reaction frame supporting the hollow plunger cylinder and the edge of the concrete slab as seen in Figure 81. The test was stopped prior of the eccentric shear test specimen in order to prevent further damage to the slab.

Figure 81: Spall at Edge of Concrete Slab Experienced by Test One of Test Group C

Another type of failure mode observed was a shear and tension interaction failure of both load side anchors, as seen in tests two, three, four, and six. Test three resulted in a complete detachment of the test specimen from the concrete slab while tests two, four, and six remained attached by the rear anchors. It was observed that test three did not have the high-strength rods projecting through the stiffened seat to test specimens behind the load

side, while tests two, four, and five did. The high-strength rods helped to restrain the rotational deformation of tests two, four, and five, which may have prevented the rear anchors from becoming overloaded to a point of fracture failure. Figure 82 shows the typical shear and tension interaction failure of the two load side anchors exhibited by Test Group C.

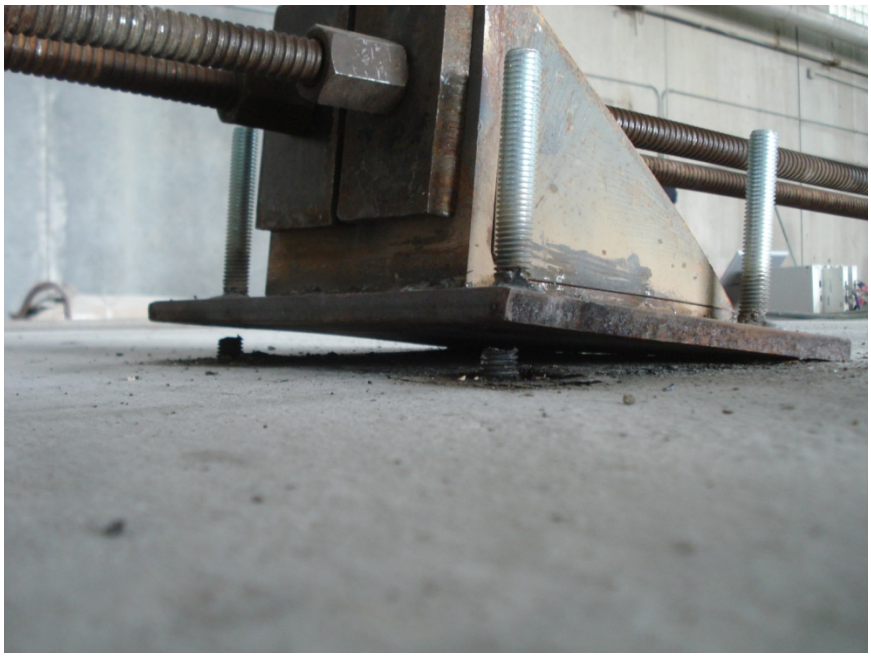

Figure 82: Test Group C Shear and Tension Failure of Two Top (Load Side) Steel Anchor Elements

Tests five, seven, and eight exhibited shear and tension failures of the load side anchors similar to tests two, three, four, and six, however, only one load side anchor fractured while the second load side anchor remained in place. The failure loads of tests five, seven, and eight are considerably lower than those of tests two, three, four, and six because testing was terminated due to test specimens' inability to take additional load. A prying deformation occurred at the same corner when the fractured steel anchor element as

additional load was applied. Figures 83 and 84 show the prying deformation located at the same corner as the fractured steel anchor element.

Figure 83: Test Group C Shear and Tension Failure of Single Top (Load Side) Steel Anchor Element

Figure 84: Prying of Corner of Test Group C Test Specimen due to Shear and Tension Failure of Single Top (Load Side) Steel Anchor Element

A similar observation was encountered with Test Group C that was experienced with Test Group A. It appeared that for tests three and six of Test Group C the failure plane of the fractured anchors occurred near the plane of the root weld between the anchors and the base plates. Test three and six specimens were removed from the slab to examine the failure planes of the fractured anchors. Examination of tests three and six produced similar findings to tests three, five, six, seven, and eight from Test Group A. The failure planes of the anchors were located at about the midpoint of the base plate thickness, which is near the root weld applied between the steel anchor elements and the base plates. The anchor projections of the fractured load side anchors out the top surface of the concrete slab were similar to those experienced by Test Group A. Figure 85 shows the anchor projections from one of the removed test specimens of Test Group C. Figures

86 and 87 illustrate the typical failure plane locations observed in relation to the bottom side of the base plates for Test Group C.

Figure 85: Test Group C Projection of Top (Load Side) Steel Anchor Elements from Concrete Surface

Figure 86: View of Bottom of Base Plate Showing Steel Anchor Element Failure Plane of Test Group C

Figure 87: Test Group C Steel Anchor Element Failure Plane near the Root Weld Plane

For all of the tests resulting in steel anchor element failures in Test Group C, no visual signs of any adhesive bond performance issues were present. Similar to the observations of Test Group A, no observed displacements between the adhesive anchor system and the concrete slab in Test Group C were discovered. Seven of the eight failure loads were steel related. Tests three and six appeared to relate to the welding performance between the steel anchor element and the base plate, which further suggests welding compatibility issues with the ASTM F 568M Class 5.8 steel anchor elements.

4.4 Comparison of Load Tests versus Predicted Capacities and Design Values

Table 35 compares the load test values obtained in Section 4.3 to the predicted failure loads of Table 2 and design values of Table 3 presented in Chapter 2. Table 35 presents a summary eccentric shear tests load values of Section 4.3 as well as the percentage of the predicted failure load and design load values the tested load values attained. In addition to Table 35, Figures 88, 89, and 90 are presented to graphically compare the tested loads values to both the predicted failure load values and design values.

For Test Group A, three of the eight tests did not meet or exceed the design load value of 28,007 lb. (124.6 kN) (Chapter 2, Table 3). The average load test value of the group did exceed the design load value, at 30,530 lb. (135.8 kN) but only by a 9.0% margin. All eight tests of Test Group A fell significantly short of meeting or exceeding the predicted failure load value. The average tested load value was 32.6% less than the predicted failure value (Chapter 2, Table 2). The observed fracture planes along the root weld plane of tests three, five, six, seven, and eight the predominantly low tested load values of tests six, seven, and eight weighed heavily on this large variation. Figure 88

shows a plot of the tested load values of Test Group A and illustrates the large variations in test values as well as the considerably large deviations from the predicted and design load values.

Table 35: Comparison of Eccentric Shear Tests Failure Loads to Design Loads and Predicted Loads

Test Group	Test	Tested Failure Load, lb. (kN)	% of Design Load Attained	% of Predicted Failure Load Attained
A	1	31,148 (138.6)	111.2%	68.8%
	2	39,115 (174.0)	139.7%	86.4%
	3	37,377 (166.3)	133.5%	82.6%
	4	33,466 (148.9)	119.5%	73.9%
	5	31,144 (138.5)	111.2%	68.8%
	6	24,914 (110.8)	89.0%	55.0%
	7	25,059 (111.5)	89.5%	55.4%
	8	22,017 (97.9)	78.6%	48.6%
	Average	30,530 (135.8)	109.0%	67.4%
B	1	66,640 (296.4)	225.1%	101.3%
	2	63,743 (283.5)	215.3%	96.9%
	3	65,916 (293.2)	222.6%	100.2%
	4	62,873 (279.7)	212.4%	95.6%
	5	65,384 (290.8)	220.8%	99.4%
	6	61,031 (271.5)	206.1%	92.8%
	7	64,318 (286.1)	217.2%	97.8%
	8	65,042 (289.3)	219.7%	98.9%
	Average	64,368 (286.3)	217.4%	97.9%
C	1	49,835 (221.7)	116.5%	72.1%
	2	46,938 (208.8)	109.7%	67.9%
	3	62,873 (279.7)	146.9%	90.9%
	4	57,513 (255.8)	134.4%	83.2%
	5	33,755 (150.1)	78.9%	48.8%
	6	41,723 (185.6)	97.5%	60.3%
	7	35,349 (157.2)	82.6%	51.1%
	8	35,783 (159.2)	83.6%	51.8%
	Average	45,471 (202.3)	106.3%	65.8%

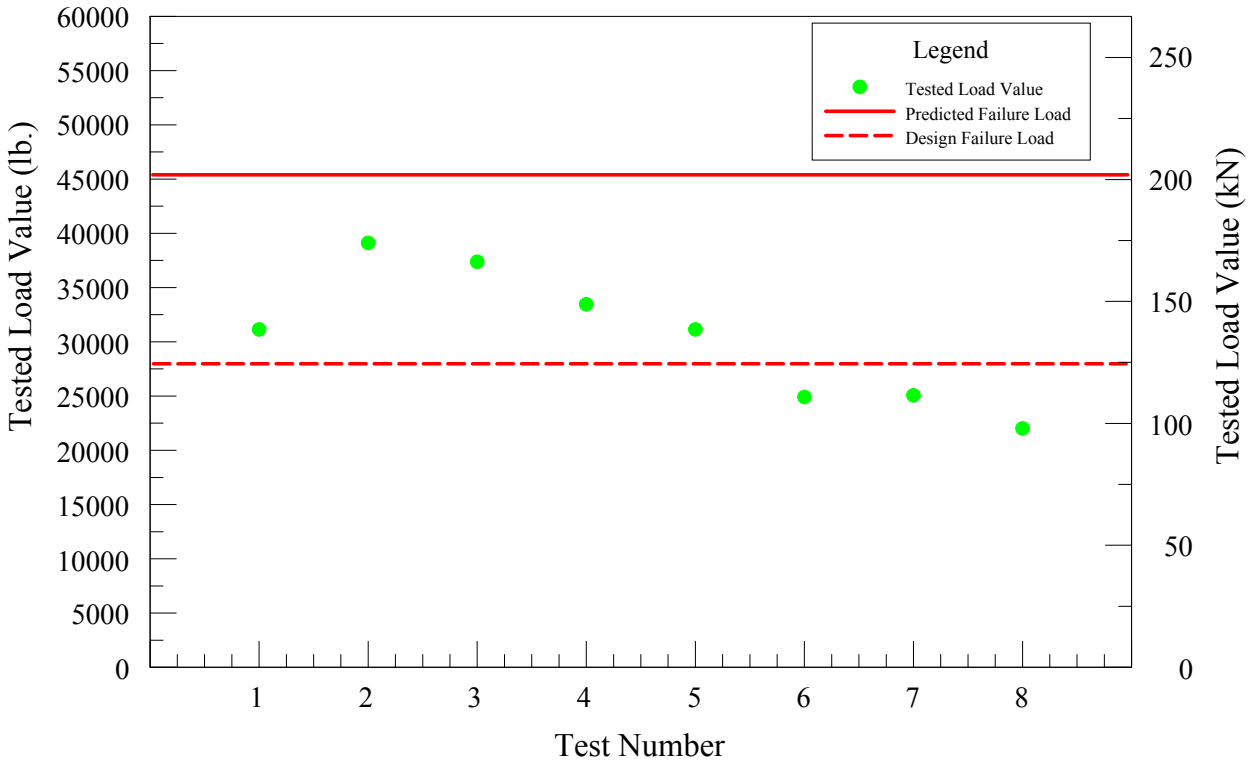

Figure 88: Plot of Test Group A Tested Load Values Compared to Predicted and Design Failure Loads

The load test results from Test Group B were very consistent in comparison to Test Groups A and C. All eight tests exceeded the design value by an average of 217.4%. It is important to note that this was due to the limitation of the specified tensile strength of the steel anchor elements by Sections D.5.1.2 and D.6.1.2 of ACI318-11.

Figure 89 plots the tested load values of Test Group B, and illustrates the small variations in test values as well as the considerably small deviations from the predicted load value. It also important to note that the predicted load values of Test Group B were based upon the actual tensile strength of the steel anchor elements as tested and presented

in Section 2.6. This is why there is a larger gap between the design value and predicted load value of Figure 89 as compared to Figures 88 and 90.

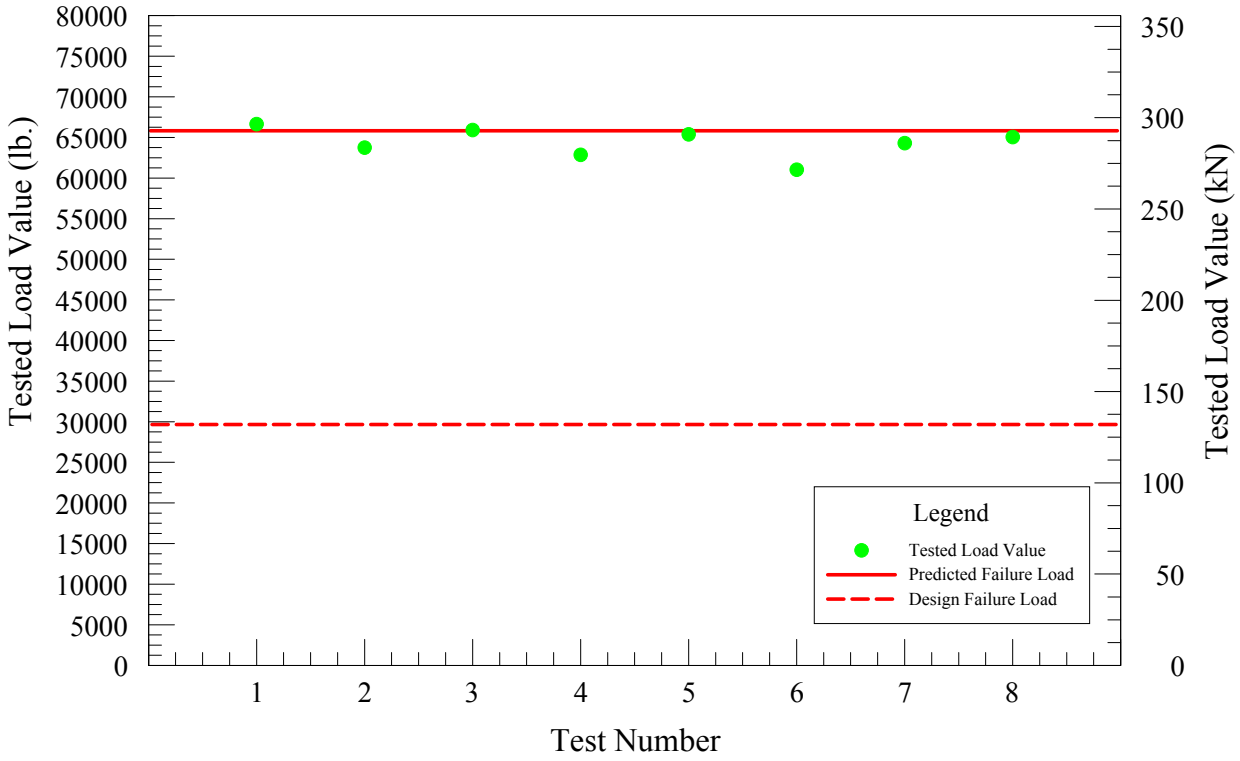

Figure 89: Plot of Test Group B Tested Load Values Compared to Predicted and Design Failure Loads

The results of Test Group C were similar to Test Group A. For Test Group C, four of the eight tests did not meet or exceed the design load value of 42,787 lb. (190.3 kN) (Chapter 2, Table 3). The average load test value of the group exceeded the design load of the group only by a 6.3% margin. All eight of the tested load values in this group were significantly below the predicted failure load, with an average tested load value 34.2% below the predicted failure load (Chapter 2, Table 2). This is a slightly larger margin than that exhibited by Test Group A.

The large variations and deviations from the predicted failure loads in Test Group C were due to the inconsistent failure modes observed in this test group. Tests five, seven, and eight played a significant role in the test group variation, as these three tests were stopped due the failure of only one load side anchor. Figure 90 shows a plot of the tested load values of Test Group C, and illustrates the large variations in test values as well as well as the considerably large deviations from the predicted and design load values.

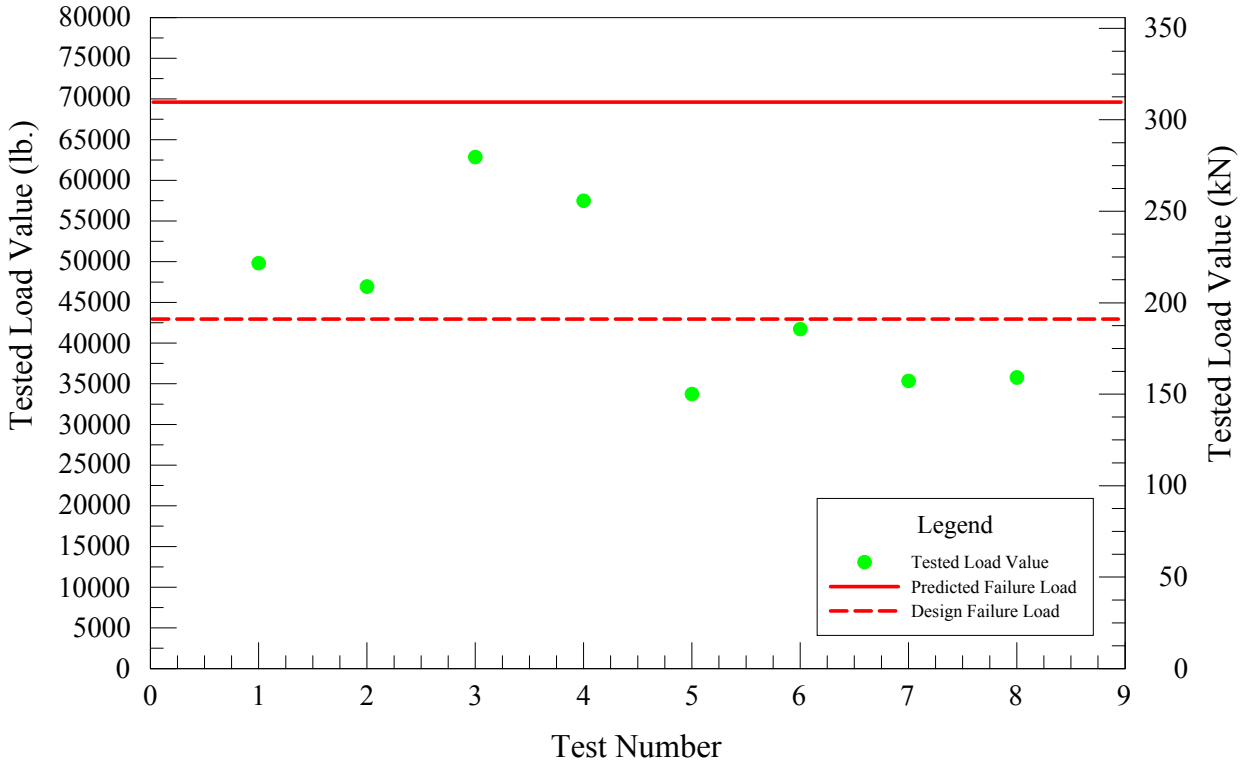

Figure 90: Plot of Test Group C Tested Load Values Compared to Predicted and Design Failure Loads

4.5 Evaluation of Split Core Samples

After testing was complete on the first eight load tests, four split cores samples were taken from the concrete slab to visually observe the adhesive surrounding the steel anchor element after welding and load exposure. The split cores were taken using a concrete drill with a wet diamond core bit then scored and split along the diametrical axis exposing the adhesive. Figure 91 shows the four cores prior to being scored and split. These core locations were taken from Test Groups A and B. Table 36 provides the specific locations of where the split cores where taken.

Figure 91: Four Core Samples taken from Test Groups A and B

Table 36: Reference of Split Core Locations

Split Core Number	Load Test Reference	Anchor Location
1	Test Group A – Test 1	Bottom (Rear)
2	Test Group B – Test 2	Top (Load Side)
3	Test Group B – Test 2	Bottom (Rear)
4	Test Group A – Test 3	Top (Load Side)

Based on visual observations, the adhesive appeared to show no signs of charring in all four split core samples. There appeared to be no discoloration of the adhesive along the entire length of all four cores. Figures 92 through 95 show the split cores referenced in Table 36. Some of the split core samples appear to have some adhesive delaminating from the steel anchor elements, such as shown in Figures 92, 93, and 94. It is important to note that this was induced by the prying action needed to remove half the concrete from the core, and not by welding influences.

Figure 92: Split Core One

Figure 93: Split Core Two

Figures 94: Split Core Three

Figure 95: Split Core Four

4.6 Discussion

Test Group B resulted in consistent failure modes that well represented the predicted failure loads, while Test Groups A and C resulted in inconsistent failure modes. Though Test Groups A and C resulted in some shear and tension failures of the load side anchors, large deviations from the predicted failure and design loads existed. This suggests that using the nut and washer fastening of the steel anchor elements to the steel base plates is a better design than welding the steel anchor elements to the steel base plates. The similar coefficients of variation, percentage of predicted and design loads attained, and similarities in the observed failures of Test Groups A and C, as well as the low coefficient of variation and consistent test results of Test Group B help reinforce this conjecture.

Based on the observations of tests three, five, six, seven, and eight of Test Group A, and tests three and six of Test Group C, there appears to be welding compatibility concerns for the ASTM F 568M Class 5.8 material. Consistent test results and low coefficient of variation of Test Group B confirms the concern of welding compatibility issues with the steel anchor elements.

The split cores were important in verifying that the adhesive is capable of enduring welding exposure. A visual inspection of the four split core samples taken from Test Groups A and B showed no signs of charring or discoloration. This suggests that welding applications using the hybrid adhesive anchoring system is acceptable for fastening conditions that use nuts and washers. It also suggests that directly welding to the steel anchor elements is acceptable, if the steel anchor elements show adequate welding compatibility.

CHAPTER 5

EVALUATION OF TEMPRATURE GRADIENT TEST SPECIMENS

5.1 Introduction

This chapter discusses the testing procedure, collection of data, test results, and observations of the twenty temperature gradient tests defined per Table 7 in Chapter 2. A brief description of the testing procedure and data collection means and methods are presented in Section 5.2. Descriptions of test observations are given with test results in Section 5.3. A discussion of the test results and observations is included as Section 5.4.

5.2 Testing Procedure and Collection of Data

The temperature gradient tests were installed as described in Section 2.7. Thermocouples were pre-attached to the steel anchor elements prior to installation, as described in Section 2.7.1. The thermocouples placed along the steel anchor elements correlated the predetermined locations shown in (a) and (b) of Figure 24. The adhesive anchor system was installed with the thermocouples projecting out the annular gap past the top surface of the concrete slab and allowed to cure per the manufacturer's printed installation instructions.

The temperature gradient testing required three people to complete. One certified welder and two others to monitor the handheld thermocouple thermometers and record data as described in Section 2.7.1. For Test Groups D and F, as described in Table 7, welding of the steel anchor elements to the base plates occurred prior to the welding of the stiffened seats to the base plates. For Test Groups E and G the nut and washer fasteners

were applied to the steel anchor elements and then the stiffened seats were welded to the base plates.

Temperature data for all tests was recorded after the completion of welding to ensure no increase in maximum temperatures occurred at thermocouples located at deeper anchor embedments. Figure 96 shows the general testing arrangement during the temperature gradient testing.

Figure 96: General Arrangement of Temperature Gradient Testing

5.3 Results of Temperature Gradient Tests and Observations

The maximum temperature test results for Test Groups D, E, F, and G temperature gradient tests are presented in Tables 37 through 44. Each test group is represented by two tables. One table representing the maximum temperatures recorded along the top (front) anchors of the test specimens and one table representing the maximum

temperatures recorded along the bottom (rear) anchors of the test specimens. Temperature gradient plots, similar to those presented in Chapter 3, follow each table of maximum temperature results. A brief discussion of the test results and observations is presented with each table and plot component.

Table 37: Test Group D Recorded Maximum Temperatures at Top (Front) Anchors

	Maximum Recorded Temperatures, °F (°C)				
Thermocouple Location, in. (mm)	Test 1	Test 2	Test 3	Test 4	Test 5
+4.0 (+102)	215 (102)	419 (215)	387 (197)	434 (223)	506 (263)
-0.5 (-13)	194 (90)	170 (77)	221 (105)	157 (69)	189 (87)
-1.75 (-45)	91 (33)	81 (27)	98 (37)	93 (34)	89 (32)
-3.0 (-76)	68 (20)	76 (24)	67 (19)	66 (19)	68 (20)
-6.0 (-152)	55 (13)	53 (12)	54 (12)	55 (13)	54 (12)
Maximum Recorded Temperatures in Surrounding Concrete, °F (°C)					
Surface (0)	55 (13)	55 (13)	56 (13)	55 (13)	58 ()
-3.0 (-76)	55 (13)	54 (12)	60 (16)	55 (13)	55 (13)
-6.0 (-152)	52 (11)	51 (11)	55 (13)	52 (11)	53 (12)
Initial Base Material Temperature, °F (°C)				51 (11)	

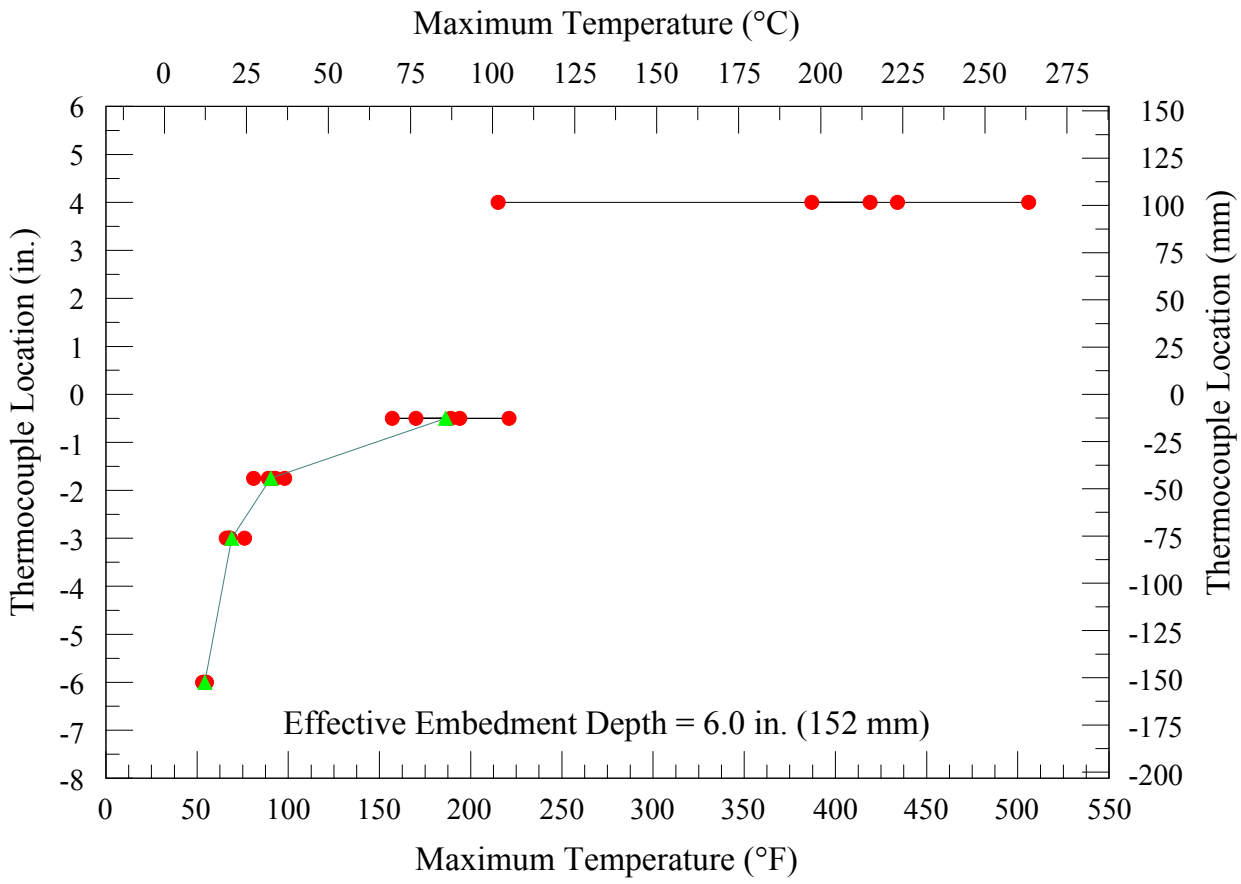

Figure 97: Weld Temperature Gradient for Test Group D Top (Front) Anchors

Table 38: Test Group D Recorded Maximum Temperatures at Bottom (Rear) Anchors

	Maximum Recorded Temperatures, °F (°C)				
Thermocouple Location, in. (mm)	Test 1	Test 2	Test 3	Test 4	Test 5
+4.0 (+102)	384 (196)	348 (176)	383 (195)	396 (202)	491 (255)
-0.5 (-13)	210 (99)	179 (82)	168 (76)	229 (109)	231 (111)
-1.75 (-45)	96 (36)	90 (32)	85 (29)	100 (38)	85 (29)
-3.0 (-76)	66 (19)	63 (17)	64 (18)	66 (19)	69 (21)
-6.0 (-152)	54 (12)	53 (12)	54 (12)	54 (12)	54 (12)
Maximum Recorded Temperatures in Surrounding Concrete, °F (°C)					
Surface (0)	57 (14)	61 (16)	55 (13)	55 (13)	58 (14)
-3.0 (-76)	52 (11)	53 (12)	54 (12)	53 (12)	56 (13)
-6.0 (-152)	51 (11)	51 (11)	51 (11)	51 (11)	52 (11)
Initial Base Material Temperature, °F (°C)				51 (11)	

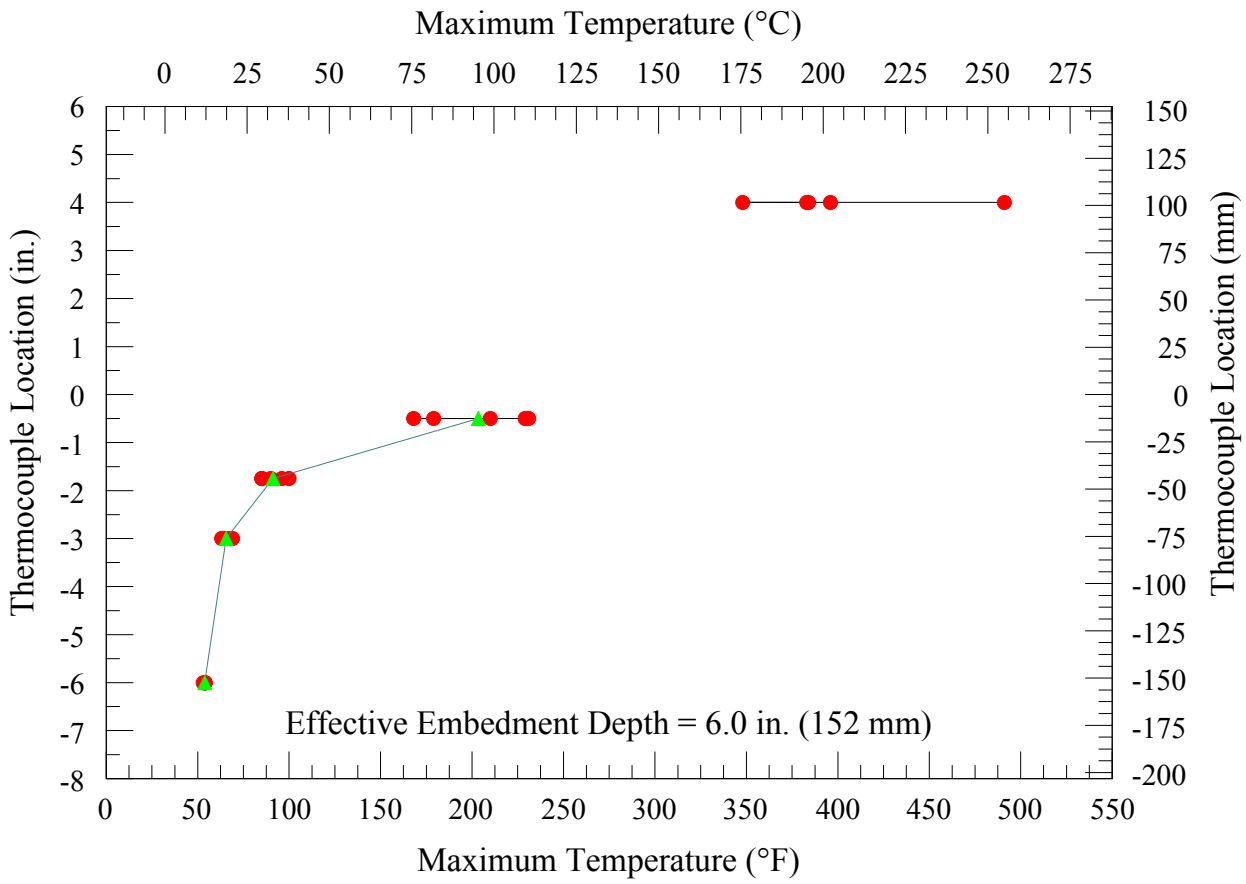

Figure 98: Weld Temperature Gradient for Test Group D Bottom (Rear) Anchors

Both the top (front) and bottom (rear) steel anchor elements of Test Group D experienced similar maximum temperatures at all thermocouple locations. Variance in maximum temperatures decreased as the effective anchor embedment into the concrete slab increased. The top of the front anchor projecting into free air above the surface of the concrete slab experienced a greater variance in maximum temperatures. This was most likely due to presence of return weld at the front of the stiffened seat element. The return weld, as shown per Figure 15 of Chapter 2, most likely subjected the front anchors projecting above the concrete surface to greater welding temperatures than the rear

anchors. Maximum temperatures recorded in the concrete surrounding the adhesive anchoring system experienced little increase in temperature from the initial base value.

Table 39: Test Group E Recorded Maximum Temperatures at Top (Front) Anchors

	Maximum Recorded Temperatures, °F (°C)				
Thermocouple Location, in. (mm)	Test 1	Test 2	Test 3	Test 4	Test 5
+4.0 (+102)	105 (41)	97 (36)	90 (32)	94 (34)	107 (42)
-0.5 (-13)	86 (30)	88 (31)	78 (26)	78 (26)	85 (29)
-1.75 (-45)	64 (18)	106 (41)	56 (13)	54 (12)	58 (14)
-3.0 (-76)	46 (8)	46 (8)	46 (8)	45 (7)	46 (8)
-6.0 (-152)	40 (4)	40 (4)	41 (5)	40 (4)	41 (5)
Maximum Recorded Temperatures in Surrounding Concrete, °F (°C)					
Surface (0)	44 (7)	49 (9)	45 (7)	52 (11)	49 (9)
-3.0 (-76)	41 (5)	41 (5)	41 (5)	41 (5)	46 (8)
-6.0 (-152)	40 (4)	40 (4)	40 (4)	41 (5)	41 (5)
Initial Base Material Temperature, °F (°C)				39 (4)	

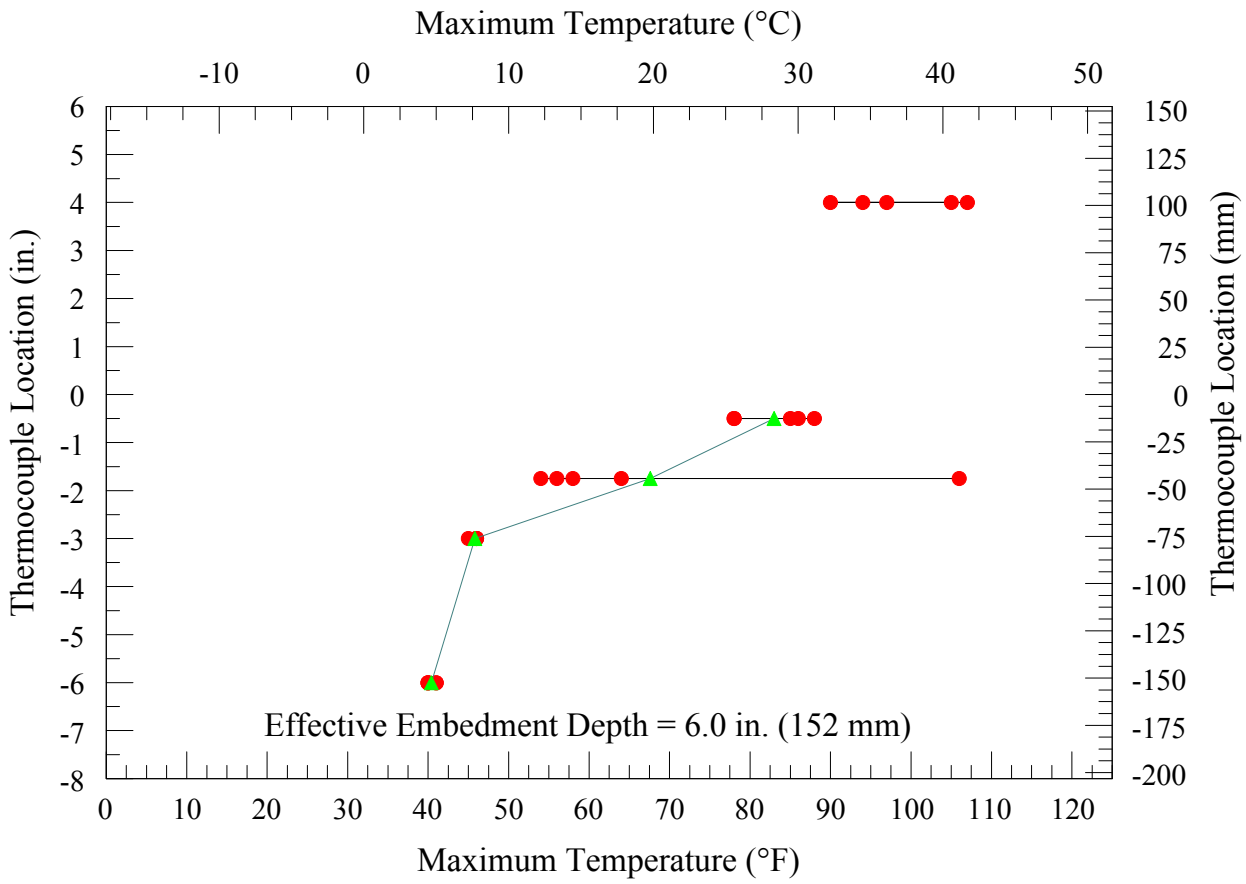

Figure 99: Weld Temperature Gradient for Test Group E Top (Front) Anchors

As seen in Table 39 and Figure 99 for Test Group E Test 2, the maximum recorded temperature at the thermocouple located at 1.75 inches (45 mm) below the concrete surface was significantly higher than the other four tests. This was most likely due to breakage of the wire securing the thermocouple to the steel anchor element where the thermocouple was shifted closer to the surface when the anchor was installed into the concrete borehole. All other maximum temperatures experienced by the steel anchor element are relatively close to the other four tests' maximum temperature values.

Table 40: Test Group E Recorded Maximum Temperatures at Bottom (Rear) Anchors

	Maximum Recorded Temperatures, °F (°C)				
Thermocouple Location, in. (mm)	Test 1	Test 2	Test 3	Test 4	Test 5
+4.0 (+102)	75 (24)	89 (32)	139 (59)	78 (26)	89 (32)
-0.5 (-13)	65 (18)	79 (26)	79 (26)	64 (18)	78 (26)
-1.75 (-45)	48 (9)	57 (14)	55 (13)	49 (9)	55 (13)
-3.0 (-76)	43 (6)	46 (8)	45 (7)	43 (6)	46 (8)
-6.0 (-152)	39 (4)	39 (4)	40 (4)	40 (4)	41 (5)
Maximum Recorded Temperatures in Surrounding Concrete, °F (°C)					
Surface (0)	52 (11)	45 (7)	46 (8)	46 (8)	45 (7)
-3.0 (-76)	41 (5)	41 (5)	41 (5)	41 (5)	42 (6)
-6.0 (-152)	39 (4)	40 (4)	41 (5)	40 (4)	41 (5)
Initial Base Material Temperature, °F (°C)				39 (4)	

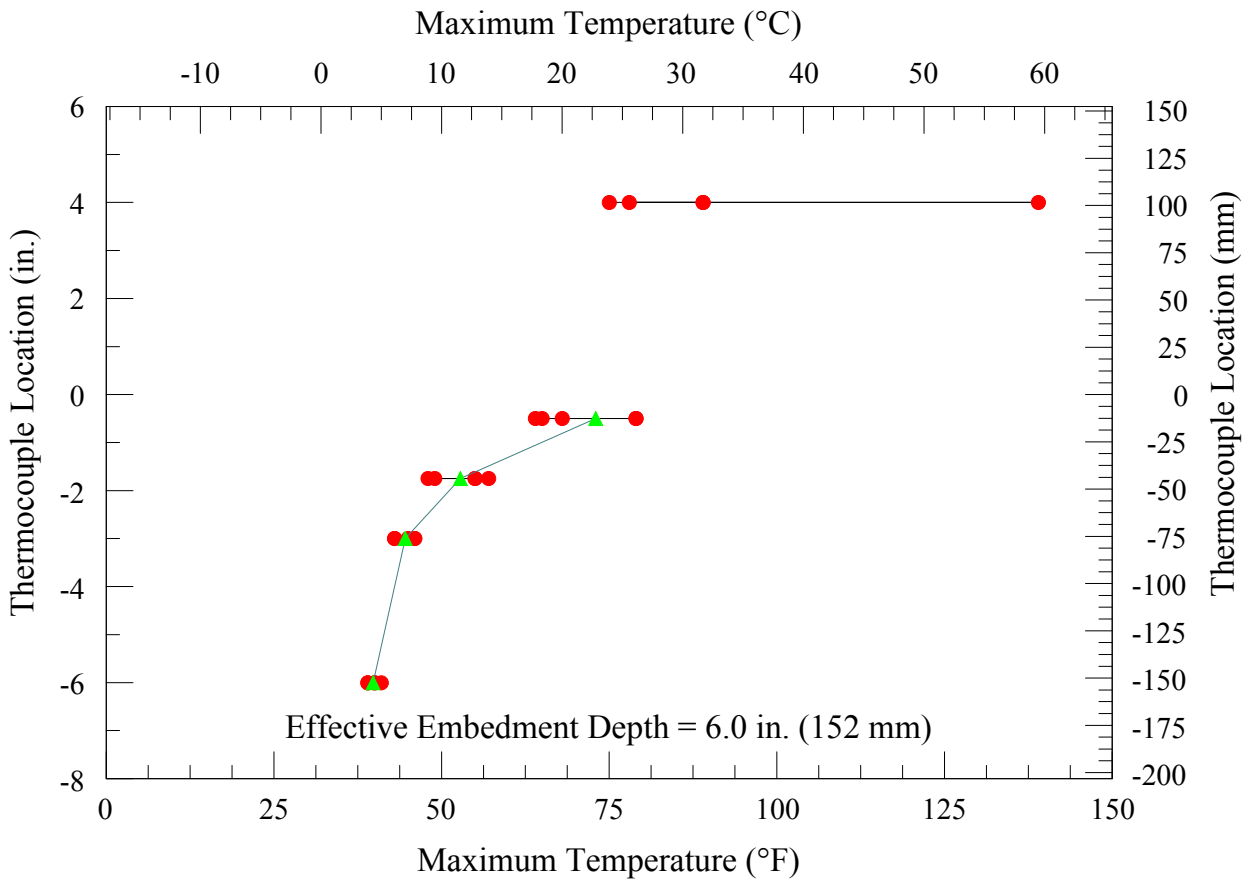

Figure 100: Weld Temperature Gradient for Test Group E Bottom (Rear) Anchors

Both the front and rear steel anchor elements of Test Group E experienced similar maximum temperatures at all thermocouples locations. Variance in maximum temperatures decreased as the effective anchor embedment into the concrete slab increased. For the front anchor, at a distance of 0.5 inches (13 mm) below the concrete surface, slightly greater maximum temperatures than the rear anchor were recorded. Again, this was most likely due to presence of return weld at the front of the stiffened seat element. For temperatures recorded at distances greater than 0.5 inches (13 mm) below the concrete surface, consistent and relatively similar maximum temperatures were recorded along the steel anchor element. Maximum temperatures recorded in the concrete

surrounding the adhesive anchoring system experienced very little increase in temperature from the initial base value.

Both front and rear anchors of Test Group D experienced larger maximum recorded temperatures than Test Group E at thermocouple locations 0.5 inches (13 mm) and 1.75 inches (45 mm) below the concrete surface. Intuitively, this makes sense as the anchors of Test Group D experienced direct welding for fastening to the base plates, where nuts and washers were used in Test Group E. For thermocouple locations located at 3 inches (76 mm) and 6 inches (152 mm) below the concrete surface, relatively low increases were experienced for both Test Groups D and E. A maximum average increase of 18° F (9.4° C) and 3.2° F (1.4° C) from the initial base material temperature occurred at 3 inches (76 mm) and 6 inches (152 mm) below the concrete surface, respectively.

Table 41: Test Group F Recorded Maximum Temperatures at Top (Front) Anchors

	Maximum Recorded Temperatures, °F (°C)				
Thermocouple Location, in. (mm)	Test 1	Test 2	Test 3	Test 4	Test 5
+4.5 (+114)	375 (191)	372 (189)	357 (181)	323 (162)	274 (134)
-0.5 (-13)	401 (205)	489 (254)	435 (224)	421 (216)	394 (201)
-2.125 (-54)	133 (56)	149 (65)	149 (65)	145 (63)	118 (48)
-3.75 (-95)	75 (24)	77 (25)	79 (26)	79 (26)	71 (22)
-7.5 (-191)	56 (13)	56 (13)	56 (13)	56 (13)	55 (13)
Maximum Recorded Temperatures in Surrounding Concrete, °F (°C)					
Surface (0)	61 (16)	77 (25)	62 (17)	61 (16)	60 (16)
-3.0 (-76)	56 (13)	58 (14)	58 (14)	57 (14)	57 (14)
-6.0 (-152)	52 (11)	52 (11)	53 (12)	52 (11)	53 (12)
Initial Base Material Temperature, °F (°C)				51 (11)	

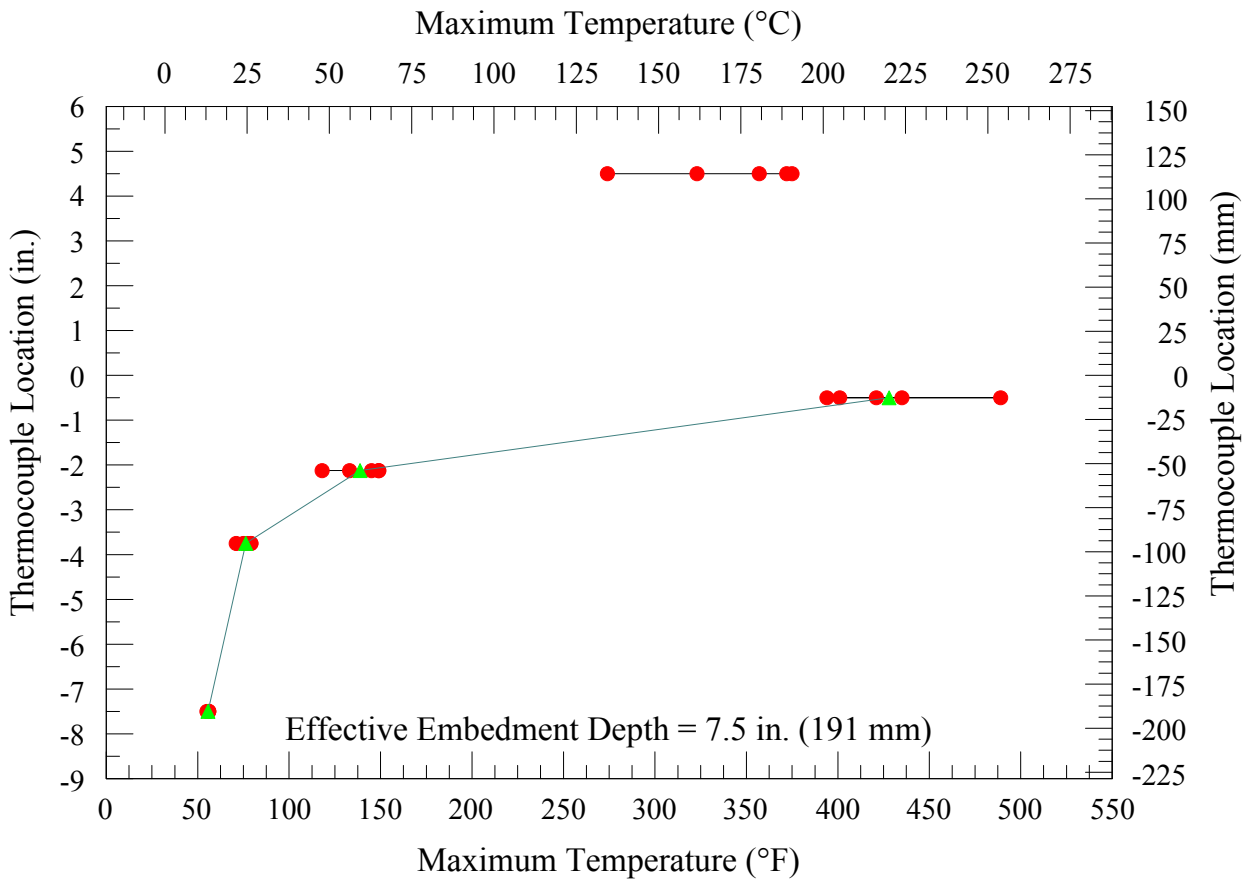

Figure 101: Weld Temperature Gradient for Test Group F Top (Front) Anchors

The front anchors of Test Group F experienced the largest recorded maximum temperatures experienced by all of the test groups. This almost certainly coincides with the larger fillet weld size required for the larger 0.625 inch (15.9 mm) diameter steel anchor elements of the test group. The maximum recorded temperatures at thermocouple locations were relatively consistent and variance in maximum temperatures decreased as the effective anchor embedment into the concrete slab increased as has been observed with all test groups.

Table 42: Test Group F Recorded Maximum Temperatures at Bottom (Rear) Anchors

	Maximum Recorded Temperatures, °F (°C)				
Thermocouple Location, in. (mm)	Test 1	Test 2	Test 3	Test 4	Test 5
+4.5 (+114)	369 (187)	359 (182)	332 (167)	312 (156)	338 (170)
-0.5 (-13)	312 (156)	326 (163)	394 (201)	380 (193)	316 (158)
-2.125 (-54)	115 (46)	138 (59)	139 (59)	118 (48)	122 (50)
-3.75 (-95)	71 (22)	76 (24)	78 (26)	73 (23)	73 (23)
-7.5 (-191)	54 (12)	55 (13)	55 (13)	55 (13)	56 (13)
Maximum Recorded Temperatures in Surrounding Concrete, °F (°C)					
Surface (0)	57 (14)	64 (18)	60 (16)	61 (16)	61 (16)
-3.0 (-76)	54 (12)	56 (13)	55 (13)	56 (13)	59 (15)
-6.0 (-152)	51 (11)	51 (11)	52 (11)	52 (11)	53 (12)
Initial Base Material Temperature, °F (°C)				51 (11)	

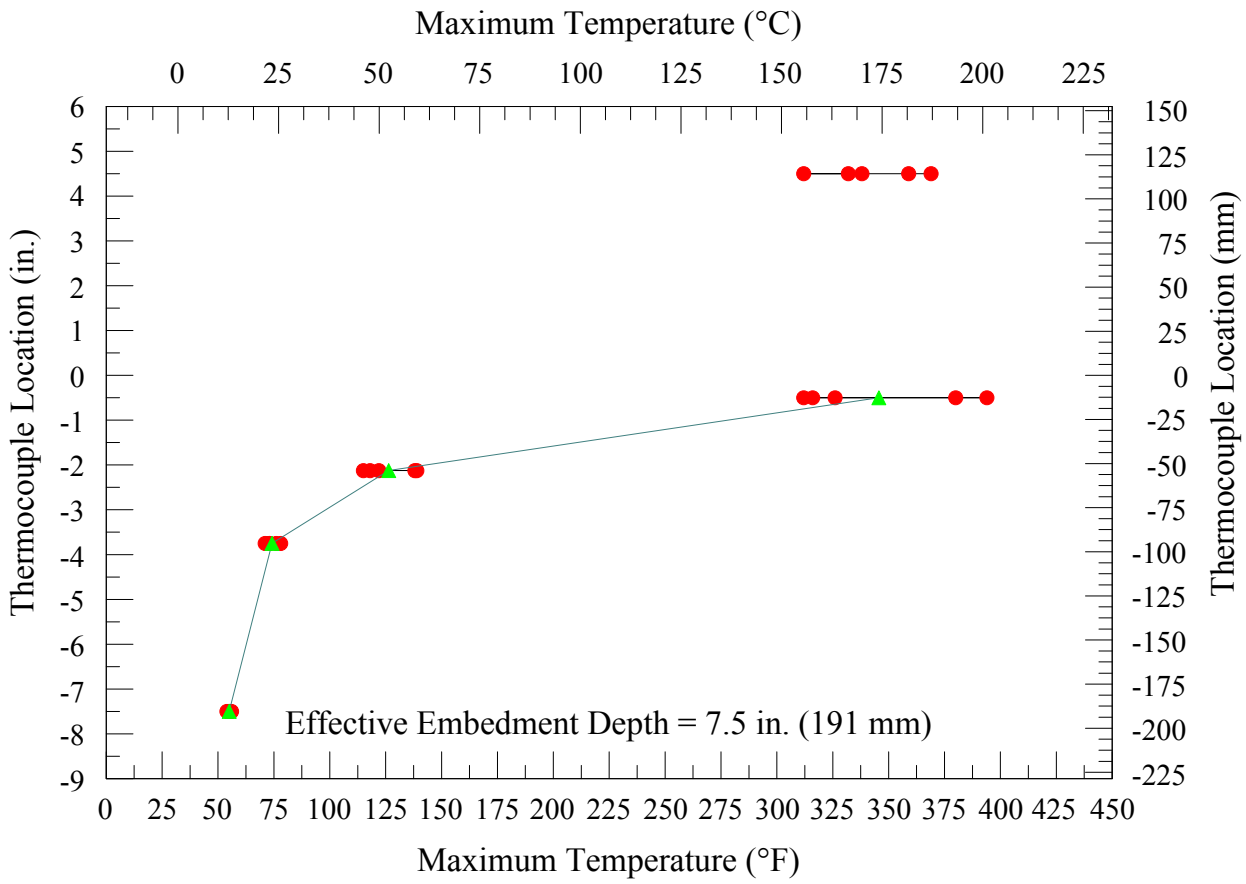

Figure 102: Weld Temperature Gradient for Test Group F Bottom (Rear) Anchors

The rear anchors of Test Group F experienced the second largest recorded maximum temperatures experienced by all of the test groups. This reinforces that the larger fillet weld size required for the larger 0.625 inch (15.9 mm) diameter steel anchor elements of the test group increase the maximum temperatures experienced by the steel anchor elements during welding. Even though the front and rear anchors of Test Group F experienced the largest maximum temperatures of all the test groups, the maximum temperatures dropped significantly at a distance of 2.125 inches (54 mm) below the concrete surface and the maximum temperatures recorded in the concrete surrounding the

adhesive anchoring system experienced very little increase in temperature from the initial base value, which is a common observation of all the test groups.

Table 43: Test Group G Recorded Maximum Temperatures at Top (Front) Anchors

	Maximum Recorded Temperatures, °F (°C)				
Thermocouple Location, in. (mm)	Test 1	Test 2	Test 3	Test 4	Test 5
+4.5 (+114)	104 (40)	94 (34)	97 (36)	102 (39)	112 (44)
-0.5 (-13)	130 (54)	119 (48)	141 (61)	114 (46)	119 (48)
-2.125 (-54)	63 (17)	60 (16)	71 (22)	59 (15)	67 (19)
-3.75 (-95)	46 (8)	45 (7)	61 (16)	44 (7)	48 (9)
-7.5 (-191)	41 (5)	39 (4)	45 (7)	38 (3)	59 (15)
Maximum Recorded Temperatures in Surrounding Concrete, °F (°C)					
Surface (0)	39 (4)	41 (5)	43 (6)	46 (8)	44 (7)
-3.0 (-76)	38 (3)	42 (6)	39 (4)	48 (9)	45 (7)
-6.0 (-152)	39 (4)	38 (3)	39 (4)	43 (6)	47 (8)
Initial Base Material Temperature, °F (°C)				35 (2)	

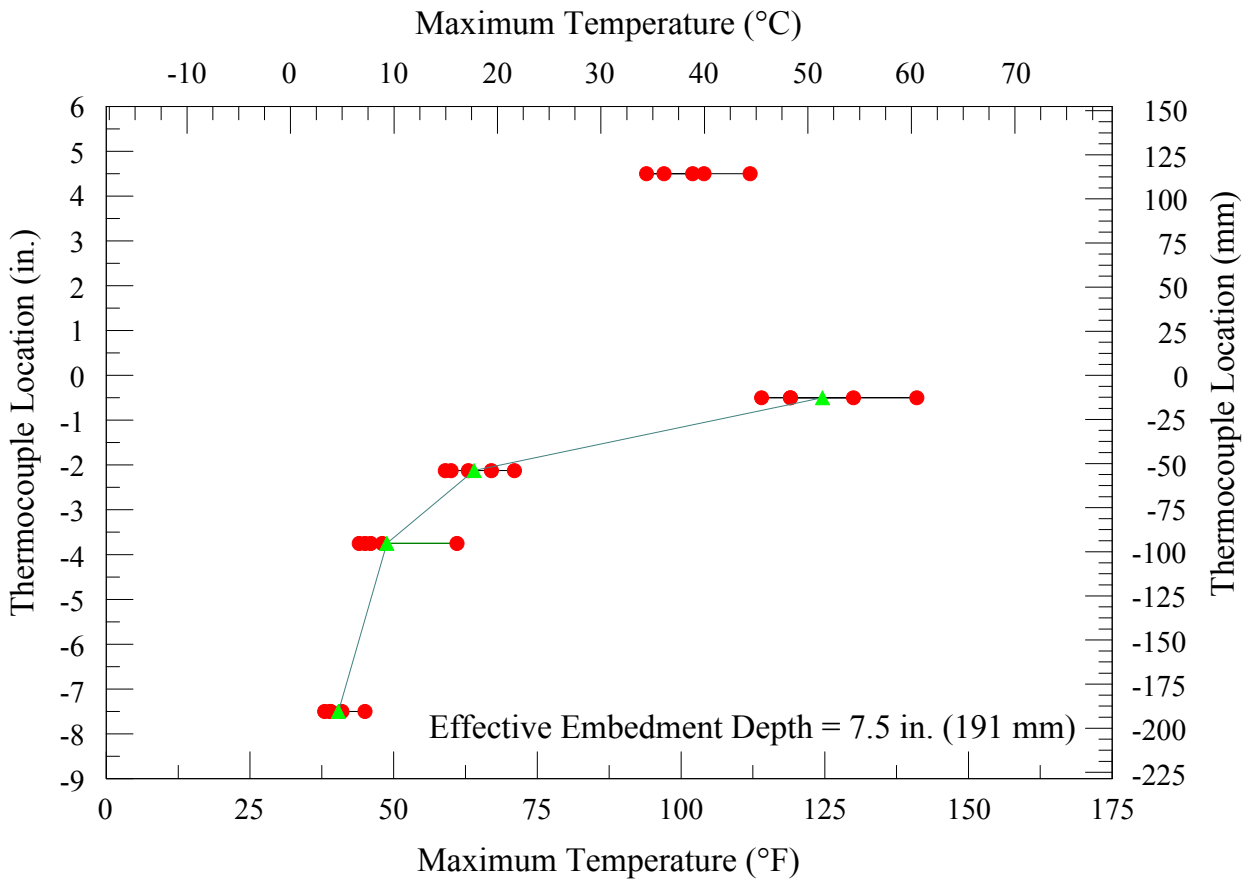

Figure 103: Weld Temperature Gradient for Test Group G Top (Front) Anchors

Table 44: Test Group G Recorded Maximum Temperatures at Bottom (Rear) Anchors

	Maximum Recorded Temperatures, °F (°C)				
Thermocouple Location, in. (mm)	Test 1	Test 2	Test 3	Test 4	Test 5
+4.5 (+114)	79 (26)	84 (29)	85 (29)	86 (30)	87 (31)
-0.5 (-13)	96 (36)	100 (38)	103 (39)	131 (55)	119 (48)
-2.125 (-54)	55 (13)	57 (14)	58 (14)	73 (23)	61 (16)
-3.75 (-95)	43 (6)	44 (7)	44 (7)	59 (15)	46 (8)
-7.5 (-191)	39 (4)	37 (3)	38 (3)	37 (3)	45 (7)
Maximum Recorded Temperatures in Surrounding Concrete, °F (°C)					
Surface (0)	42 (6)	41 (5)	54 (12)	66 (19)	39 (4)
-3.0 (-76)	38 (3)	36 (2)	35 (2)	35 (2)	55 (13)
-6.0 (-152)	37 (3)	36 (2)	36 (2)	35 (2)	51 (11)
Initial Base Material Temperature, °F (°C)				35 (2)	

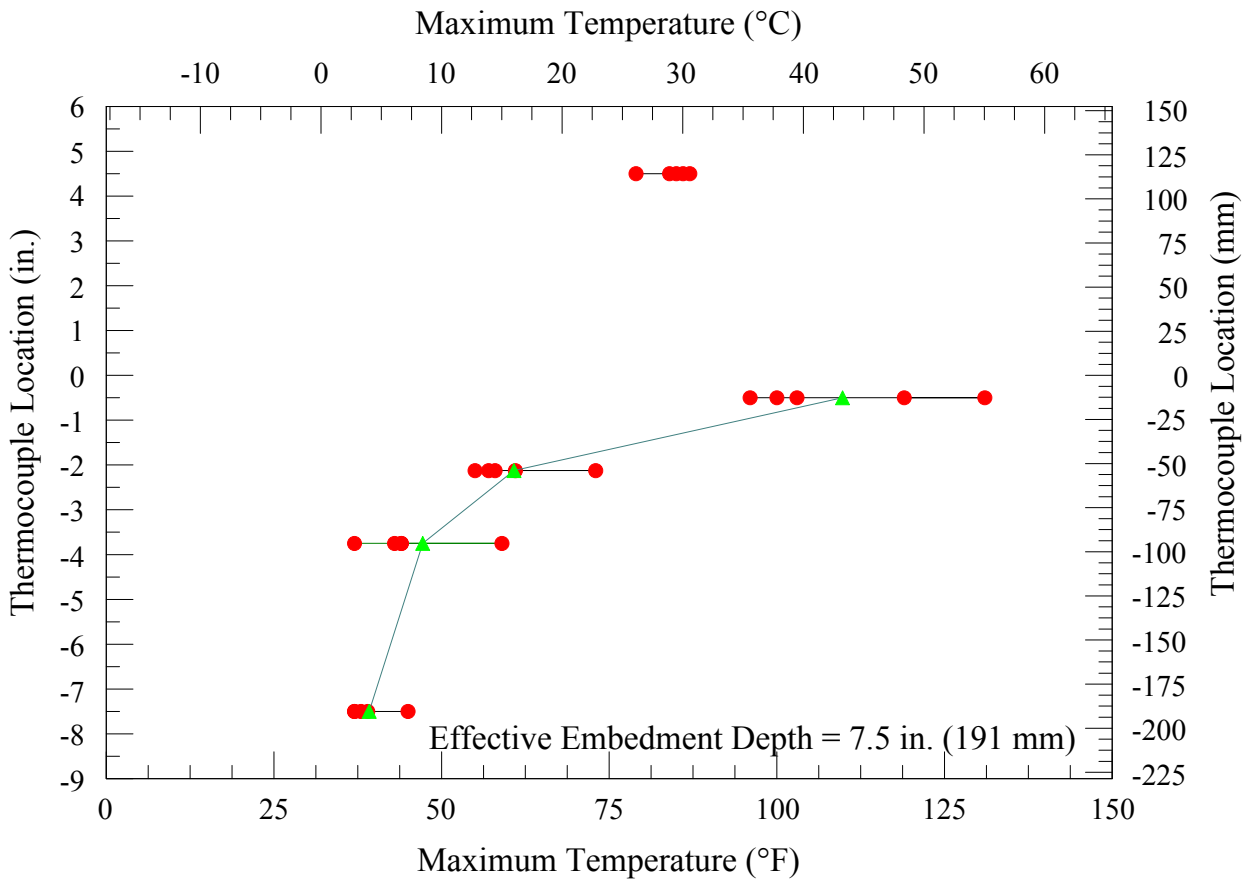

Figure 104: Weld Temperature Gradient for Test Group G Bottom (Rear) Anchors

The maximum temperatures experienced by Test Group G were slightly larger than Test Group E. This is presumably due to the larger diameter anchors used in Test Group G compared to Test Group E. Temperature values were relatively consistent in Test Group G and the temperature gradients of the front and rear anchors closely replicated that of the previous test groups. Test Group G experienced lower maximum temperatures than Test Group F. This is similar to the comparison made between Test Groups D and E and reinforces that the steel anchor elements subjected to direct welding experience higher maximum temperatures than those fastened with nuts and washers.

Maximum temperatures recorded in the concrete surrounding the adhesive anchoring systems for both Test Groups F and G were similar in behavior to Test Groups D and E, and experienced relatively small temperature increases from the initial base temperatures.

5.4 Discussion

From Test Groups D, E, F, and G, it was observed that welding directly to the steel anchor elements to fasten them to the base plates did result in higher maximum temperatures than fastening the anchors to the steel base plates using nuts and washers. Logically, the highest temperatures typically occurred within the upper half of the embedment depth of the steel anchor elements. For Test Group D, based on the average maximum temperatures of the five tests, temperatures were 300% and 173% higher at anchor embedment depths 0.5 inches (13 mm) and 1.75 inches (45 mm), respectively, below the concrete surface than corresponding anchor embedment depths of Test Group E. For Test Group F, based on the average maximum temperatures of the five tests, temperatures were 343% and 217% higher at anchor embedment depths 0.5 inches (13 mm) and 2.125 inches (54 mm), respectively, below the concrete surface than corresponding anchor embedment depths of Test Group G.

For the Test Groups D and F, where the steel anchor elements were welded directly to the steel base plates, the larger diameter anchors experienced higher maximum temperatures than the smaller diameter anchors, by 170% to 230%.

From this temperature investigation, it was also observed that the return welds applied at the front of the stiffened seats resulted in higher maximum temperatures along the front anchors than those experienced by the rear anchors, and that the concrete

surrounding the adhesive anchoring system showed no significant increase in temperatures when compared to the initial base temperatures of the concrete slab.

The temperature gradient test results show similar behavior to the temperature gradients observed in the confined static tension tests presented in Chapter 3. For all specimens tested in Chapters 3 and 5, the maximum temperatures were greatest at or near the surface and then drastically decayed as the effective anchor embedment increased from the concrete surface. To compare the overall temperature gradient regardless of the fastening condition of the steel anchor elements to the steel base plates, the temperature gradients for all temperature gradient tests are combined and shown in Figure 105.

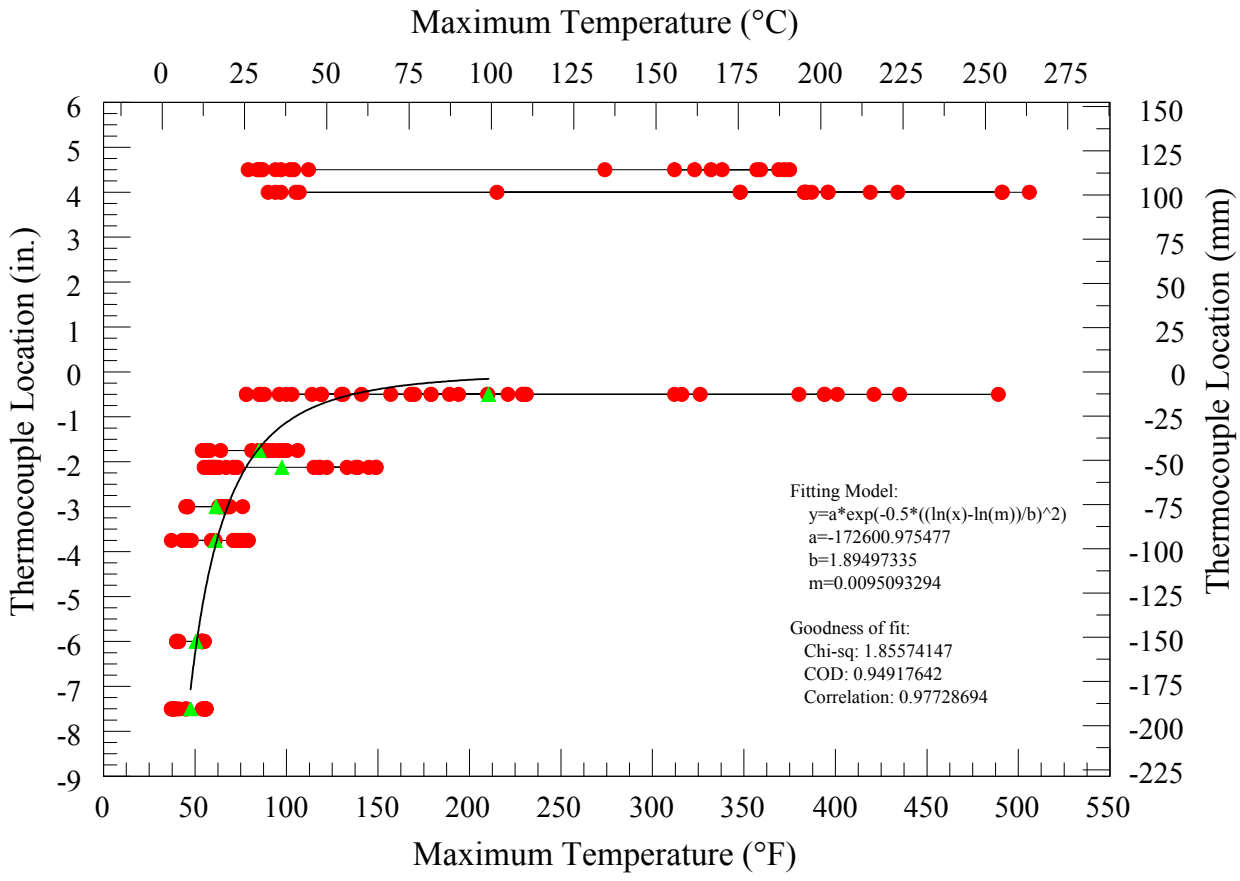

Figure 105: Combined Maximum Temperature Gradient for All Temperature Gradient Tests

As seen in Figure 105, the combined maximum temperature gradient of the temperature gradient test specimens are very similar in behavior to the welded confined static tension test specimens shown per Figure 66 of Chapter 3. Just as it was observed in the welded confined static tension test specimens, at about 2 inches (50.8 mm) below the concrete surface (point of welding), the highest recorded temperatures fall below the maximum short-term temperatures defined for "Temperature Range B" of the adhesive anchoring system's ICC-ES ESR. This suggests the proposal of disregarding the top 2 inches (50.8 mm) in the upper temperature gradient and adding this disregarded embedment as additional overall anchor embedment will provide a capacity that will meet or exceed the design capacity is applicable to eccentric shear applications subjected to welding applications.

CHAPTER 6

RECOMMENDATIONS, CONCLUSIONS, AND FUTURE WORK

This research attempts to provide the construction industry and design professionals with test data and recommendations for the design of precast concrete welded repair applications using a hybrid adhesive anchoring system subjected to tensile and eccentric shear loads. The recommendations, conclusions, and future work resulting from this testing program are presented in Sections 6.1, 6.2, and 6.3, respectively.

6.1 Recommendations

6.1.1 Direct Welding to Threaded Steel Anchor Elements

Based on test results and observations of test specimens where welding was applied directly to the steel anchor elements, it is not recommended that welding be applied directly to threaded steel anchor elements. Tests three, five, six, seven, and eight of Test Group A and tests three and six of Test Croup C presented in Section 4.3 all exhibited anchor fracture planes near or along the root weld pass made between the steel anchor elements and the steel base plates. This failure mode accounted for 29.2% of the failures observed with the eccentric shear test specimens where the steel anchor elements were fastened to the base plates by means of direct welding. Of these seven tests where the failure plane occurred near or along the weld plane, four exhibited failure loads below the design load value.

The weld failures of test one of Test Group J and test one of Test Group L as presented in Tables 17 and 21 of Section 3.5, respectively, accounted for only 6.67% of the welded confined static tension tests failure modes presented in Chapter 3. This is a

relatively small percentage, but still reinforces issues associated with welding directly to the steel anchor elements.

Based on the test results presented in Chapters 3 and 4, the use of DBA material conforming to ASTM A 496 or weldable rebar conforming to ASTM A 706 as steel anchor elements in the adhesive anchoring system appears to be a more appropriate selection of material when welding is applied directly to the steel anchor elements as means of fastening. When threaded steel anchor elements are required in the design of the adhesive anchoring systems, nuts and washers compatible with the threaded anchor material should be utilized instead of fastening methods that involve direct welding.

6.1.2 Bond Performance of Welded Steel Anchor Elements

The test results of the confined static tension tests presented in Chapter 3 confirm that reductions in ultimate bond capacity are present when direct welding is applied to the steel anchor element. Based on the magnitude of these reductions in bond strength and the observed maximum temperature gradient presented in Figure 66 of Section 3.8, the proposed method of compensating the effective anchor embedment for the heat affected zone of the adhesive exceeding the maximum short-term ICC-ES ESR temperatures can be used. Equations 27, 28, and 29 of Section 3.8 present this method for determining a nominal compensated bond strength capacity for steel anchor elements subjected to direct welding.

It is important to note that while the general design philosophy of this method can be applied to a multitude of different adhesive anchoring systems subjected to similar welding conditions tested in this work, reference and welded tests similar to those presented in Chapter 3 should be performed for specific adhesive anchoring systems to

establish the bond capacity needed to determine the nominal compensated bond capacity. The bond capacity values presented in Figure 67 of Section 3.8 are specific to the hybrid and epoxy adhesive anchoring system tested in this research program.

Though bond related failures were not observed during the eccentric shear testing presented in Chapter 4, the welding temperature investigation presented in Chapter 5 reveal that maximum temperatures induced by welding on or near the steel anchor elements exceed the short-term temperatures prescribed by the product specific ICC-ES ESR in a similar heat affected zone as experienced by the welded confined static tension test specimens. In practice, it is recommended the same proposed design procedure presented in Equations 27, 28, and 29 of Section 3.8 be used for the design of tensile and eccentrically loaded welded precast repair applications.

6.2 Conclusions

From the data and observations of confined static tension testing, eccentric shear tests, and temperature gradient tests, the following conclusions can be summarized as follows:

- Confined static tension tests exhibited a reduction of bond capacity when subjected to direct welding, but with proper compensation of the effective anchor embedment, which disregards a heat affected zone, the hybrid and epoxy adhesive anchoring systems tested in this research can meet or exceed required design load capacities.
- Though testing was limited, it was observed that the epoxy based adhesive anchoring system experienced less reductions in bond capacity than the

hybrid adhesive anchoring system when subjected to direct welding and confined static tensile loads.

- Maximum temperature gradients experienced by direct welding to or near the steel anchor elements reveal that temperatures exceeding the maximum short-term temperatures prescribed per the product specific ICC-ES ESR occur at the surface (point of welding) and the immediate upper portions of the effective anchor embedment, but rapidly decay below this heat affected zone.
- Split core specimens that exposed the hybrid adhesive anchoring system after welding and load testing revealed no visual signs of charring or adhesive discoloration.
- The eccentric shear test specimens utilizing nuts and washers to fasten the threaded steel anchor elements to the steel base plates exhibited more consistent failure modes and failure loads than the specimens that used direct welding to fasten the steel anchor elements to the base plates.

6.3 Future Work

Overall, the research performed to date accomplished its objective in serving as a basis for test data and guidance to the construction industry and design professionals. Based on the test results and recommendations of this work, future research needs have become apparent, and should be considered as opportunities to further enhance this work. The future work opportunities generated from this current research can be summarized as follows:

- Testing of the welding compatibility of threaded steel anchor elements used in this research program and the use higher strength welding electrodes.
- Testing to validate the proposed nominal compensated bond strength capacity design methodology for steel anchor elements subjected to direct welding.
- Round Robin testing to validate the maximum temperature gradients of steel anchor elements subjected to welding on or near steel anchor elements.
- Numerical study of the temperature gradient experimental data to develop a general temperature gradient model.

APPENDIX A

SAMPLE HAND CALCULATIONS OF ECCENTRIC SHEAR TEST SPECIMEN PREDICTED FAILURE AND DESIGN LOADS

TEST GROUP A

Test Group A – Given Parameters:

$A_e = 0.1341 \text{ in}^2$ ⟶ From Ancillary Testing

$b = 7$ in

$d = 8.5$ in

$e = 4.5$ in

$f'_c = 7.805$ ksi

$f_u = 115.9$ ksi

Predicted Failure Load for Test Group A using Equation (11):

$$V = \left[\frac{2}{\frac{4.5}{(2)(0.1341)(115.9)(8.5) - \frac{(0.1341)^2(115.9)^2}{(0.85)(7.805)(7)}} + \frac{1}{(2.4)(0.1341)(115.9)}} \right]$$

$$= \left[\frac{2}{\frac{4.5}{259.02} + \frac{1}{37.30}} \right]$$

$$= \left[\frac{2}{(0.0174) + (0.0268)} \right]$$

$= 45.276$ kips

∴ V = 45,276 lb. (220.6 kN)

Predicted Factored Nominal Design Load for Test Group A using Equation (12):

$$\varphi V_n = \left[\frac{2}{\frac{4.5}{(0.65)(259.02)} + \frac{1}{(0.6)(37.30)}}\right]$$

$$= \left[\frac{2}{(0.0267) + (0.0447)}\right]$$

= 28.007 kips

∴ φV_n = 28,007 lb. (130.0 kN)

APPENDIX B

STRESS VS. ELONGATION PLOTS FOR ANCILLARY TENSILE TESTS

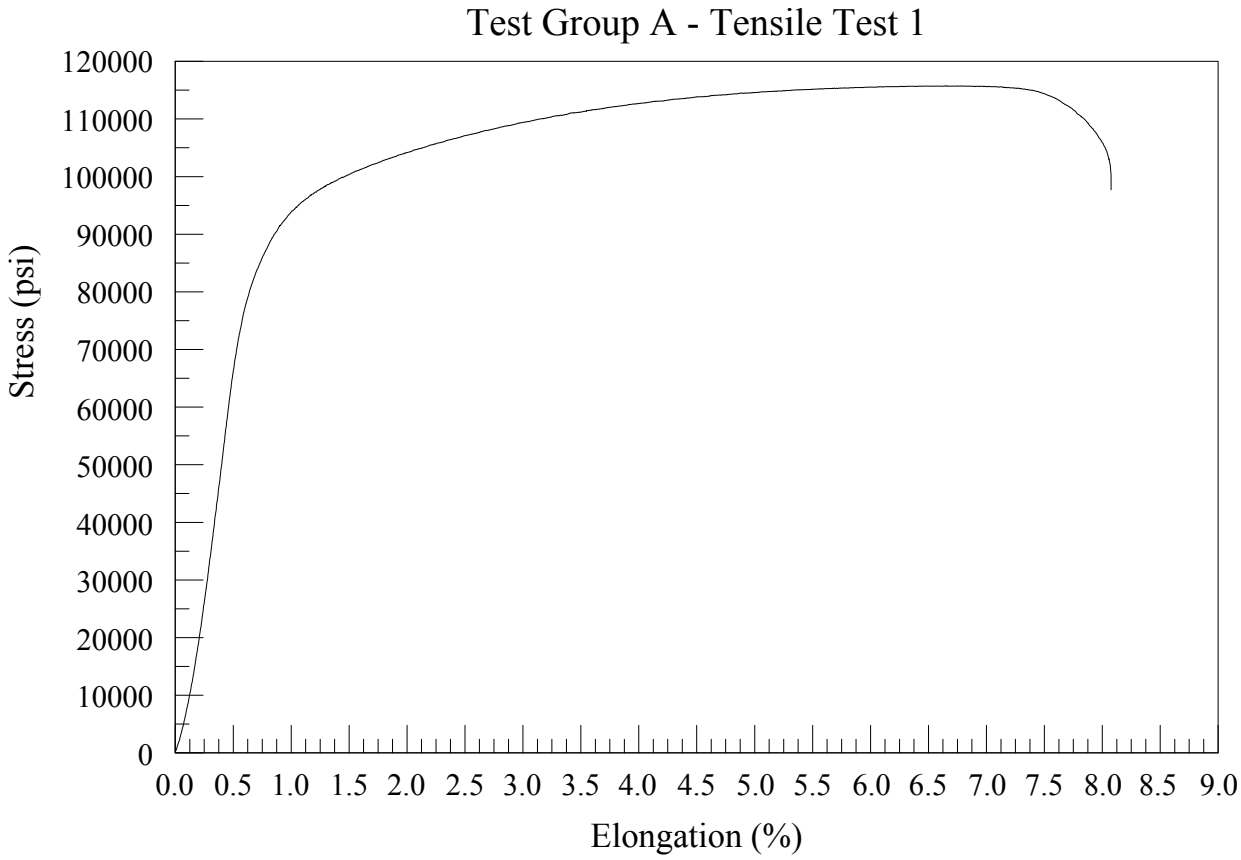

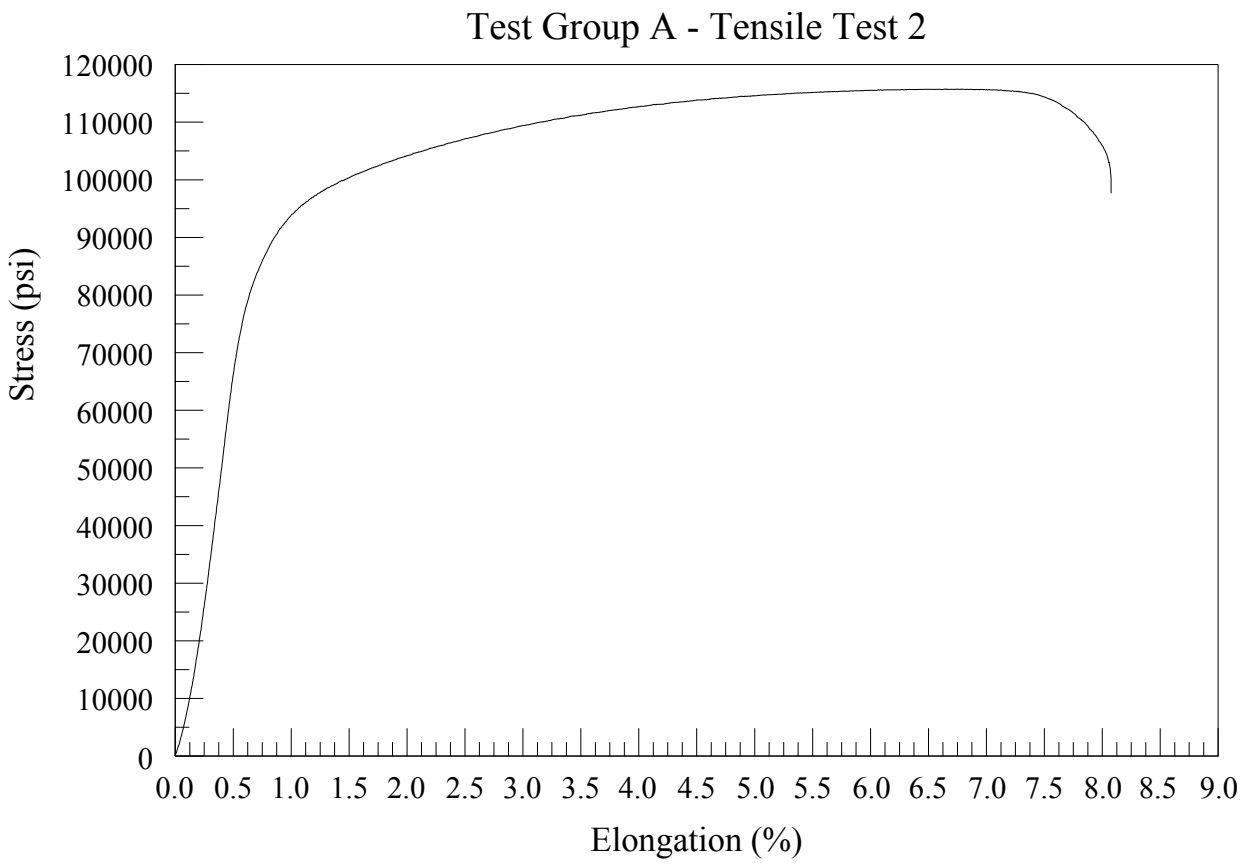
Test Group A - Tensile Test 2
Stress (psi)
120000
110000
100000
90000
80000
70000
60000
50000
40000
30000
20000
10000
0
0.0 0.5 1.0 1.5 2.0 2.5 3.0 3.5 4.0 4.5 5.0 5.5 6.0 6.5 7.0 7.5 8.0 8.5 9.0
Elongation (%)

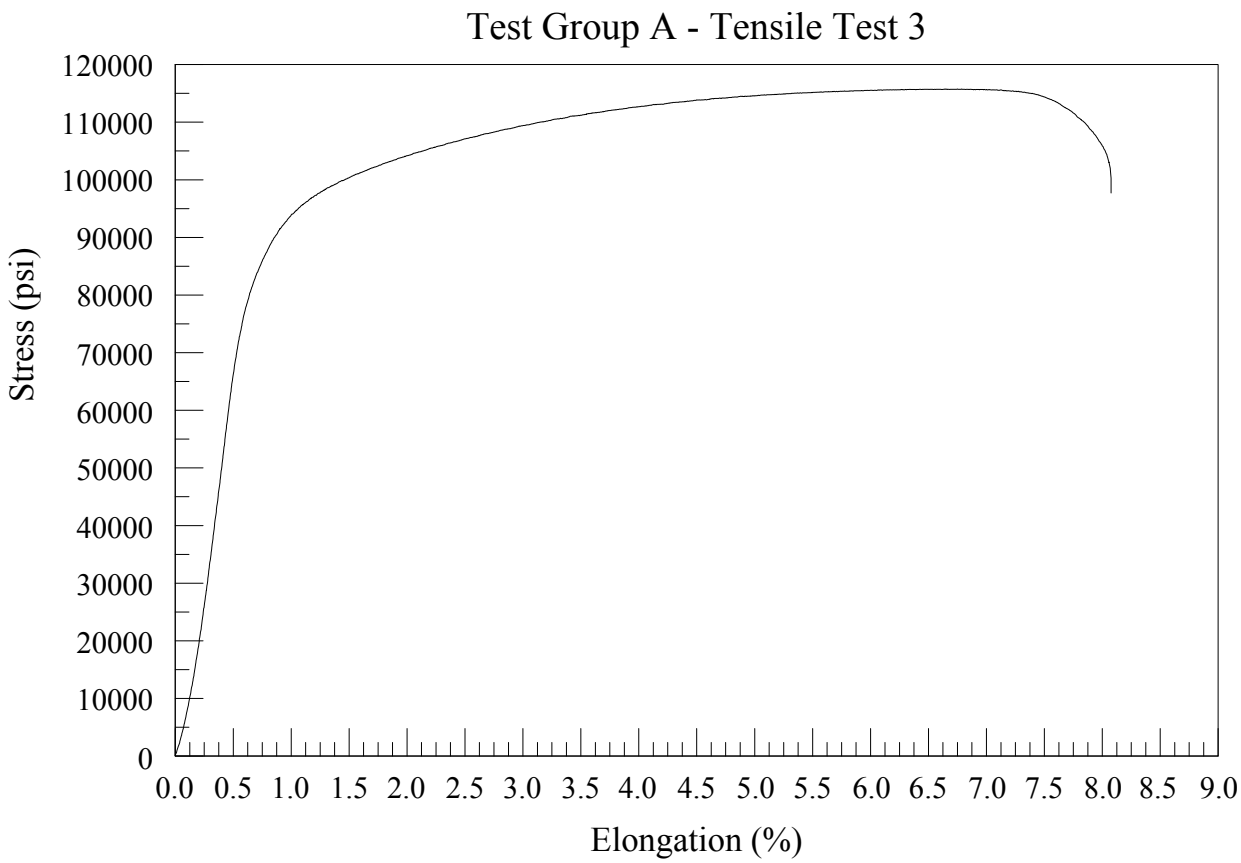
Test Group A - Tensile Test 3
Stress (psi)
120000
110000
100000
90000
80000
70000
60000
50000
40000
30000
20000
10000
0
0.0 0.5 1.0 1.5 2.0 2.5 3.0 3.5 4.0 4.5 5.0 5.5 6.0 6.5 7.0 7.5 8.0 8.5 9.0
Elongation (%)

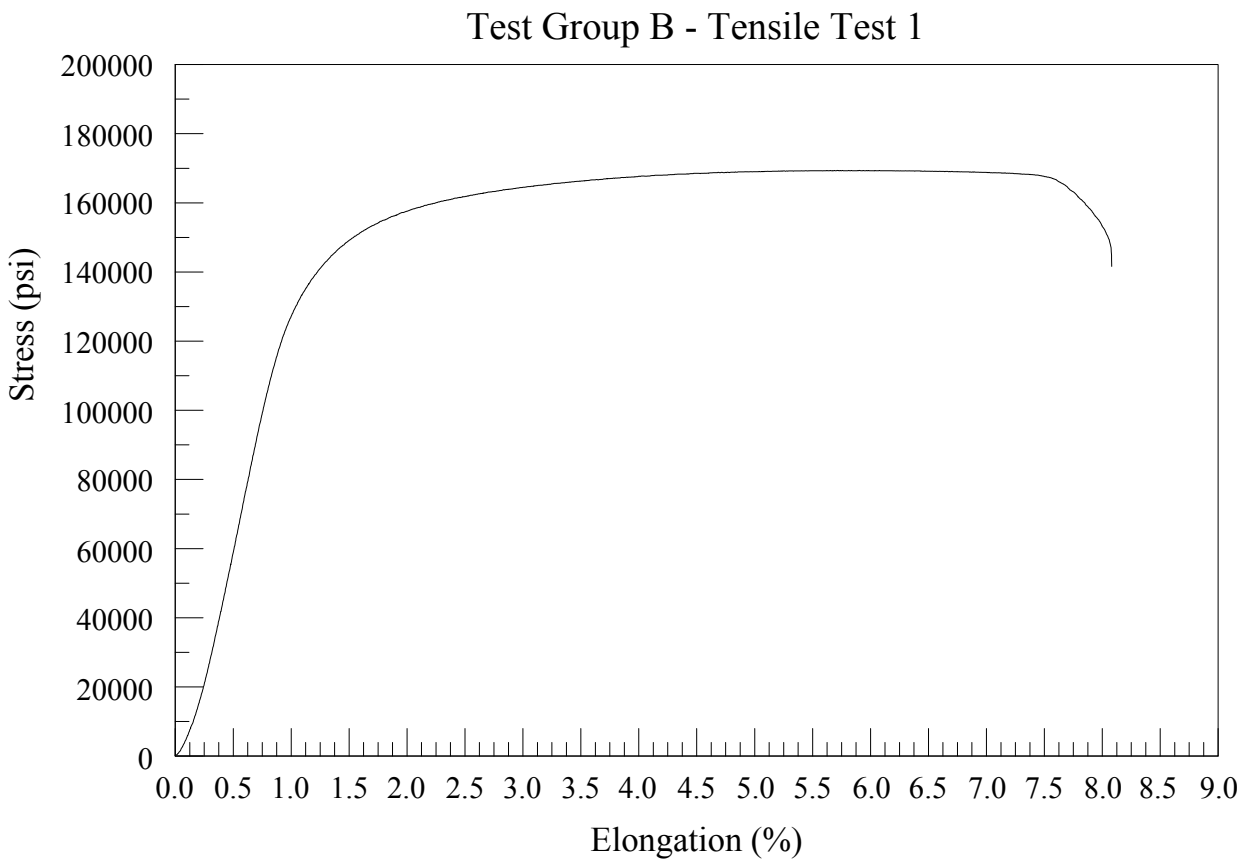
Test Group B - Tensile Test 1
Stress (psi)
200000
180000
160000
140000
120000
100000
80000
60000
40000
20000
0
0.0 0.5 1.0 1.5 2.0 2.5 3.0 3.5 4.0 4.5 5.0 5.5 6.0 6.5 7.0 7.5 8.0 8.5 9.0
Elongation (%)

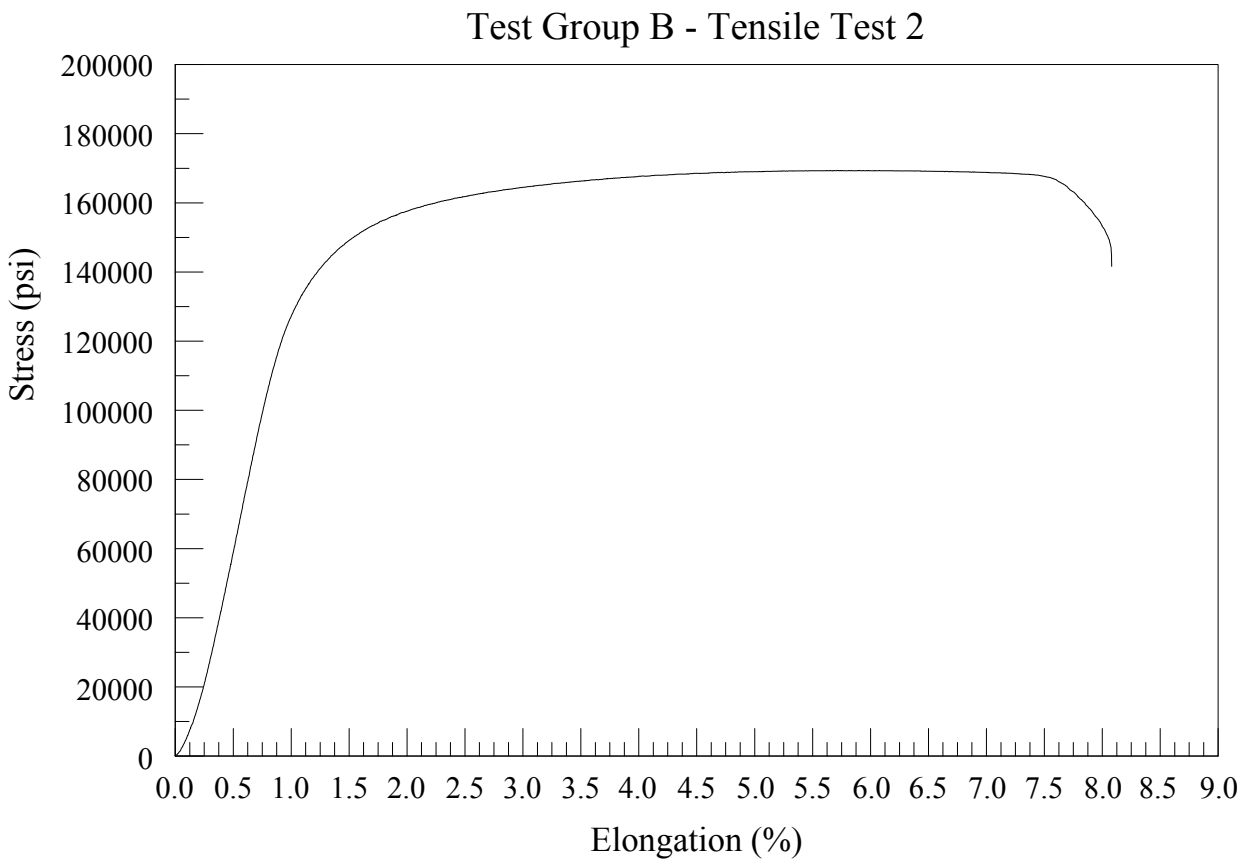
Test Group B - Tensile Test 2
Stress (psi)
200000
180000
160000
140000
120000
100000
80000
60000
40000
20000
0
0.0 0.5 1.0 1.5 2.0 2.5 3.0 3.5 4.0 4.5 5.0 5.5 6.0 6.5 7.0 7.5 8.0 8.5 9.0
Elongation (%)

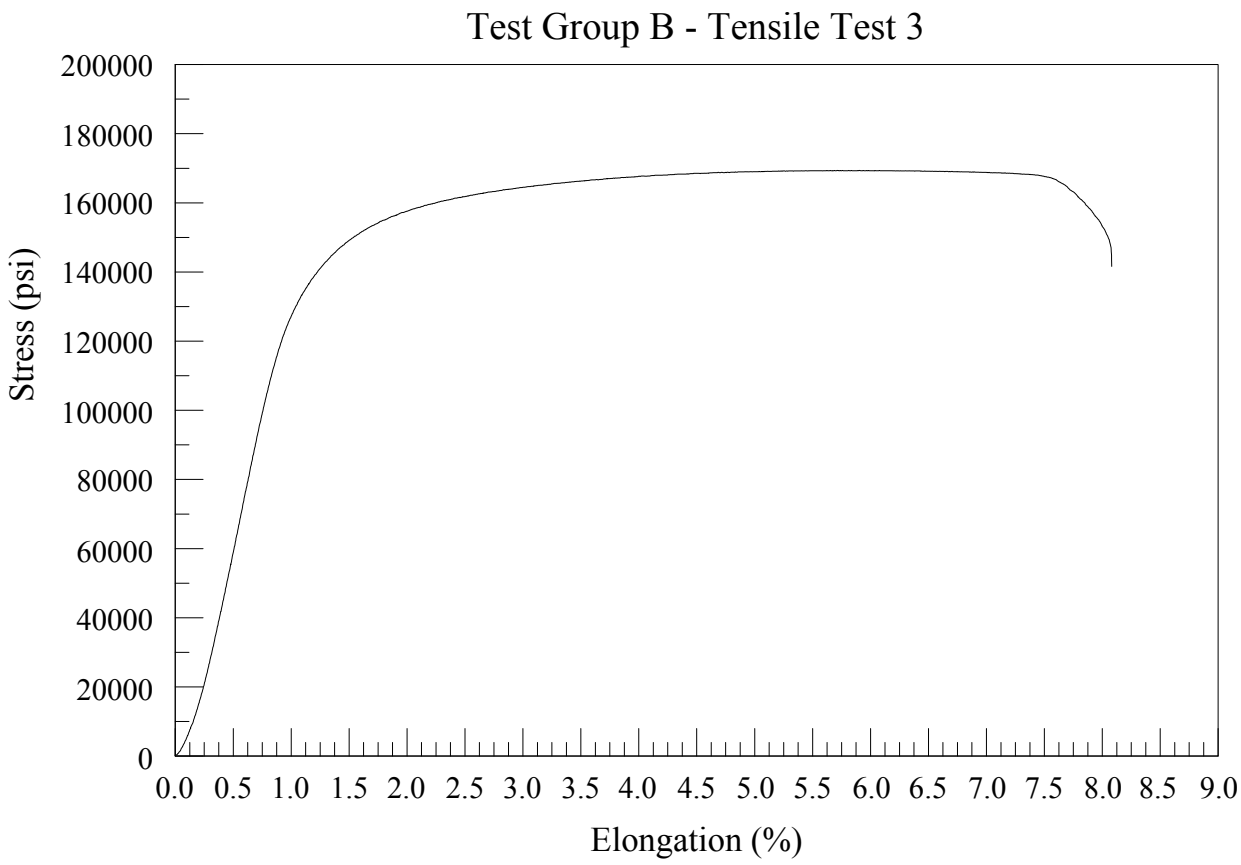
Test Group B - Tensile Test 3
Stress (psi)
200000
180000
160000
140000
120000
100000
80000
60000
40000
20000
0
0.0 0.5 1.0 1.5 2.0 2.5 3.0 3.5 4.0 4.5 5.0 5.5 6.0 6.5 7.0 7.5 8.0 8.5 9.0
Elongation (%)

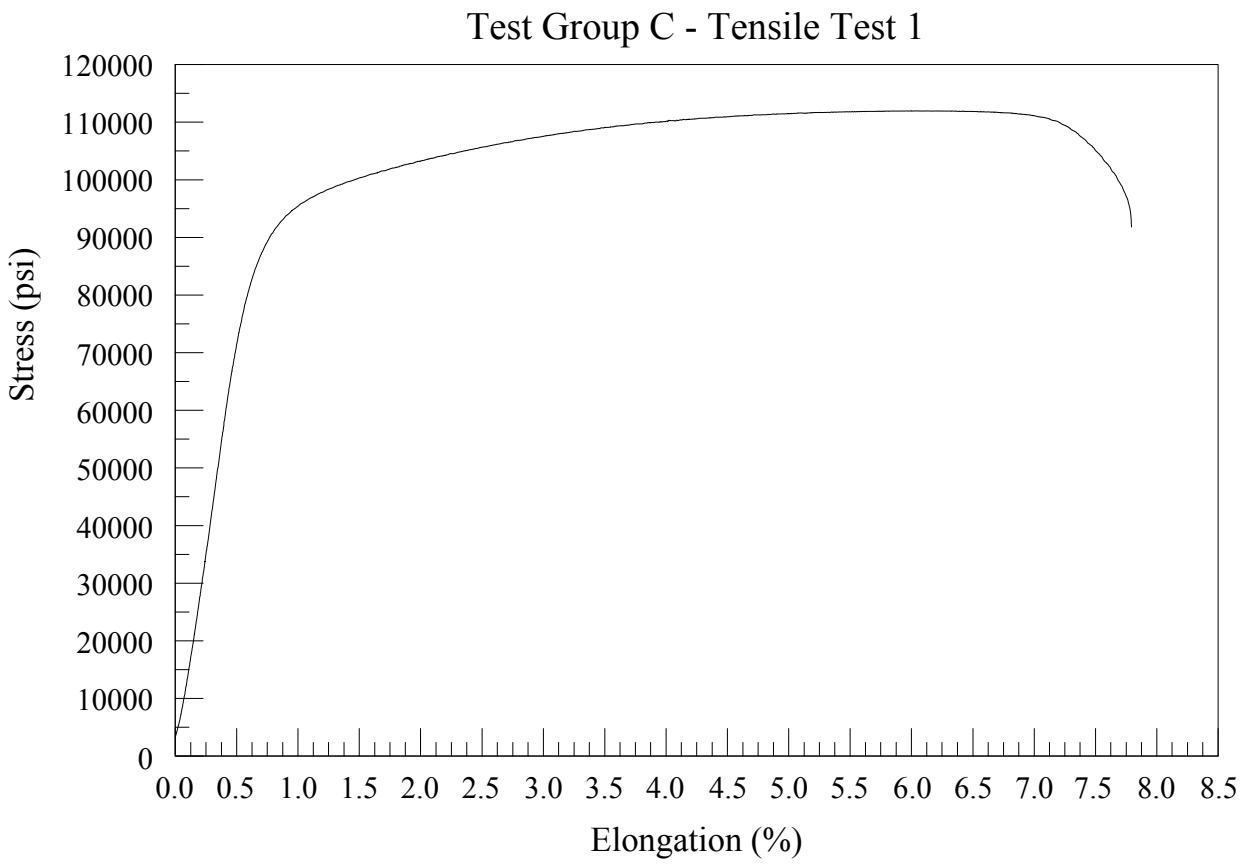
Test Group C - Tensile Test 1
Stress (psi)
120000
110000
100000
90000
80000
70000
60000
50000
40000
30000
20000
10000
0
0.0 0.5 1.0 1.5 2.0 2.5 3.0 3.5 4.0 4.5 5.0 5.5 6.0 6.5 7.0 7.5 8.0 8.5
Elongation (%)

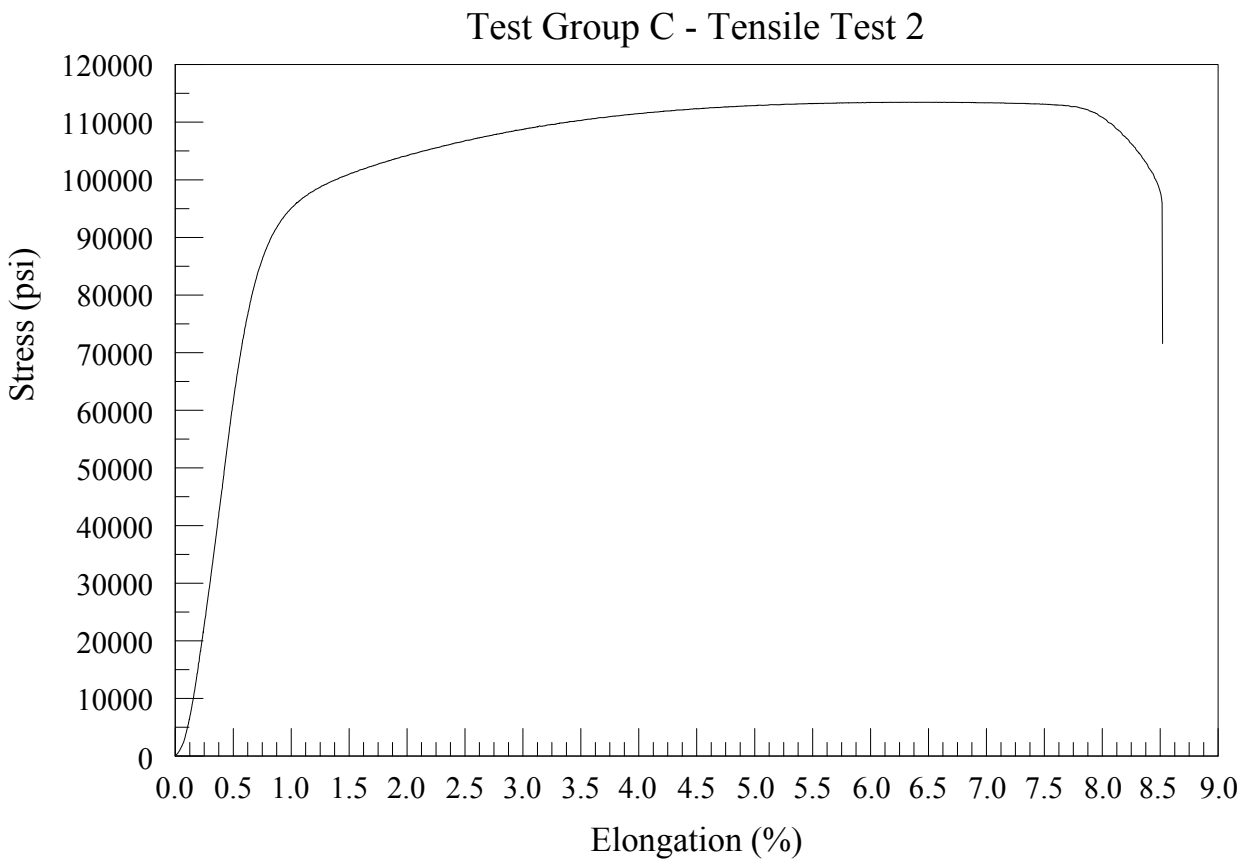
Test Group C - Tensile Test 2
Stress (psi)
120000
110000
100000
90000
80000
70000
60000
50000
40000
30000
20000
10000
0
0.0 0.5 1.0 1.5 2.0 2.5 3.0 3.5 4.0 4.5 5.0 5.5 6.0 6.5 7.0 7.5 8.0 8.5 9.0
Elongation (%)

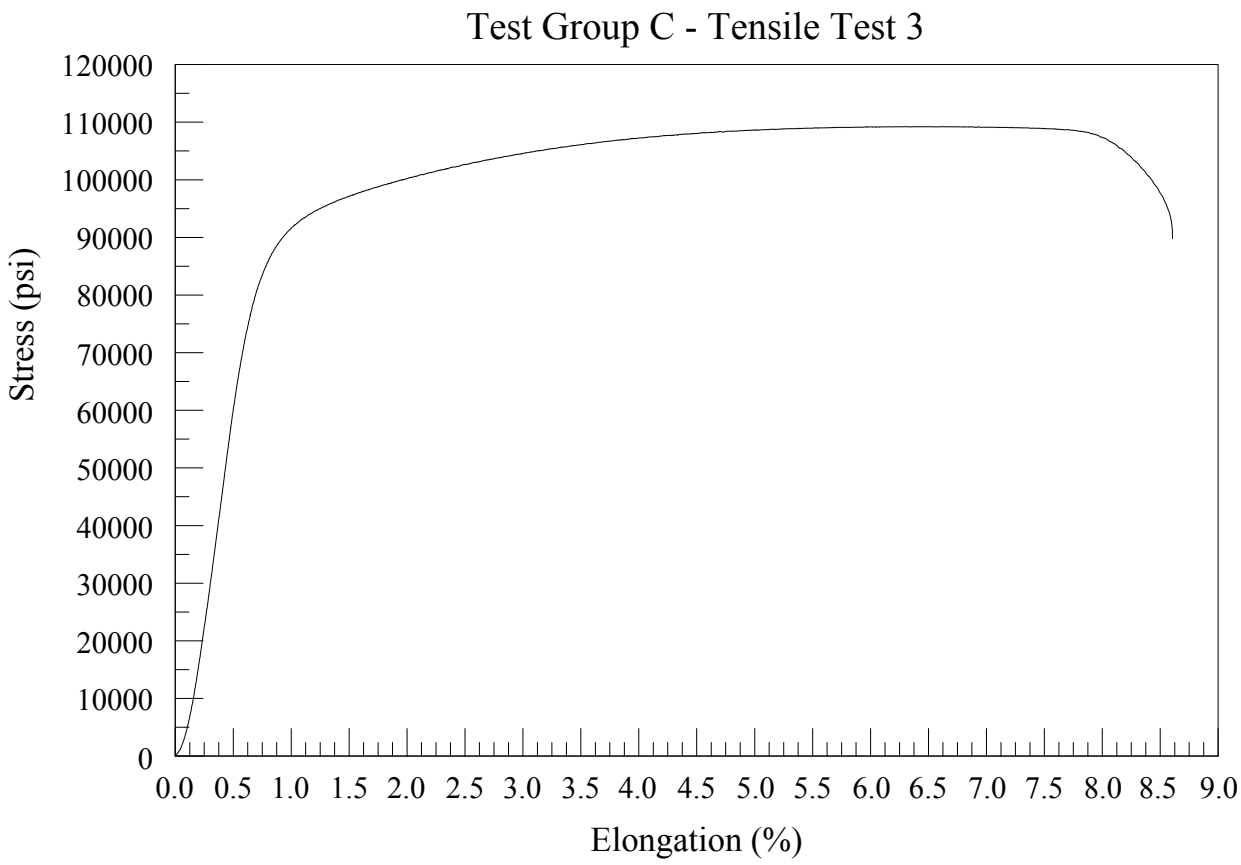
Test Group C - Tensile Test 3
Stress (psi)
120000
110000
100000
90000
80000
70000
60000
50000
40000
30000
20000
10000
0
0.0 0.5 1.0 1.5 2.0 2.5 3.0 3.5 4.0 4.5 5.0 5.5 6.0 6.5 7.0 7.5 8.0 8.5 9.0
Elongation (%)

APPENDIX C

LOAD VS. DISPLACEMENT PLOTS OF CONFINED STATIC TENSION TESTS

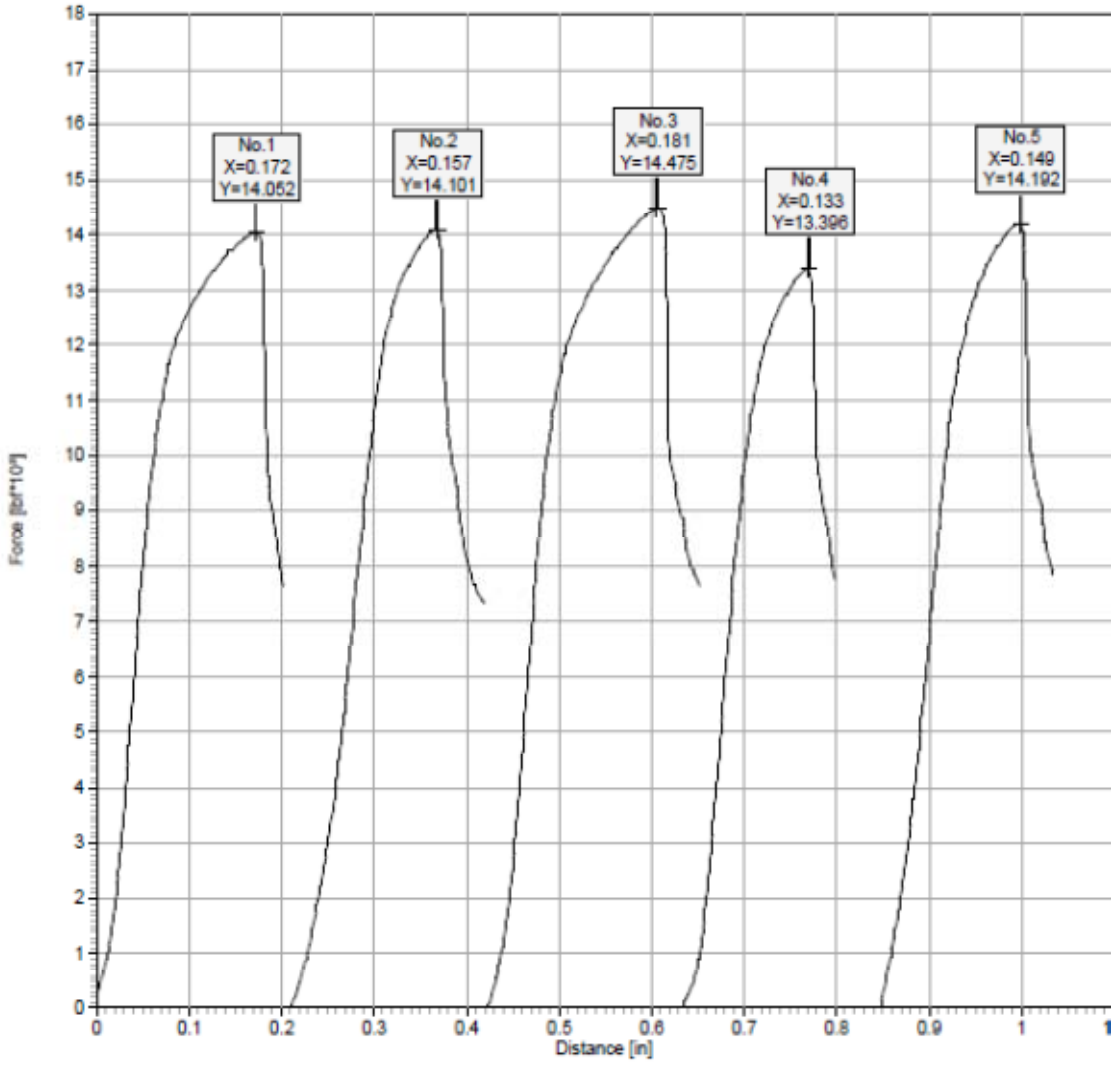

Test Group H Reference Tests Load-Displacement Plot

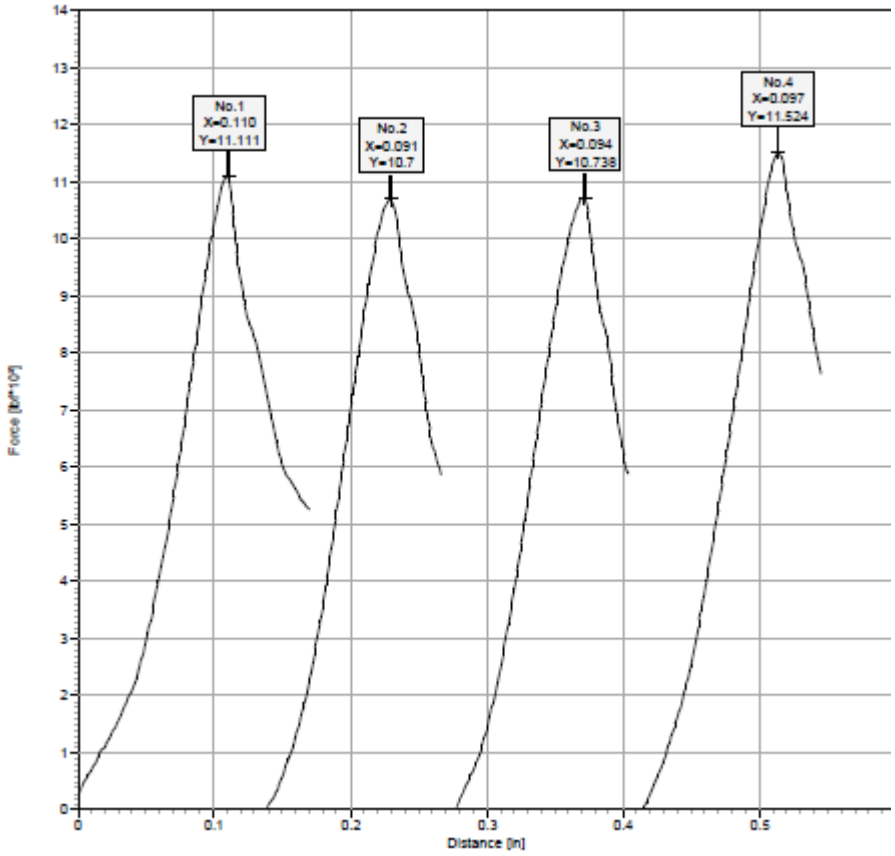

Test Group H Welded Tests Load-Displacement Plot

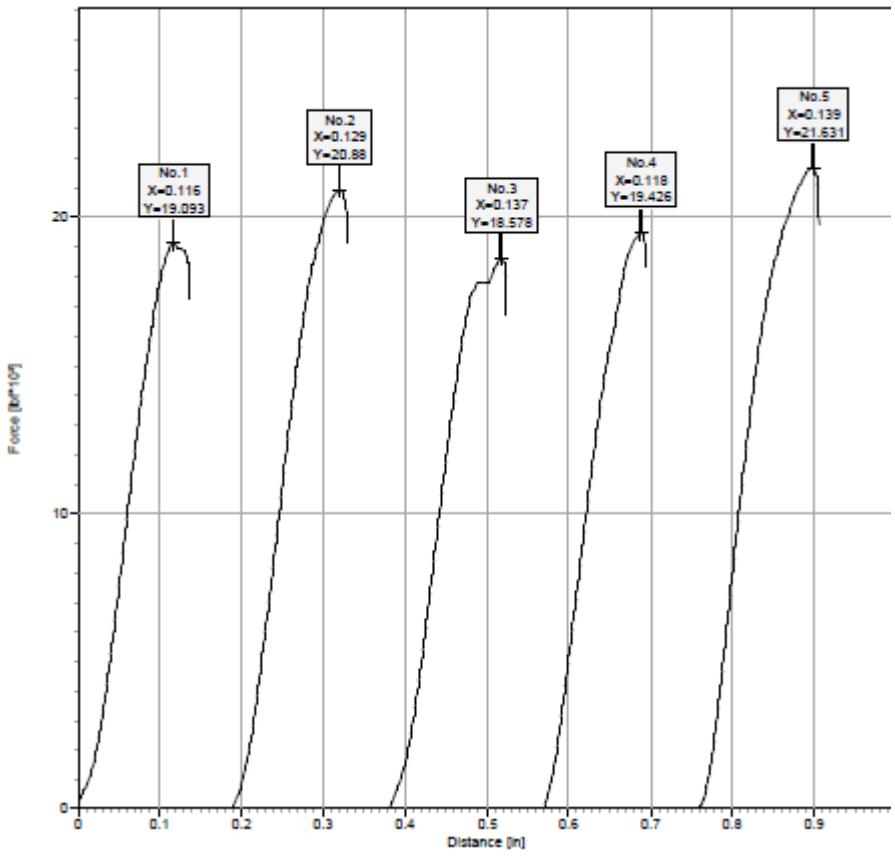

Test Group I Reference Tests Load-Displacement Plot

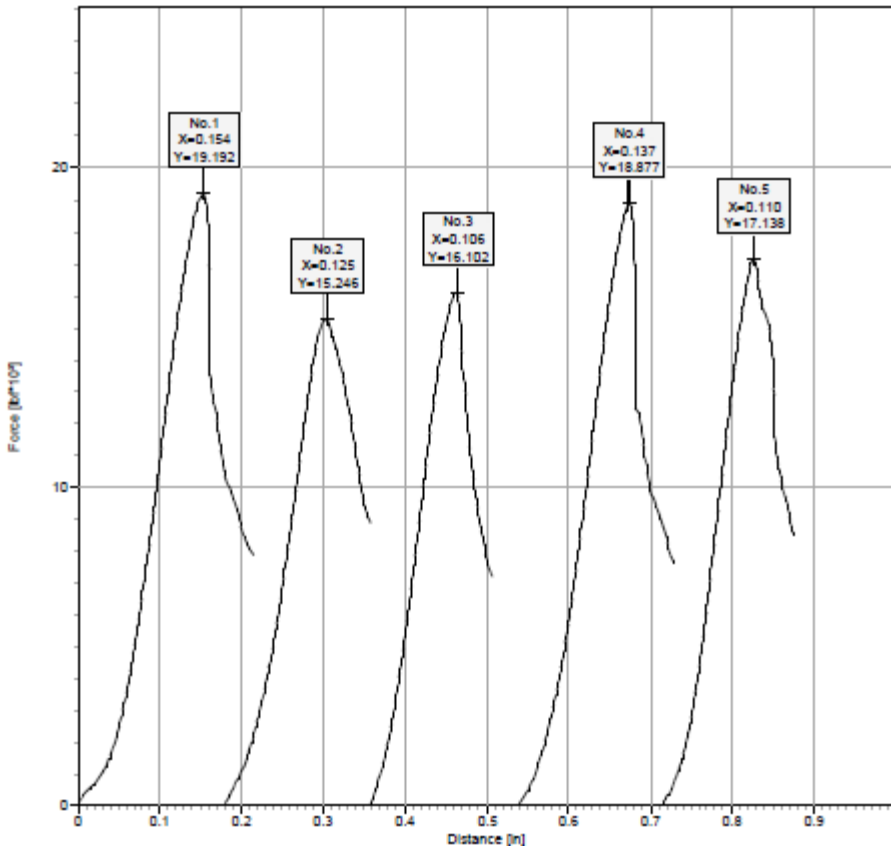

Test Group I Welded Tests Load-Displacement Plot

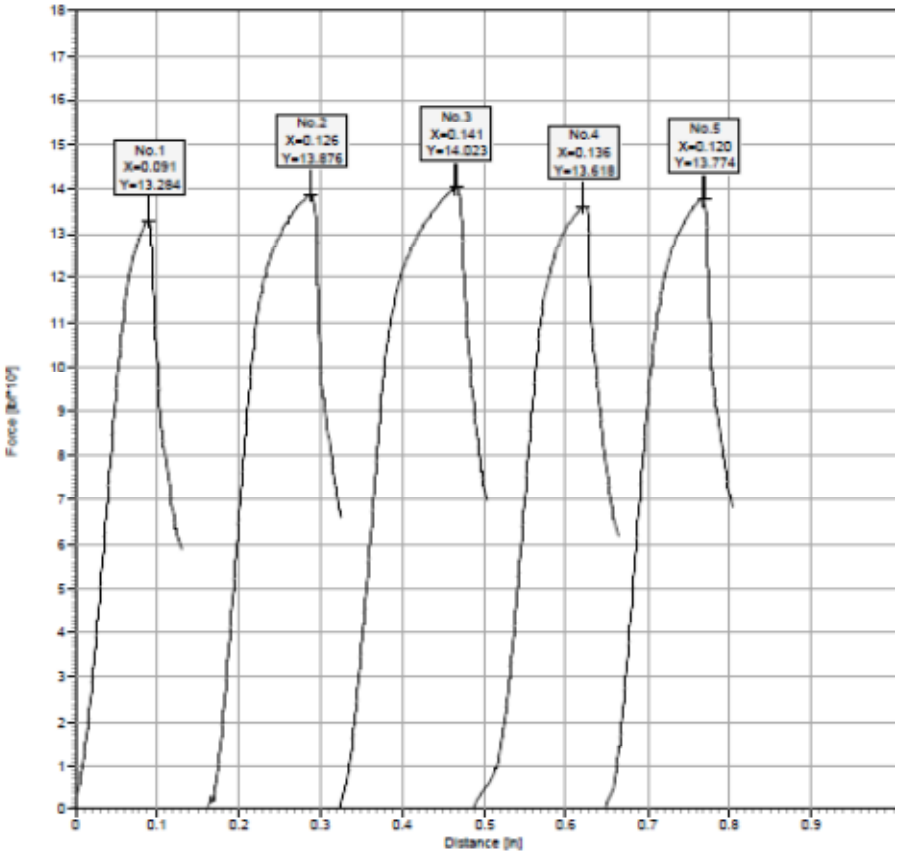

Test Group J Reference Tests Load-Displacement Plot

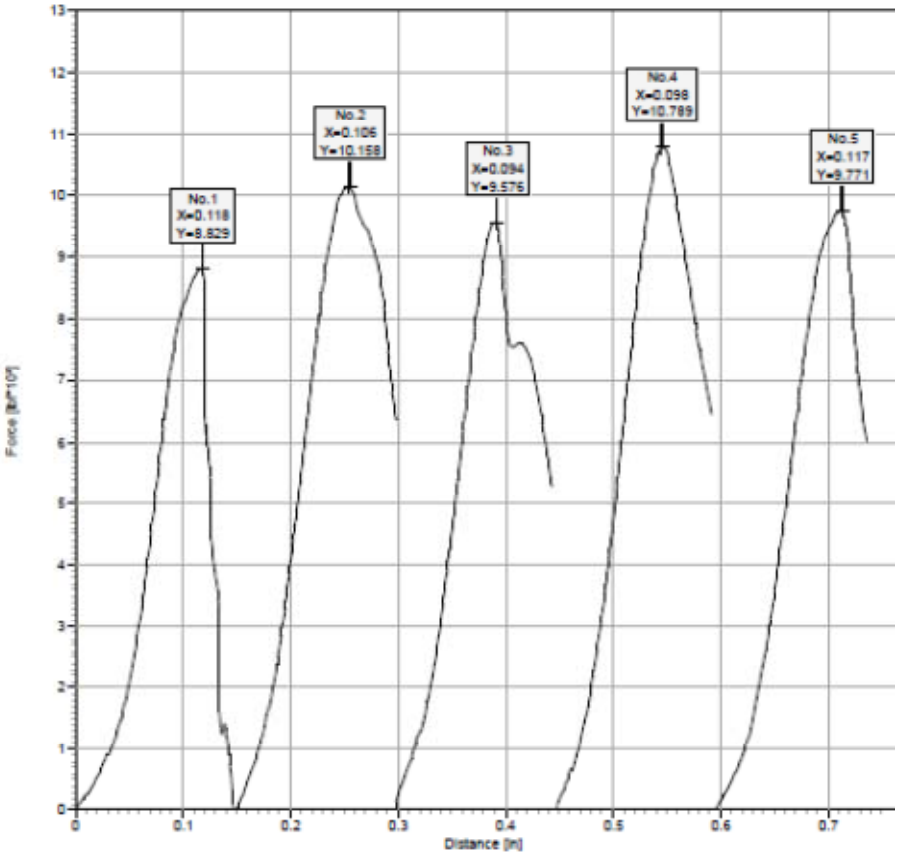

Test Group J Welded Tests Load-Displacement Plot

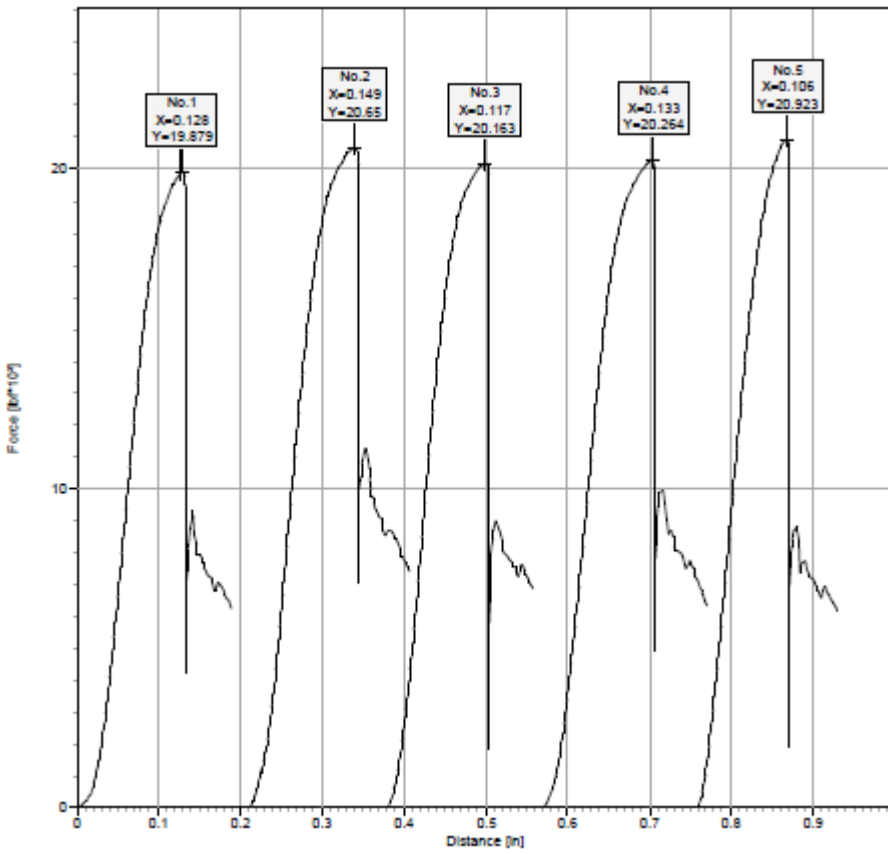

Test Group K Reference Tests Load-Displacement Plot

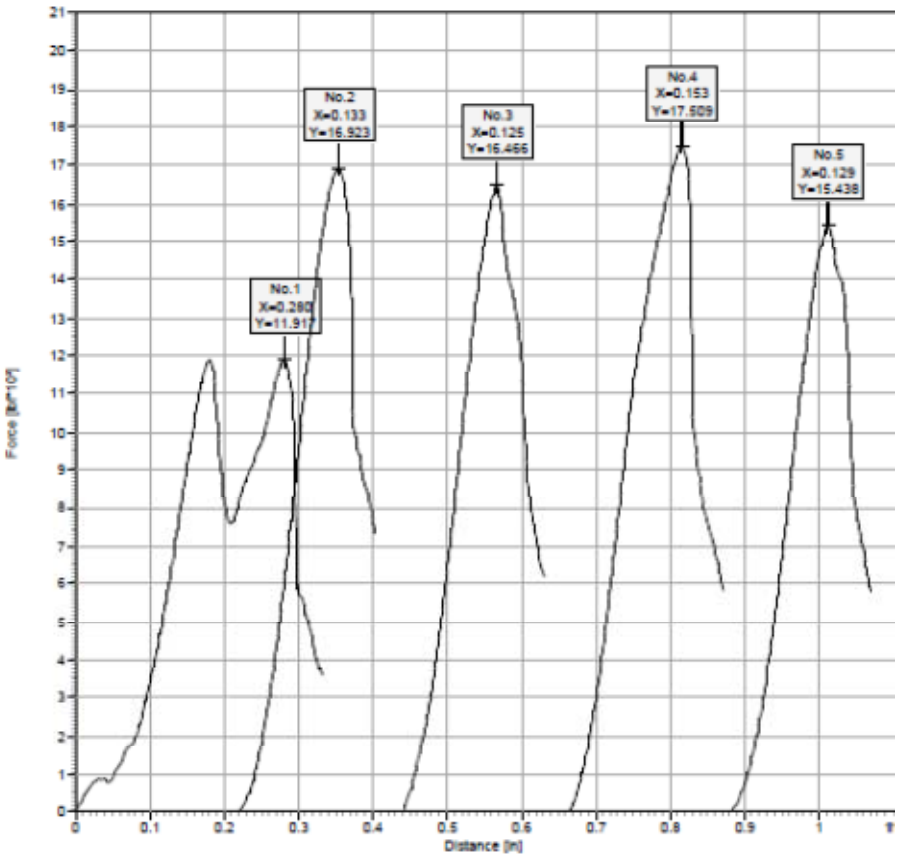

Test Group K Welded Tests Load-Displacement Plot

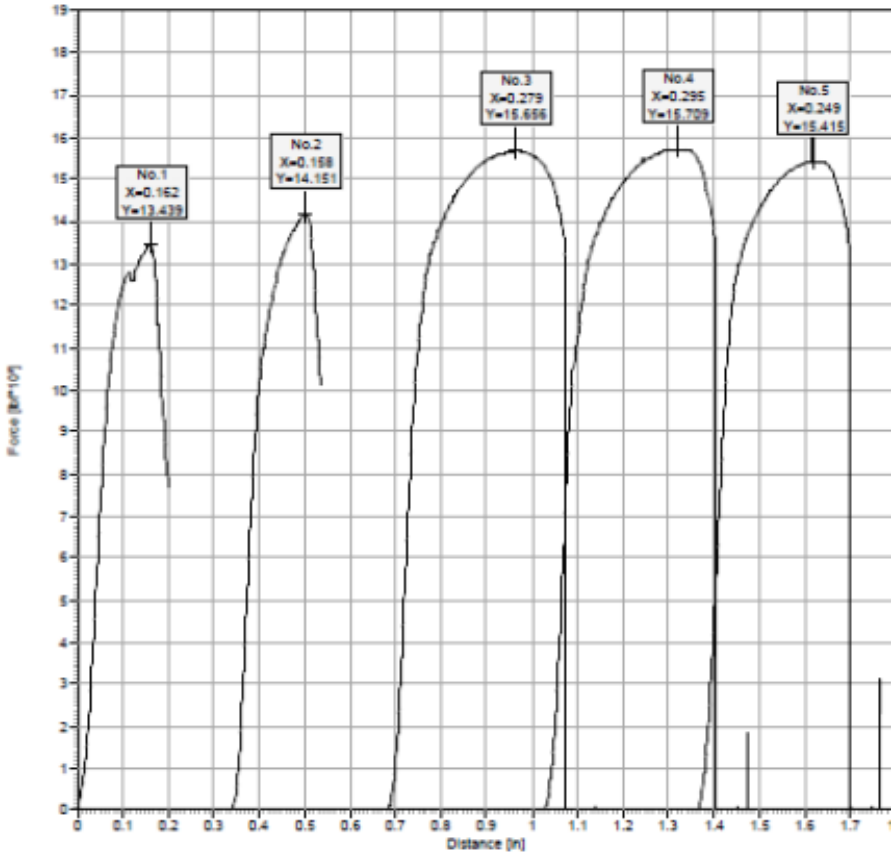

Test Group L Reference Tests Load-Displacement Plot

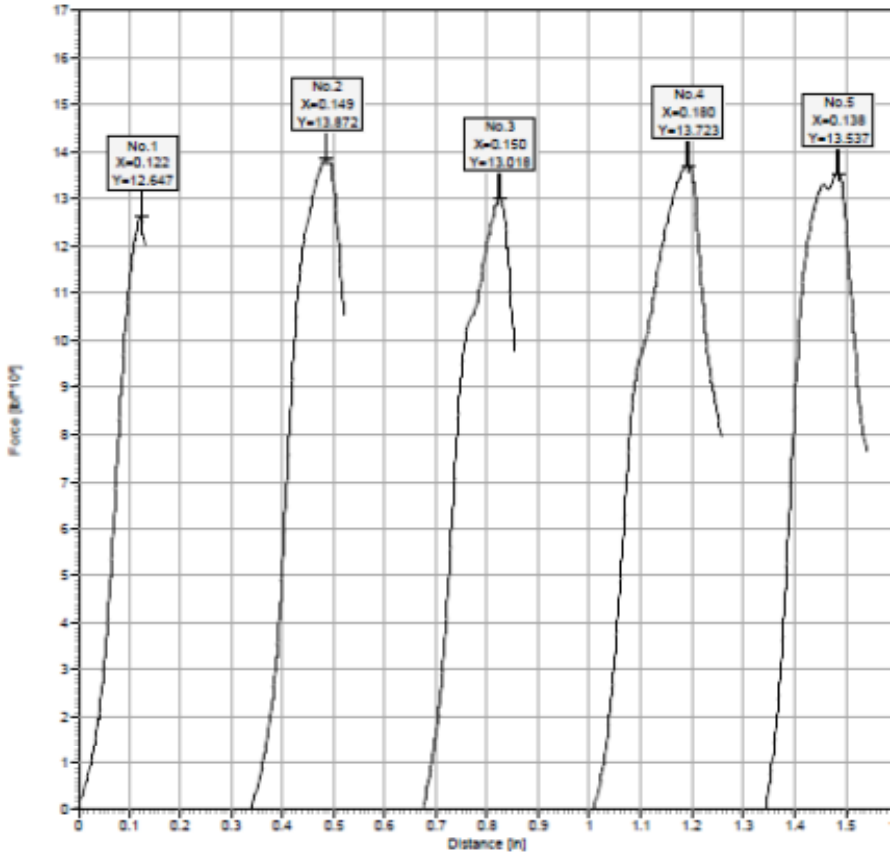

Test Group L Welded Tests Load-Displacement Plot

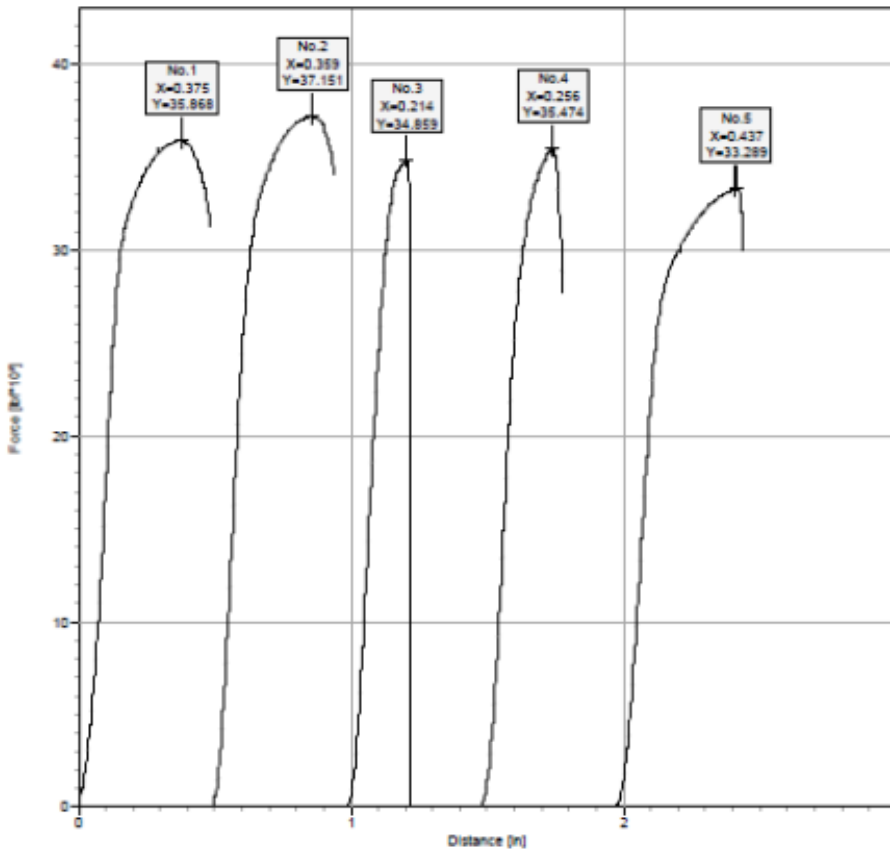

Test Group M Reference Tests Load-Displacement Plot

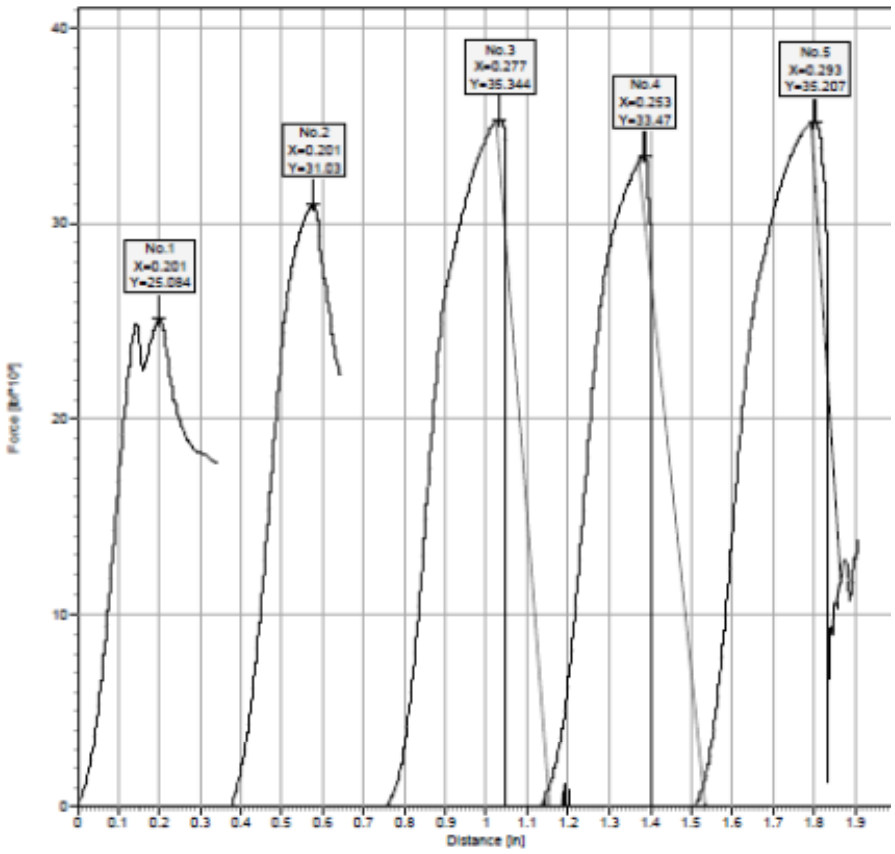

Test Group M Welded Tests Load-Displacement Plot

REFERENCES

The following references are cited in this dissertation:

American Concrete Institute. ACI Committee 355 Home. American Concrete Institute Technical Committees. http://www.concrete.org/COMMITTEES/committeehome.asp?committee_code=0000355-00 (accessed May 17, 2002).

ACI Committee 318. 2011. Building Code Requirements for Structural Concrete (ACI 318-11) and Commentary. Farmington Hills, MI: American Concrete Institute.

ACI Committee 318. 2008. Building Code Requirements for Structural Concrete (ACI 318-08) and Commentary. Farmington Hills, MI: American Concrete Institute.

ACI Committee 318. 2005. Building Code Requirements for Structural Concrete (ACI 318-05) and Commentary. Farmington Hills, MI: American Concrete Institute.

ACI Committee 318. 2002. Building Code Requirements for Structural Concrete (ACI 318-02) and Commentary. Farmington Hills, MI: American Concrete Institute.

ACI Committee 355. 2010. Acceptance Criteria for Qualification of Post-Installed Adhesive Anchors in Concrete (ACI 355.4-10) and Commentary. Farmington Hills, MI: American Concrete Institute.

ACI Committee 355. 2007. *Qualification of Post-Installed Mechanical Anchors in Concrete (ACI 355.2-07)*. Farmington Hills, MI: American Concrete Institute.

ASTM Subcommittee E06.13. 2003. ASTM E 488-96 Standard Test Methods for Strength of Anchors in Concrete and Masonry Elements. West Conshohocken, PA: ASTM International.

ASTM Subcommittee E06.13. 1993. ASTM E 1512-93 Standard Test Methods for Testing Bond Performance of Adhesive-Bonded Anchors. West Conshohocken, PA: ASTM International.

Bickel, T.S., and Shaikh, A.F. 2002. Shear Strength of Adhesive Anchors. *PCI Journal*, Vol. 47, No. 5 (September – October): 92-102.

Chin, J., Hunston, D., and Forster, A. 2009. *Thermo-viscoelastic Analysis of Ambient Cure Epoxy Adhesives Used in Construction Applications*. NISTIR 7429. National Institute of Standards and Technology, Washington D.C.

Cognard, P. 2005. "Technical Characteristics and Testing Methods for Adhesives and Sealants" (Chapter 2). In *Handbook of Adhesives and Sealants: Volume 1*. Elsevier, 21-99.

Colak, A. 2007. Estimation of Ultimate Tension Load of Methylmetahcrylate Bonded Steel Rods into Concrete. *International Journal of Adhesion and Adhesives*, Vol. 27, No. 8: 653-660.

Colak, A. 2001. Parametric Study of Factors Affecting the Pull-Out Strength of Steel Rods Bonded into Precast Concrete Panels. *International Journal of Adhesion and Adhesives*, Vol. 21, No. 6: 487-493.

Cook, R.A., Douglas, E.P., and Davis, T.M., 2009. *Adhesive Anchors in Concrete Under Sustained Loading Conditions*. NCHRP Report 639. Transportation Research Board. Washington, D.C.: Transportation Research Board.

Cook, R.A. and Jain, P. 2005. Effect of Coarse Aggregate on the Strength of Adhesive-Bonded Anchors. University of Florida, Gainesville, FL.

Cook, Ronald A. and Konz, R.C. 2001. Factors Influencing Bond Strength of Adhesive Anchors. *ACI Structural Journal*. Vol. 98, No. 1: 76-86.

Cook, Ronald A., Kunz, Jacob, Fuchs, Werner, and Konz, Robert C. 1998. Behavior and Design of Single Adhesive Anchors under Tensile Load in Uncracked Concrete. *ACI Structural Journal*. Vol. 95, No. 1: 9-26.

Elighausen, R. and Balogh, T. 1995. Behavior of Fasteners Loaded in Tension in Cracked Reinforced Concrete. *ACI Structural Journal*. Vol. 92, No. 3: 365-379.

Eligehausen, R., Cook, R., Appl, J. 2006. Behavior and Design of Adhesive Bonded Anchors. *ACI Structural Journal*. Vol. 103, No. 6: 822-831.

Eligehausen, R. and Silva, J. 2008. *The Assessment and Design of Adhesive Anchors in Concrete for Sustained Loading*. [Online]. Available from http://www.us.hilti.com/fstore/holus/techlib/docs/technical%20publications/anchoring/hiltiadhesivesustainedloading.pdf. 24 February 2011.

European Organization for Technical Approvals. 1997. ETAG 001 Guideline for European Technical Approval of Metal Anchors for use in Concrete – Annex B: Tests for Admissible Service Conditions. Brussels, Belgium: EOTA.

Fuchs, W., Eligehausen, R., and Breen, J.A. 1995. "Concrete Capacity Design (CCD) Approach for Fastening to Concrete". *ACI Structural Journal*. Vol. 92, No. 1: 73-94.

Grosser, P., Fuchs, W., and Eligehausen, R. 2011. "A Field Study of Adhesive Anchor Installations". *Concrete International*, January, 57-63.

Hilti. 2011. *Volume 2: Anchor Fastening Technical Guide.* North American Product Technical Guide. Tulsa, OK: Hilti, Corp.

ICC Evaluation Service, Inc. 2012. ICC-ES Evaluation Report ESR-2322, Hilti HIT-RE 500-SD Adhesive Anchors in Concrete. Whittier, CA: International Code Council.

ICC Evaluation Service, Inc. 2010. ICC-ES Evaluation Report ESR-2262, Hilti HIT-HY 150MAX Adhesive Anchoring System in Uncracked Concrete. Whittier, CA: International Code Council.

ICC Evaluation Service, Inc. 2009. AC308 Acceptance Criteria for Post-Installed Adhesive Anchors in Concrete Elements. Whittier, CA: International Code Council.

ICC Evaluation Service, Inc. 1995. *AC58 Acceptance Criteria for Adhesive-Bonded anchors in Concrete and Masonry*. Whittier, CA: International Code Council.

Krishnamurthy, K. 1996. "Development of a Viscoplastic Consistent-Tangent FEM Model with Applications to Adhesive-Bonded Anchors" Doctoral thesis. University of Florida, Gainesville, FL.

Meinheit, D.F., Wollmershauser, R.E., Pearson, J.E. 2007. Bonded Anchors: A Convenient Solution or Potential Liability. *STRUCTURE Magazine,* November, 50-51.

Messler, R.W. 2004, *Joining of Materials and Structures*. Elsevier Butterworth-Heinemann, Oxford, UK.

Meszaros, J. 1999 "Tragverhalten Von Verbunddübeln Im Ugerissenen Und Gerissenen Beton". Doctoral thesis. University of Stuttgart, Stuttgart, Germany.

PCI Industry Handbook Committee. 2010. *PCI Design Handbook: Precast and Pretressed Concrete.* MNL-120. 7th ed. Chicago, IL: Precast/Prestressed Concrete Institute.

Wollmershauser, Richard, Mattis, Lee. 2008. "Adhesive Anchor Installation and Inspection". *Concrete International*, December, 36-40.

Wollmershauser, Richard. 2003. *The Latest Word on Building Codes for Anchoring Concrete.* [Online]. Available from http://www.us.hilti.com/fstore/holus/techlib/docs/technical%20publications/anchoring/article_building_codes-anchoring_to_concrete.pdf, 24 February 2011.

VITA

Michael Glenn Eilers was born on July 25, 1978, in Sedalia, Missouri. He was educated in Marshall, Missouri public schools and graduated from Marshall High School in 1997. He received several scholarships to the University of Missouri-Rolla in Rolla, Missouri, from where he graduated in 2002 with a degree of Bachelor of Science in Civil Engineering. While at the University of Missouri-Rolla, he was an active member of Phi Kappa Theta fraternity and participated in four internships with Coreslab Structures (formerly Rinker Materials).

After working as a structural engineer for one year at Structural Engineering Associates, Inc. in Kansas City, Missouri, Mr. Eilers returned to Coreslab Structures as a structural engineer and began a Master's program in civil engineering at the University of Missouri-Kansas City. He was awarded the Master of Science degree in Civil Engineering in December 2006.

Upon completion of his Master's degree, Mr. Eilers began work toward his Ph.D. in Civil Engineering and Mathematics at the University of Missouri-Kansas City and continued to work for Coreslab Structures. During his graduate studies at the University of Missouri-Kansas City, he became a Graduate Teaching Assistant and Adjunct Instructor.

Mr. Eilers is a member and past board member of the Missouri Chapter of the American Concrete Institute as well as a member of the Precast/Prestressed Concrete Institute. Mr. Eilers is a Registered Professional Engineer in Arkansas, Kansas, Missouri, and Texas.